Forschungszentrum Karlsruhe
in der Helmholtz-Gemeinschaft

Wissenschaftliche Berichte
FZKA 7011

ECO Steam Explosion Experiments – Documentation and Evaluation of Experimental Data

W. Cherdron, F. Huber, A. Kaiser, W. Schütz

Institut für Reaktorsicherheit
Programm Nukleare Sicherheitsforschung

Dezember 2005

Forschungszentrum Karlsruhe

in der Helmholtz-Gemeinschaft

Wissenschaftliche Berichte

FZKA 7011

ECO STEAM EXPLOSION EXPERIMENTS – DOCUMENTATION AND EVALUATION OF EXPERIMENTAL DATA

W. Cherdron, F. Huber, A. Kaiser, W. Schütz

Institut für Reaktorsicherheit

Programm Nukleare Sicherheitsforschung

Forschungszentrum Karlsruhe GmbH, Karlsruhe

2005

Impressum der Print-Ausgabe:

Als Manuskript gedruckt

Forschungszentrum Karlsruhe GmbH
Postfach 3640, 76021 Karlsruhe

Mitglied der Hermann von Helmholtz-Gemeinschaft
Deutscher Forschungszentren (HGF)

ISSN 0947-8620

urn:nbn:de:0005-070116

Abstract

Steam explosions are a safety concern during analysis of LWR core melt accidents. In case of a steam explosion, part of the thermal energy of the melt is transferred into mechanical energy, imposing loads to reactor vessel, reactor roof, and and in-vessel structures. As a consequence of these loads, part of these structures might fail.

The ECO experiments have been conducted at the Forschungszentrum Karlsruhe to measure the explosion pressures and actually measure the Energy COnversion directly under well-defined conditions with relevant melt masses (up to 18 kg), which has never been done before. These tests were using molten alumina (Al_2O_3) from a thermite reaction (2600 K) to simulate the high temperature core melt.

In principle, the facility consists of a piston and cylinder system. The melt is injected from above into the water which is situated in the piston. Under the pressure forces due to the explosion, the piston moves downwards compressing a stack of crushing material with well-defined forces. This gives a direct measurement of the mechanical energy.

Very low energy conversion ratios were obtained in the first three tests (less than 0.1 %). Therefore, in the following tests, essential test conditions were changed. The water-to-melt mass ratio was decreased and the melt jet was partly fragmented before it penetrated into the water.

Under these conditions, the energy conversion became more effective: up to 2.39 % were reached. In test 05, the strongest explosion of the test series occurred, with pressures well beyond the registration limit of 50 MPa. The last two tests produced pressures in excess of the extended registration limit of 100 MPa, the energy conversion ratios remained below one percent, however.

We report here about the results of the full test series which comprises eight successful tests.

Zusammenfassung

ECO-Versuche zur Dampfexplosion – Dokumentation und Auswertung der experimentellen Ergebnisse

Dampfexplosionen sind Bestandteil der LWR-Sicherheitsanalysen, in denen Kernschmelzunfälle betrachtet werden. Im Falle einer Dampfexplosion wird ein Teil der thermischen Energie der Schmelze in mechanische Arbeit umgesetzt, die zu Lasten auf den Reaktordruckbehälter und den Reaktordeckel führt. Als Folge dieser Lasten könnte ein Teil dieser Strukturen versagen

Die so genannten ECO-Experimente wurden am Forschungszentrum Karlsruhe durchgeführt, um zum einen die Explosionsdrücke, zum anderen die Energiekonversion (engl. Energy COnversion) direkt unter wohl definierten Bedingungen mit Schmelzemassen von bis zu 18 kg zu messen, was bisher einmalig ist. Die heiße Kernschmelze wurde durch flüssiges Aluminiumoxid (Al_2O_3) von etwa 2600 K simuliert, das durch eine Thermitreaktion erzeugt wurde.

Die Testeinrichtung besteht im Prinzip aus einem Kolben-Zylinder-System. Die Schmelze wird von oben in das Wasser eingeleitet, das sich im Kolben befindet. Letzterer bewegt sich unter der Wirkung der Drücke, die mit der Dampfexplosion einhergehen, nach unten und komprimiert dabei eine Lage von energieverzehrendem Knautschmaterial mit bekannten Verformungseigenschaften. Der Verformungsweg kann somit direkt in mechanische Energie umgerechnet werden.

Die Energiekonversionrate war in den ersten drei Versuchen mit Werten unter 0,1% sehr niedrig. In den folgenden Versuchen wurden daher wesentliche Versuchsbedingungen geändert. So wurde das Massenverhältnis von Wasser und Schmelze verkleinert, und es wurde der Schmelzestrahl vorfragmentiert, bevor er in das Wasser eindrang.

Diese Maßnahmen erhöhten die Energiekonversionrate auf bis zu 2,39 %. Der Versuch 05 verzeichnete die stärkste Dampfexplosion der Versuchsserie, wobei die Drücke den Messbereich von 50 MPa weit überschritten. In den letzten zwei Versuchen wurden noch höhere Drücke gemessen, die sogar über den auf 100 MPa erweiterten Messbereich hinaus gingen. Die Energiekonversionraten blieben jedoch unter einem Prozent.

Der Bericht gibt alle Ergebnisse der Versuchsserie wieder, die acht erfolgreiche Einzelversuche umfasst.

CONTENTS

List of Figures

List of Tables

1. INTRODUCTION

1.1. General remarks

Steam explosions are encountered often when liquids of very different temperatures are intermixed accidentally. Quenching of molten materials in water pools is a widely used technique, e.g. in the foundry, to granulate and cool them effectively. This dualism indicates the necessity of a careful treatment of the problem.

A steam explosion develops in several stages: premixing (i.e. fragmentation of the hot material and mixing without much heat loss), triggering, propagation and expansion. Steam explosions occur when, after triggering, a large amount of heat is transferred to the vaporizable liquid at a temperature far above its boiling point and at such a rate that the system cannot expand fast enough. As a result, very high pressures develop within a short time with the potential of a destructive effect.

In spite of an extremely small probability of occurrence, steam explosions are also a safety concern during analysis of LWR core melt accidents. For more details see the review papers /1-4/. In case of a steam explosion, part of the thermal energy of the melt is transferred into mechanical energy. These types of interaction are called thermal interaction or - in the field of nuclear reactor safety - fuel-coolant interaction (FCI). The ECO experiments, carried out at Forschungszentrum Karlsruhe, have been conducted to measure the energy conversion under well-defined conditions.

1.2. Remarks on the ECO experiments and on alumina melt

The purpose of the ECO experiments was to obtain an experimental upper limit of interaction pressure and energy conversion, to observe how these depend on initial and boundary conditions, and to collect relevant and well defined experimental data for verifying computer models.

To this end, explosions are triggered externally and contained in a system of cylinder and piston in which the piston can move only by compressing crushing material with a well defined force. This gives a direct measurement of the work that the steam explosion can do on its surroundings.

The direct transfer of experimental results to reactor accident conditions is always handicapped by the need to extrapolate from relatively small experiments to large dimensions (and masses) and, if simulant materials are used, from the material properties in the experiment to those of the molten core materials. Therefore, the use of large masses and of prototypical materials is desirable. Unfortunately, for technical and administrative reasons, we are not able to handle amounts of UO_2 worth mentioning at Forschungszentrum Karlsruhe.

Consequently, we have developed the technique of producing large amounts of molten alumina (Al_2O_3) at about 2600 K by thermite reactions. The molten iron produced in the same reaction is separated from the alumina and retained in the source. This works so well that the oxide that actually is released consists of more than 90 weight % of Al_2O_3, the rest being unreacted iron oxide and iron. (Note: at 2600 K, the density of alumina is about 2800 kg/m^3, that of iron 6300 kg/m^3.)

The use of a non-toxic and non-radioactive simulant material under realistic temperatures (and, thus, almost realistic heat transfer) had the big advantage that a large variety of instrumentation including video and high-speed photography could be applied. No elaborate protection was needed in post-test debris examination.

The information can be used as well for comparison with experiments carried out with a prototypical corium melt on a similar scale. This comparison is important since

the more pronounced tendency of alumina towards steam explosion compared to corium is still an open question. Experiments with prototypical materials have been performed at JRC Ispra, using the FARO and KROTOS facilities /5-7/. The KROTOS facility has also been used for tests with alumina on a two-kg scale. These experiments may be also considered in scaling studies.

The melt is released through a circular tube at a controlled driving pressure. This technique has also been used in the PREMIX experiments /8, 9/ performed to study the premixing phase that must precede any large-scale steam explosion in situations in which hot melt and water are separated in space initially.

We consider alumina as a good substitute for actual core melts for several reasons: It is essentially an oxide as is the expected main component of core melt. Its initial temperature comes close to the expected core melt temperatures. Note that all phases of steam explosions are essentially driven by heat transfer and that this is controlled by the temperature of the hot melt and its surface area.

Differences in the properties of the melts are in the composition, in the density, in the absolute temperature, and in the temperature span above solidus. The excess enthalpy influences, among other properties, premixing during the initial period of interaction.

On the other hand, good agreement is given in the total enthalpies. The thermal content per unit volume of Al_2O_3 is similar to that of UO_2. So, from an energetic point of view, alumina represents an equal volume of UO_2, i.e. roughly three times its mass of UO_2. Also, as far as the droplet size is similar, so is the heat transfer surface per unit thermal energy.

Al_2O_3 is known to produce violent explosions easily. So it is prudent (conservative) to perform steam explosion studies with this material. If no explosion occurs in an experiment, it is sure that this is not due to the hot melt not tending to explode.

In Table 1, physical properties and conditions are compared of a melt typical of ECO with those of corium melt /10/ estimated for a light water reactor (LWR). Note that the composition of the melt used in FARO is similar to that given here for an LWR. The melt release temperature in the L-28 and L-31 FARO tests was 3000 – 3050 K. In any case, the use of computer codes is essential to properly find the influence on the results of the different test conditions.

Table 1. Actual properties of the melt in ECO compared with properties estimated for corium melt (cf. Ref. 10).

	ECO	LWR
Composition of melt, wt%	>90% alumina <10% iron and iron oxide	UO_2 + 22.2%ZrO_2
Average melt density, kg/ m^3	2800	7350
Melt release temperature, K	2600	3300
Temperature at solidus, K	≈2313	2815
Total enthalpy, MJ/m^3	$10.64 \cdot 10^3$	$12.3 \cdot 10^3$
Excess enthalpy above solidus, MJ/m^3	$\approx 1.45 \cdot 10^3$	$\approx 5 \cdot 10^3$

Extrapolation to reactor accident conditions must be done by numerical simulation anyhow. By this, many of the different material properties (e.g. density, freezing tem-

perature) are accounted for automatically. For others it might be necessary to tune models in the codes. But with the KROTOS and FARO results available as well, there is a large body of information on the behavior of these materials under comparable conditions. Actually, two of the later PREMIX experiments have been performed as similar as possible to two of the last FARO tests within a common European project /11/.

On this basis, we expect to obtain data relevant for reactor accident conditions when using this alumina in quantities above 10 kg for premixing and explosion tests. Such data are improving our understanding of the physical phenomena involved and are suited to test, improve, and finally validate corresponding computer codes for the intended purpose.

2. TEST FACILITY AND PERFORMANCE

2.1. Test facility

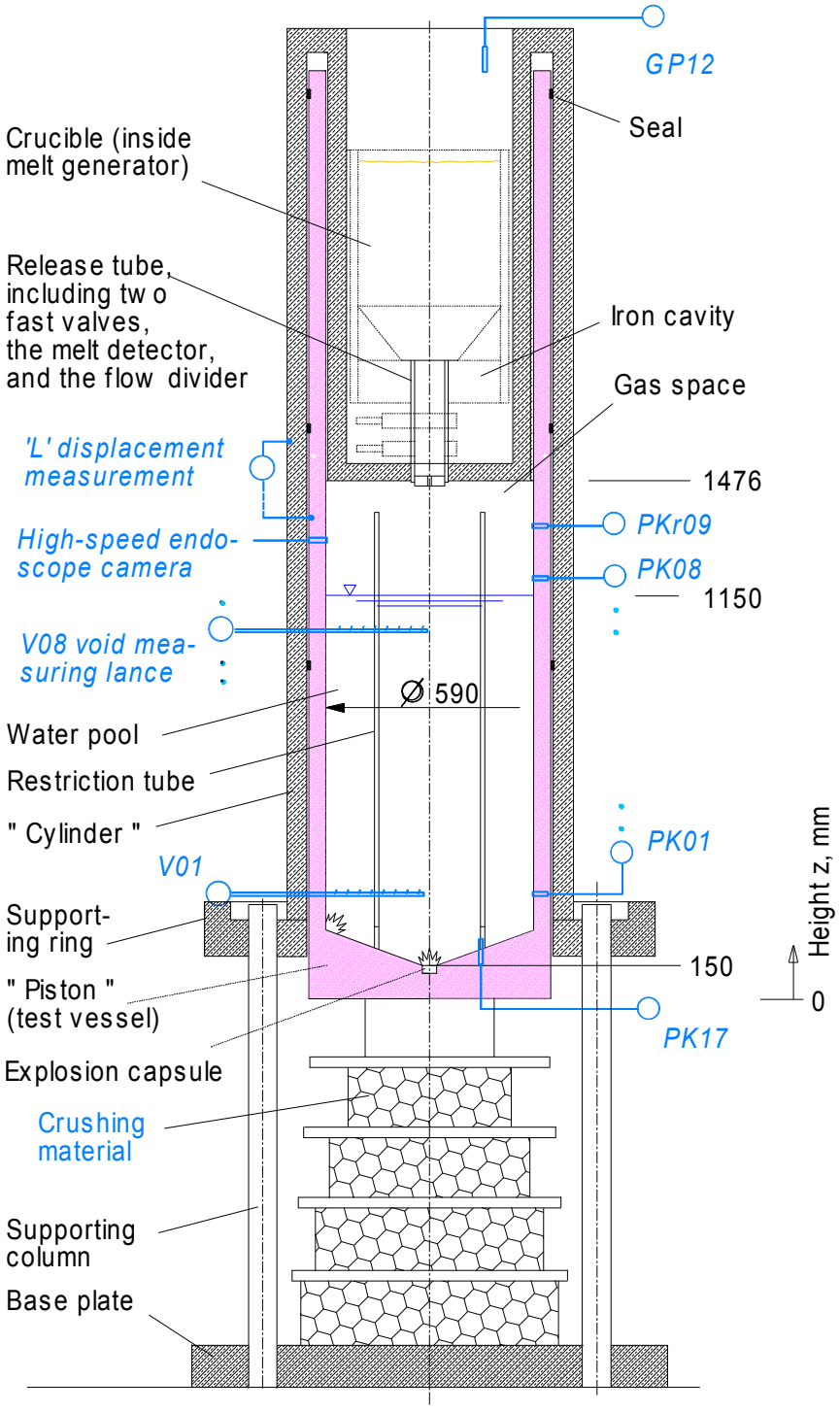

Fig. 2.1 ECO test facility. For details of the melt generator see Figure A1.

The test apparatus is shown in Fig. 2.1. The measurement of the mechanical energy is achieved by confining the explosion in a closed volume (cylinder) equipped with a piston that contains the water pool. In response to the explosion pressure, the piston moves down compressing a stack of crushing material with a known force. The movement of the piston is guided by three annular flat seals made of Teflon positioned at different axial positions.

The melt generator forms the upper (closed) lid of the stationary cylinder. The middle part, labelled “cylinder” in Fig. 2.1, is welded to the supporting ring. It is equipped with six narrow grooves in which the measuring instruments fastened to the piston can move in the axial direction. The six supporting columns are connected to the supporting ring by big screws.

The test vessel (piston) has an inner diameter of 0.59 m. To reduce the amount of water involved in the melt penetration and condensation processes taking place during the premixing and explosion phases, a restriction tube with an internal diameter of 0.3 m was introduced in the test vessel in tests 04, 05, 06, and 09. Its upper rim is at 1390 mm height. The water is initially about 1 m deep, and there is a free gas space of 0.3 m above it forming a volume of about 0.08 m^3. The whole facility is 4 m high and weighs about 10^4 kg.

The tests proper are controlled by an automated procedure that is started by igniting the thermite mixture in the crucible. For details see Section 2.2 and Appendix A.

2.2. Test performance

Melt supply and release system

The melt to be released into the water is generated in the crucible by an exothermal reaction of an aluminium/iron oxide thermite mixture. The equation of the chemical reaction reads:

$2Al + Fe_2O_3 = 2\,Fe + Al_2O_3 + 3800$ J/g

From the two reaction products, only alumina is used. The temperature of the melt depends on the initial temperature and the composition of the thermite mixture, on the completeness of the chemical reaction (cf. Section 1.2 above), and on the heat losses. To avoid evaporation of iron, the temperature of the melt was lowered to about 2600 K by adding 4% alumina to the stoichiometric thermite mixture.

The thermite reaction is started by means of four electrical igniters mounted in the top region of the mixture. Gas and smoke can escape from the crucible atmosphere through a venting line, from the very beginning until close to the end of reaction. The reaction products, iron and alumina, separate during and after the reaction due to their different densities. This effect is used in the construction of the melt generator: When the reaction front reaches the bottom of the crucible, an annular compartment (named 'iron cavity', see Figs. 2.1 and A2.1), initially closed by a steel foil and evacuated, is opened by melting. The heavier iron fully drains into the cavity.

The reaction front proceeds through the bottom into the melt release tube. Melt detectors (two-wire cables), installed 30 mm (50 mm from test 06 on) above another steel foil which closes the thermite filling towards the bottom, indicate the arrival of the reaction front and with it the near end of the chemical reaction. This event triggers the closure of the crucible venting line as well as the activation of the gas pressure monitoring system. In a first action, the melt generator is pressurized to a certain level above the test vessel pressure in order to obtain the desired rate of melt release. The pressurization is performed by connecting a gas line to a high-pressure argon reservoir. This pressure rise and the following variations of the pressure difference are controlled by pressure transducers and a couple of fast acting valves mounted in that line.

It should be mentioned that the melt released always contains a small portion of non-condensable gas. It is assumed that the gas, attached to the particles and contained in the porosity of the thermite mixture does not escape completely from the

melt during the time available. The gas content is estimated to be about 10 – 20 % of volume.

Two types of melt generator with different capacities were used in ECO. The smaller one had a maximum capacity of 9 kg of alumina melt. The diameters of the crucible and the melt release tube were 180 and 45 mm, respectively. It was only used in the first test, ECO-01.

Figure A2.1 (Appendix A) shows the two designs of the larger melt generator which had a capacity of 18 kg of alumina melt. The diameters of the crucible and the melt release tube were 200 and 60 mm, respectively. In all cases, the thermite filling in the crucible was tightly separated from the test vessel by the second steel foil mentioned before. The steel foil was generally located at a distance of 90 mm below the bottom of the crucible.

The smaller melt generator and the variation 1 of the larger one were equipped with only one fast slide valve that was used to terminate melt release. The melt release started with melt-through of the steel foil mentioned. Variation 2, used from test 04 on, was equipped with an additional (opening) valve.

One of the primary goals of our test preformance was to get the maximum of melt released. In persuing this goal, the driving pressure and the pattern of melt flow, i.e., a rather compact jet or a dispersed type of flow, have been the most important parameters.

Results of the first three experiments as well as calculations on a simple numerical model (see Appendix A4) led to the conclusion that the process of complete melt through of the steel foil took some time, so that melt release occurred in an uncontrolled manner. Therefore, a second fast acting slide valve was mounted to start melt release in a more predictable manner. The space between the valve and the steel foil is evacuated so that the melt can easily enter this volume. To be sure that the steel foil is completely molten, the valve is opened 400 ms after the start of melt through.

Preparation of a typical test and the course of events

In the following description, characteristic data of one of the more successful tests, ECO-06, are used in some points.

In preparing the test, the test vessel was filled with demineralised water to the desired level while it was open to the environment. This means that air was one component of the gas overlying the water. Salt (NaCl) was added to the water to get a certain degree of electrical conductivity necessary to enable the void measurement. The dose was 125 g per 1000 litre of water.

The water was heated up close to boiling conditions by electrical heaters mounted at the inner surface of the vessel wall. Natural circulation and heat losses caused the formation of temperature stratification from top to bottom as indicated in Table 4. A short time before the proper start of the experiment, the test vessel was pressurized to the desired value (0.25 MPa) by adding argon to the gas overlying the water. The pressurization was enabled by a special annular seal between the piston and the cylinder which made the test vessel gas tight, at least in its initial position.

As mentioned, the proper test was started by igniting the thermite mixture. About 26 seconds later, melt release was started by opening valve 1. (Remember: in the first three experiments, this occurred by melt through of the steel foil). Seventeen milliseconds later, the melt front passed the lower end of the release tube; another 12 ms later, the water surface was reached. Both events were recorded by the high-speed endoscope video system. The actual passage of melt at the tube exit was in-

dicated by a step in the melt detector signal which triggered the start of the data and (outer) video recording systems.

The start of melt penetration into the water was indicated by a pressure increase caused by evaporation. When, during the melt release, the pressure difference dropped below a given value (e.g. 0.7 MPa), gas was added to the melt generator atmosphere to keep the pressure difference constant. This goal could not really be achieved since the pressure rise in the test vessel turned out to be too fast. This was true in tests 03 to 07. Consequently, the pressure difference decreased and even became negative for a short period of time. Still flow reversal did not occur since the pressure difference used to recover. Towards the end of melt release, another pressure increase in the crucible was observed. We presume that this was caused by the evaporation of water intruded into the almost empty melt generator.

The melt release was terminated by closing the lower slide valve (valve 2). Valve closure was triggered as soon as one of the following criteria was fulfilled:

(1) Steam is detected at two out of three void probe positions. These are V03.1 and V02.1 at 450 mm level and V01.1 at 300 mm level. This means that melt has almost reached the bottom of the pool. The goal was to avoid premature destruction of the explosion capsule by melt attack.

(2) The pressure in the test vessel exceeds a preset high value (typically 3 MPa), e.g. due to a spontaneous steam explosion.

(3) The pressure difference between the melt generator and the test vessel becomes negative by more than a preset value (around 0.2 MPa). The goal was to avoid melt flow reversal.

(4) An interval of time, typically 0.3 s, is exceeded, counted from the instant when the melt passes the melt detector located at the lower end of the release tube.

The steam explosion was triggered, from test 03 on, by two explosion capsules, about 10 milliseconds after closure of valve 2. The capsules were located in the center and at the edge of the vessel bottom, respectively. Under the pressure forces due to the steam explosion, the test vessel moved down compressing, as a rule from top to bottom, the various layers of crushing material. (Test 09, in which two different materials were used, is an exception of this rule.)

Typically one day after the experiment, the water from the test vessel was drained and with it part of the melt fragments. The other part remained in the vessel and was collected after dismantling of the test facility a few to several days later.

The mass of melt released was determined by weighing the melt fragments collected. The result was controlled by a balance of the masses of the melt generator before and after the experiment.

2.3. Instrumentation

The instrumentation of the facility (Fig. 2.1) was copious. It was especially designed to measure the release of meachanical energy during steam explosion. The various types of instruments mounted in the reach of the “piston” and of the “cylinder” help in the interpretation of the course of events. Table 2 gives a comprehensive list of the instruments taking test 06 as an example.

Dynamic pressure transducers were generally mounted in the 60° - 240° azimuth direction angles at several axial heights (e.g., PK17 and PK08 in Fig. 2.1). Up to three instruments were located at one height at different azimuthal directions. Most of the transducers were of the piezo-electric type. The manufacturer is Kistler, Switzer-

land; we used the so-called 6000 and 7000 series with charge characteristics of around 7.5 and 78 pC/bar, respectively. Some transducers were of the piezo-resistive type (manufacturer: Kulite, USA), giving absolute pressure data. The measuring heads of the transducers were generally mounted flush with the inner surface of the test vessel. In test 06, two instruments have been shifted radially, such that their measuring heads were flush with the inner surface of the restriction tube.

The *deformation* of the crushing material was an important integral measurement of the *mechanical energy released*. The areas of the crushing material layers increased from top to bottom so that increasingly high forces were required to compress them, one after the other. An exception occurred in test 09 (cf. Appendix B).

Two *displacement transducers* measured on-line the movement of the piston, L, relative to the cylinder. The instruments use the principle of electric potentiometers. Additionally, this movement and that of the whole test facility against gravity were observed by two outer *high-speed video cameras*.

Twelve horizontal *measuring lances* were grouped in the 0° and 180° azimuth angles (Fig. 2.2 (a)), equipped with eight *void* probes and a *thermocouple* each. The void probes indicate changes in the local phase conditions, i.e. from liquid to steam, and vice versa. The upper photograph in Fig. 2.2 was taken from above into the (dismantled) test vessel giving an impression of how the void measuring lances were arranged. Eight of the lances, arranged in the 0° angle, formed an array of 8 axial and 8 radial positions, the other four formed one of 4 x 8 positions. The probes were situated at radial distances of 35 mm, starting at a radius of 25 mm. The thermocouple tips were at a radius of 10 mm.

The *axial forces* in the six supporting columns were determined by means of strain gauges (abbrev. DMS).

A *high speed video camera* taking 1000 f/s equipped with an endoscope was used in test 06 for the first time. The objective observed the section of the gas volume between the exit of the release tube and the water surface.

Up to four *acceleration transducers* were mounted in tests 06 to 09 at different positions. The sites were at the body of the test vessel (see e.g. AKi04, Table 2) as well as at the top of the facility (e.g. AKi03). It should be mentioned that, in principle, only qualitative results were obtained from the instruments (see e.g. Fig. 5.6.7).

Table 2. List of the measuring instruments used in test 06 (cf. Fig. 2.1).

- V: void meas. lance with one TC at its end; T13 - T16: at different radial positions;
- PKi: Kistler pressure transducer; PKu: Kulite pressure transducer;
- AKi: acceleration transducer; § Four additional instruments, used in test 09.

Azimuth / **Height**	**0°**	**60°**	**180°**	**240°**
2750 mm		**AKi03**		
1488 mm § r ≈ 220 mm	**PKi19, T18**	**PKi20, 120°**		**T19**
1445 mm		**Melt release detector**		
1350 mm			**Displacement transducers** **120°** **300°**	
	V11 measuring tips downward!		**V12** measuring tips downward!	**PKr09**
1275 mm	**Endoscope camera, T17**			
1200 mm	**V10** Measur. tips downward!	**PKi08**	**PKi13**	**PKi09**
1150 mm	**Water level**			
1050 mm	**V08**	**PKi07**	**V09**	**PKu15**
900 mm	**V07**	**PKi06**	**T13, T14** 95, 230 mm rad. respectively	**PKi12**
750 mm	**V05**	**PKi05**	**V06**	
600 mm	**V04**	**PKi04**	**PKi11**	**PKu14**
450 mm	**V02**	**PKi03**	**V03**	**T15, T16** 95, 230 mm rad., respect.
390 mm supporting ring		**AKi02**		
300 mm	**V01**	**PKi01**	**PKi10**	**PKi02**
230 mm			**120° Trigger 2, lateral position**	
200 mm pool bottom, r ≈ 147 mm	**PKi16** **30°**		**PKi17** **150°**	**PKi18** **270°**
100 mm		**Trigger 1, central position**		
0 mm piston bottom		**AKi04**		
-1030 mm		**AKi01**		

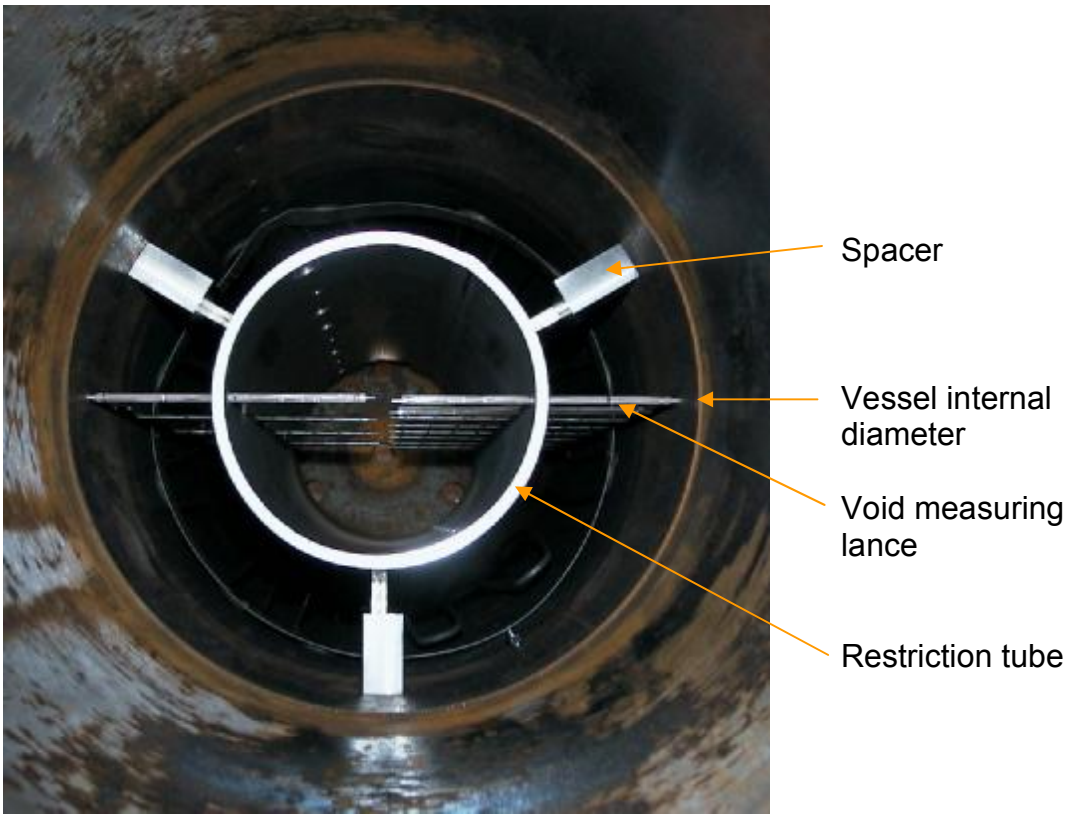

(a) View from above into the test vessel (melt generator removed).

(b) Void measuring lance, ready for mounting.

(c) Detail showing the three innermost void probes and the thermocouple. The distance between two void probes is 35 mm.

Fig. 2.2 Details of the void measuring equipment.

3. TEST CONDITIONS

Test conditions of all successful experiments are summarized in Table 3. By the addition of a few essential results, the gradual modifications (i.e. optimization) of the test conditions becomes apparent. In the following, additional remarks are given on the individual tests.

ECO-01.

The water temperature and the initial system pressure were set close to environmental conditions. The melt was provided by the smaller melt generator.

On the basis of the PREMIX results, an initial pressure difference of 0.075 MPa was projected. The actual pressure difference and with it the speed of the melt released were about three times higher, however. The reason for this was that the response of the specific measuring device that formed (by capillary action) the pressure difference between crucible and test vessel, turned out to be too slow to be effectively used by the gas pressure monitoring system.

We conclude from the void data that the melt flow had the form of a rather compact (i.e. not diverging) jet whose front penetrated very fast into the water. Melt was detected at the lowermost measuring lance already at 0.154 s. When the valve was closed thereupon, only 60% of the maximum melt mass had left the melt generator.

ECO-02.

The water temperature and the initial system pressure were set close to environmental conditions. The larger melt generator having a double charge and a larger tube diameter was used from this test on.

A special measure was taken to prevent a pressure increase in the test vessel during premixing: The gas space overlying the water pool was kept open to the environment during premixing. Two venting lines, each provided with a fast slide valve, were mounted in the bottom plate of the melt generator housing (cf. Fig. A2.1). These valves were to be closed simultaneouly with the melt closing valve before the steam explosion was triggered.

Another change was the reduction of the initial water level by 50 mm to 1150 mm height. By this, the volume overlying the water was increased.

As the pressure in the test vessel was low, the pressure difference was chosen to be low as well. In fact, the melt release took place at a smaller rate than in test 01. However, a spontaneous steam explosion occurred long before the melt front had reached the lowermost detecting level. The valves (that for melt release as well as those in the venting lines) were closed after the explosion. This occurred according to criterion no 2. In the end, only half of the melt mass was released compared with test 01 and one fifth of the possible mass.

From test 02 on, the specific device to measure the pressure difference was replaced by a fast electronic unit that determined the difference from the output signals of two separate transducers.

ECO-03.

To reduce the risk of a spontaneous steam explosion, the system pressure and the water temperature were raised from test 03 on. (The venting lines of the test vessel were kept closed.) The water was heated close to boiling conditions while a temperature gradient established in the water as indicated in Table 3. At last, the system pressure was increased to the desired value using argon gas.

The aim of this test was to release a large amount of melt using a higher pressure difference. Because of a failure of a valve in the venting system of the melt generator, the actual pressure difference was much lower than projected. Additionally, we conclude from parametric calculations on our numerical model that the melt release started with a small jet diameter that became larger according to the (slow) progress of melt-through of the steel foil (see Appendix A.4).

As a result of both conditions, only a small amount of melt (0.9 kg) was released. Melt release was terminated according to the above criterion no 4.

ECO-04.

The experimental design was modified in this and the following tests to achieve both larger melt masses and larger conversion ratios. In test 04, two major changes were made:

(1) Melt release was no longer started with the uncontrolled melting of a steel membrane but by opening a fast slide valve additionally mounted between the steel membrane and the closing valve (Fig. A2.1). This was to ensure a fairly compact melt flow within the tube with full cross-section instantly.

(2) To reduce the amount of water involved in the condensation processes taking place in the 'interaction volume' during the premixing and explosion phases a restriction tube made of steel was mounted in the vessel. The tube wall thickness was 12.5 mm, the internal diameter 299 mm, i. e. about half that of the vessel diameter.

In the end, the essential characteristics of the test were similar to those in test 01. The jet was compact and penetrated very fast into the water. Melt release was prematurely terminated according to criterion no 1. The larger amount of melt was mainly caused by the larger diameter of the release tube.

ECO-05.

From test 05 on, in addition, a flow divider (also called dispersion device) was mounted at the exit of the melt release tube to avoid the formation of a compact jet below the release tube. The device consists of four ribs forming a cross (Fig. A3.1). It divides the compact jet into four partial jets. The aim was to get a smaller penetration rate of the melt in the water and by this a larger portion of the melt involved in premixing. The other experimental conditions were similar to those in test 04.

The modification resulted in the release of almost the total mass of melt within the given time (criterion no 4). No steam was detected at the lowermost measuring lance.

ECO-06.

The aim of test 06 was to get information on the *reproducibility* of the ECO experiments. Therefore, the same initial test conditions were set as in test 05. Melt release was terminated according to criterion no 4.

ECO-07.

Test 07 was carried out without the restriction tube. It should give information on the influence of the tube on the results, especially on the fragmentation pattern. The other test conditions were the same as in test 06.

Valve 2 was closed according to criterion no 4. The same amount of melt as in test 06 was released in a time that was scheduled to be 20% shorter. No steam explosion occurred, although the triggers were fired as planned.

ECO-08.

The experiment failed soon after the start because of a failure in the operation control system. No melt was released.

In this test, the restriction tube was used again and a lower initial pressure was applied in the melt generator. The latter should give information on the effect of a smaller pressure difference on the results. From precalculations and from the results of test 01, we concluded that a smaller pressure difference should cause smaller ejection velocities and thereby a smaller pressure increase in the mixing zone. In such a case, it should be easier to maintain a more constant pressure difference than in the case of a steep pressure increase.

The other initial conditions in test 08 were the same as in the tests before.

ECO-09.

Test 09 is a successful repetition of test 08. The maximum mass of melt could be released within 0.35 s (criterion no 4). The steam explosion produced very high pressures.

Table 3. Test conditions and a few specific results.

Test Date	01 25.04.2000	02 12.12.2000	03 10.04.2001
Melt			
Mass actually released, kg	5.76	2.87	0.9
Initial pressure difference [§], MPa	0.26	0.095	0.13
Release device within tube, -	steel foil	steel foil	steel foil
Release tube diameter, m	0.045	0.060	0.060
Height of fall to water surface, m	0.275	0.325	0.325
Max. speed in tube (calc.), m/s	7.4	5.9	6.8
Release time (till valve closure) [§§], s	0.172	0.226	0.351
Average release rate, kg/s	28.5	11.2	2.4
Pool			
Water temperature (stratified!), K	293	293	363-323
Diameter available for mixing, m	0.59	0.59	0.59
Initial water level, mm	1200	1150	1150
Effective water depth, m	1.10	1.05	1.05
Pressure conditions			
Initial system pressure, MPa	0.1	0.1	0.24
Pressure before explosion, MPa	0.325	0.1 [$]	0.387
Explosion period			
Explosion mode, -	triggered	spontaneous	triggered
Compression of crushing mat., mm	4	4	2

[§] At the start of melt release; [§§] around 0.030 seconds have to be added for the time span between steel foil melt-through and zero time; [$] system open to environment.

Test Date	04 14.11.2001	05 19.06.2002	06 18.03.2003	07 04.09.2003	09 20.07.2004
Melt					
Mass released, kg	9.6	16.4	15.2	15.2	18.0
Init. press. difference [§], MPa	0.73	0.76	0.72	0.76	0.35
Release device, -	fast valve	+ me. disp.	+ me. disp.	+ me. disp.	+ me. disp.
Release tube diameter, m	0.060	0.060	0.060	0.060	0.060
Height of fall to wat. surf., m	0.325	0.325	0.325	0.325	0.325
Max. speed (calc.), m/s	12.5	13.5	12.8	13.1	8-9
Release time [§§], s	0.161	0.340	0.350	0.312	0.347
Average release rate, kg/s	60	48	43	49	52
Pool					
Water temperature, K	369-336	355-329	353-319	347-331	360-343
Diameter avail. for mixing, m	0.30	0.30	0.30	0.59	0.30
Initial water level, m	1150	1150	1150	1150	1150
Effective water depth, m	1.05	1.05	1.05	1.05	1.05
Pressure conditions					
Initial system pressure, MPa	0.25	0.23	0.247	0.23	0.227
Pressure before expl., MPa	1.17	1.9	1.54	0.98 [$]	≈1.30
Explosion period					
Explosion mode, -	triggered	triggered	triggered	No st. expl.	triggered
Compr. of crush. mat., mm	64	319	151	-	46

[§] At the start of melt release; [§§] time between opening and closing of valves 1 and 2, respectively; [$] at the end of the mixing period.

4. DATA ACQUISITION, EVALUATION, AND PRESENTATION

This section is to explain how the data were recorded and evaluated and to help in the assessment of the results presented below.

4.1. Data recording

The ranges of the measuring devices, especially those of the pressure transducers, were preset. A reset/operate order was sent to the Kistler pressure transducer group when the front of the thermite reaction had reached the space immediately above the opening valve. The signals were amplified, typically amounting up to 10 Volt after amplification.

The data were recorded by data loggers, transient recorders and digital tapes. Two sampling frequencies were used in the transient recorders, 25 kHz and 500 kHz. All registration units including the high-speed cameras were synchronized by means of a real-time online clock.

The origin of the time scale in the diagrams presented in this report was defined to agree with the step in a voltage signal that is created when melt is detected at the lower end of the release tube. In that case, the melt destroys a pair of interwoven two-wire cables mounted in the outlet cross-section (GD03/04 sensors in Fig. A2.1).

It should be noted here, and this is a general statement in all ECO tests, that the characteristic step in the melt detector signal, caused by the physical destruction of the detector, is delayed by about 20 ms relative to the first contact of the melt with the detector. This behaviour is supported by findings in the thermocouple readings which are contacted and destroyed by melt.

4.2. Dynamic pressures

The evaluation of the dynamic pressure data occurred by applying the formula: $P = a \cdot U + b$, where U is the measurement in Volt. Here, a is the amplification factor, e.g., 10 MPa/Volt; and b is chosen such that P agrees with the pressure in the test vessel at t = -0.05 s. The latter is obtained by the PK13 and PKr09 measurements for test 01 and tests 02 to 09, respectively.

4.3. Melt release

Knowledge about the time history of melt release is essential for an appropriate numerical simulation of the ECO experiments by a computer code.

Since the rate of melt release could not be measured, it was calculated by an auxiliary numerical model based on a momentum equation that describes liquid flow in a pipe with varying cross sections. Input are the impressed pressure difference and the melt mass to be released (for more details see Appendix A).

A 'leading edge' position is calculated assuming the melt to move as a piston from the start of melt release. The overall results appear to be reasonable as the total amount of melt released that is calculated is normally close to the experimental finding. For this see, e.g., the results in Fig. 5.4.2.

The calculations also help to better estimate the instant of melt through of the steel foil in the first three experiments. In the calculations for these experiments we presume that the process of melt through took some time, i.e. a few to several milliseconds, until the flow of melt occupied the full cross section of the release tube. This means that melt release started with a jet whose diameter was much smaller than that of the tube.

4.4. Evaluation of the void probe and thermocouple signals

The data of the void probes were sampled at a frequency of 25 kHz (this corresponds to a time of 0.04 ms between two inquiries). The data give the actual phase condition at the location of the measuring tip: either zero indicating liquid water or unity indicating steam (or gas). An example is shown in Fig. 4.1 (a).

In the evaluation of the void data, two different kinds of presentation were chosen. In the first way, the instants of the first changes from water to steam, complemented by the axial and radial coordinates of the respective probe, were arranged in a matrix containing three rows which was taken as an input to a small numerical interpolation program. Output are boundaries of the mixing zone to the surrounding bulk of liquid water with the time as a parameter (e.g., see Fig. 5.1.5). The figure allows a quick survey and enables an easy comparison of characteristics in the melt progression observed in the various experiments.

The second kind of presentation gives the local distribution of gas and water in the test vessel for selected times. For this see, e.g., the sequence of graphs in Fig. 5.1.9. Note that the minimum time span between two graphs is 0.2 ms (see the information given in the next paragraph). In a single graph, the void data are placed at the lines' crossings which represent the coordinates of the probes in the axial and radial directions. The data can be interpreted as local actual void, while the information is obtained from all void probes at a given time. A dark point (full circle) indicates water whereas the bright points indicate gas (or steam). An advantage of this kind of presentation is that the actual phase conditions are given also inside the mixing zone.

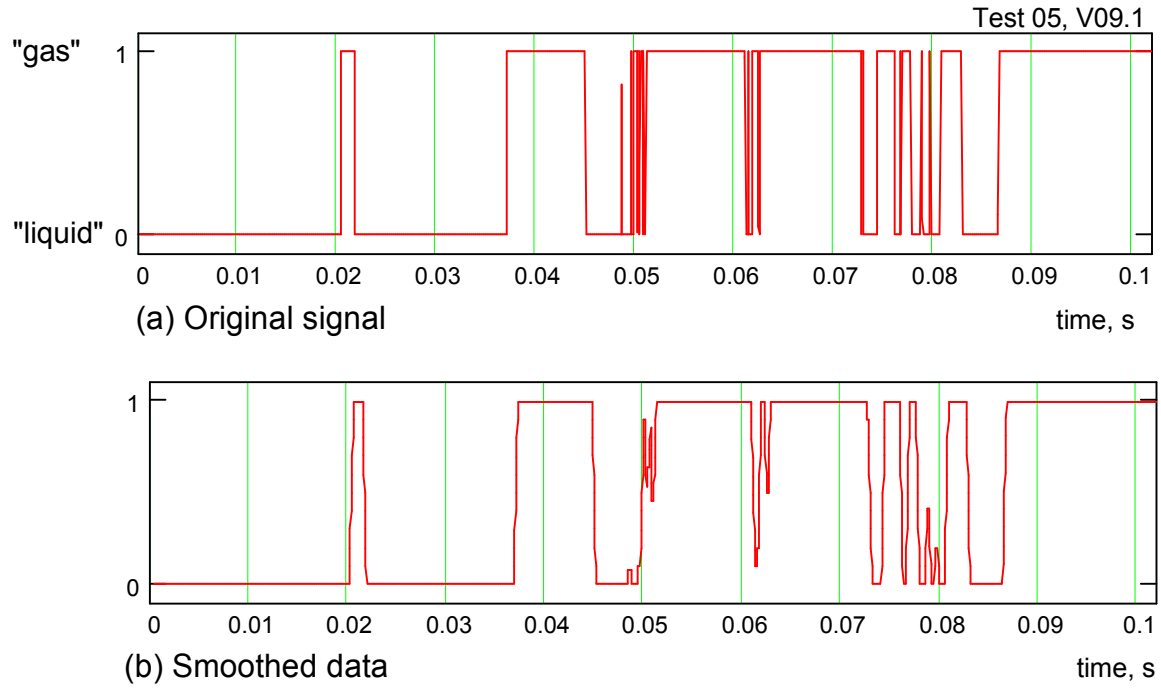

Fig. 4.1 Void signal recorded at 1050 mm level, r = 25 mm, before and after the smoothing procedure.

Information is given in the following on the procedure of void data reduction that was applied in the above second kind of presentation. The changes in phase in the void data occur at a high frequency, such that the duration in either phase is often less than 0.2 ms. To avoid a partial loss of information in the presentation of void re-

sults, e.g. in a sequence of graphs whose time intervals are larger than that of the phase duration, the data were averaged by passing a sliding window of 0.4 ms width (comprising 10 original data) over them. By this “smoothing” procedure (Fig. 4.1 b), data are produced whose numbers are between zero and unity (the related filling of the circles appearing black, grey, or white, cf. Fig. 5.1.9). This means the inclusion of changes in phase that occurred up to 0.2 ms before or after the time chosen.

Summarizing the before said, one must state that the void data give information on the phase condition valid for the very location of the probe. In case of a single probe, there is no immediate information on the spatial extension. In case of a group of neighbouring probes indicating the same kind of phase, however, the existence is probable of a coherent region characterized by a dominating phase.

The information obtained from the void data seems reliable until the instant of steam explosion. This is not true for the time after the steam explosion, i.e., we do not know whether a change in phase, e.g. from gas to liquid, is real or not. This means that the change may be due to a local replacement of water. It might also come from the destruction of the measuring tip by melt contact or by a buckling of the whole measuring lance as a result of the steam explosion. The latter circumstance is illustrated by the photograph in Fig. 4.2 which shows a set of measuring lances after the dismantling of the test vessel.

The thermocouple data primarily help in evaluating the axial progression of the mixing zone in the water. In doing so, one has to keep in mind the slow response time of the thermocouple. This leads to a typical delay in time, e.g. 0.010 s, in case of a fast change to saturation conditions. For this compare the intersection point of the tangents in the T01 signal in Fig. 5.4.3 (b) with the instant of actual change in phase that is immediately indicated by the V01.1 void probe positioned nearby.

Anyhow, depending on the rate of increase, two kinds of information can be gained from the temperature data recorded farther down in the water pool. This is especially true in the tests with the flow divider in which the largest melt penetration rates were observed outside the central region.

Fig. 4.2 Set of the measuring lances used in test 01, after disassembly.

1. A slow increase (e.g. in T06, up to 0.25 s, Fig. 5.5.3 (b)), starting from the level that corresponds to the initial axial temperature profile due to stratification, indicates the relocation of water somewhere above resulting from the expansion of the mixing zone. Note that the expansion occurs in the axial as well as in the radial direction.

2. A steep, enduring increase in temperature (T06 after 0.26 s) indicates the immediate approach and passage of the boundary of the mixing zone.

An example is touched on here regarding the instants of characteristic temperature increases, that were used in the various graphs showing the melt penetration, by referring again to Fig. 5.4.3 (b). As outlined above, the T01 characteristic time is delayed compared to the change in the void signal. Instead, we generally used the instant when the steep temperature increase started; this is, e.g., 0.127 s in T01.

4.5. Evaluation of the energy conversion

Remarks

The energy conversion that we measure with the crushing material is a lower limit. First, there is more mechanical energy released within the test vessel that is not transferred to the crushing material. Second, the force required to compress the crushing material depends to some extent on the deformation velocity (see Appendix B). Under the conditions of the tests, a variation range of ± 10 % may be possible. Furthermore, there are energy losses due to friction and leakages. The actual test design represents a compromise between these two.

Still, ripping the piston loose from its initial position (e.g. the gas tight seal) will provoke some energy loss as does the further friction. Similarly, there are leakage paths along the gap between piston and cylinder and also through equipment (like the void probe plugs) that do not fully withstand the enormous pressures and become defective. These latter losses are difficult to quantify.

Mechanical work determined from the crushing material

The mechanical work, W, set free outside of the test vessel can properly be determined only from the deformation, L, of the crushing material (abbreviated: CM in the following) in conjunction with the force of deformation. For this see the special excursion into this question in Section 5.2. The work connected to the deformation is calculated by

$$W = \Sigma\, F_i\, L_i, \qquad (1)$$

where $F_i = \sigma_{CM}\, A_{CM}$, i is the (constant) force necessary to compress layer i (e.g., layers i = 1 ... 5 in test 05). $A_{CM,i}$ and σ_{CM} are the area of layer i and its strength, respectively. For the latter, an average value of σ = 23.8 N/mm^2 (see Table B.2) was used. The L_i sub-sections are the lengths of compression found in the various layers.

The energy conversion factor used in this report is defined as

$$\eta = W/Q. \qquad (2)$$

It should be noted here that in test 01 to test 03, no permanent deformation was obtained. The maxima of elastic deformation were 2 ... 4 millimetres. In these cases, the work is calculated using the equation $W = ½\, F_1 \cdot L$ instead of eq. (1). For F_1 see Table B.3. To account for such small deformations in the evaluation and to check the strength of the crushing materials under static and dynamic conditions, calibration tests were performed. Results are given in Appendix B.

The heat content,

$$Q = m\, h, \qquad (3)$$

is the product of the melt mass and its specific enthalpy. We do not know the part of the melt that is actually involved in the steam explosion. Therefore, the whole mass of melt released is taken into account in eq. (3). In this final report, we take for the enthalpy a value of 3.8 MJ/kg, following the result of intense investigations on the heat content of alumina melt mixtures /12/. The above value is the difference in the enthalpies of the melt at the initial and boiling temperatures of water 2600 K and 373 K, respectively. Heat losses during mixing are not taken into account.

Kinetic energy put into the acceleration of masses

1. Test vessel

The mass of the empty vessel is m_{ves} = 2700 kg. The movement of the vessel is given by the L measurement. The equation for the force accelerating the vessel reads

$$F_{acc,\,ves} = m_{ves} \cdot dv/dt, \tag{4}$$

where v = dL/dt. The work is calculated by

$$E_{kin,\,ves} = \int F_{acc,\,ves}\, dL = m_{ves} \int v\, (dv/dt)\, dt. \tag{5}$$

2. Water column

It is assumed that part of the water located above the height, where the steam explosion started, is accelerated in upward direction.

The kinetic energy of this water is calculated by

$$E_{kin,\,wat} = \int F_{acc,\,wat}\, v_{wat}\, dt, \tag{6}$$

where $F_{acc,\,wat} = \Delta p_{wat}\, A_v$ is the force acting from below on the water column considered, Δp_{wat} is the pressure difference measured across the water column, A_v is the vessel cross section. On the other hand, the acceleration force is given by

$$F_{acc,\,wat} = m_{wat} \cdot dv_{wat}/dt, \tag{7}$$

The average axial speed of the water, v_{wat} , is calculated by integration over time from the equation

$$dv_{wat} = 1/(\rho_{wat}\, H_{wat})\, \Delta p_{wat}\, dt, \tag{8}$$

the mass of the water from

$$m_{wat} = \rho_{wat}\, H_{wat}\, A_v, \tag{9}$$

where H_{wat}, is the height of the water column.

Remark: The values for the kinetic energy turned out to be comparatively low. Numbers are given, e.g., at the end of the test 05 results.

4.6. Calculation of the melt-to-water mass ratio

In the Summary section, the melt-to water mass ratio is taken as a parameter that is suitable in the evaluation of the energy conversion measured in the ECO tests. This ratio is calculated, with the exception of test 03, for each test in Chapter 5. The melt mass is considered as the one released into the water pool.

The water mass is considered as the one within the radial enclosure, given by the full vessel diameter for tests 01 to 03 and by the restriction tube for tests 04, 05, 06, and 09, respectively, and within an axial length extending from the initial water level down to a level range that is indicated in Table 6.2. The upper limit of this range is gained by extrapolating the penetration data to the time of triggering (cf. Fig. 6.3). The lower one is inferred from the overall evidence, e.g. the height of the pressure transducer that indicates the start of steam explosion.

4.7. Error calculation

To get an idea of the scattering of the conversion factor calculated, the errors of the data used in the calculations were estimated and the total error was calculated.

The single errors are:

- Mass of melt released,

Test 01 to 04 Δm: ± 0.1 kg
Test 05 to 09 Δm: ± 0.4 kg

- Enthalpie of the melt based on an accuracy of the melt temperature of ±50 K,

Δh: ± 0.1 MJ/kg

- Deformation length of the crushing material,

$L \leq 40$ mm ΔL: ± 1 mm
$L \geq 40$ mm ΔL: ± 2 mm

- Strength of the crushing material during deformation,

$\Delta \sigma$: ± 10 % of σ

The total error is calculated as the sum of the squared relative single errors. The results are:

Test 01 and 02 $\Delta \eta$: ± 28 % of η
Test 04 to 09 $\Delta \eta$: ± 12 % of η

The larger value in tests 01 and 02 comes from the very small, absolute deformations of the crushing material.

4.8. Post-test examination

If still possible, the complete water and melt inventory inside the test vessel was drained through narrow filters after the experiment to collect all the debris. After drying, the mass was weighed. A sieve analysis gave the size distribution of the melt particles.

4.9. Software used to produce the diagrams

The diagrams in cartesian coordinates were made using the “TechPlot für Windows 3.1.6” software; © Software für Forschung und Technik, 38102 Braunschweig, Germany.

The graphs showing the melt penetration mode (local distribution of steam and water at increasing times) were produced using the “Mathcad, Version 11.0b” software; © Mathsoft Engineering & Education, Inc.

5. EXPERIMENTAL RESULTS

General remarks

In this chapter, the results of ECO-01 to ECO-09 are presented in chronological order. By this, improvements achieved can be easily identified. Main emphasis is laid on presenting the results of ECO-04 to ECO-09. Starting with ECO-01, typical results are discussed in more detail.

5.1. Results of ECO-01

Course of events

Taking the first maximum of the melt generator pressure (GP12 in Fig. 5.1.1) as an indication, we presume that melt through of the steel foil and with it the melt release started at around -0.05 s. The pressure difference was 0.26 MPa.

It is further assumed that the melt release started with a thin jet whose diameter was much smaller than the tube diameter. Probably, the process of melt through took some time, several up to a few tens of milliseconds, until the flow of melt occupied the full cross section of the tube.

The pressure in the test vessel (PK13) began to rise at a slow rate soon after the start of melt release. The first melt/water contact took place at 0.0065 s, indicated by the V10.1 void signal. This event launched a stronger pressure rise in the test vessel.

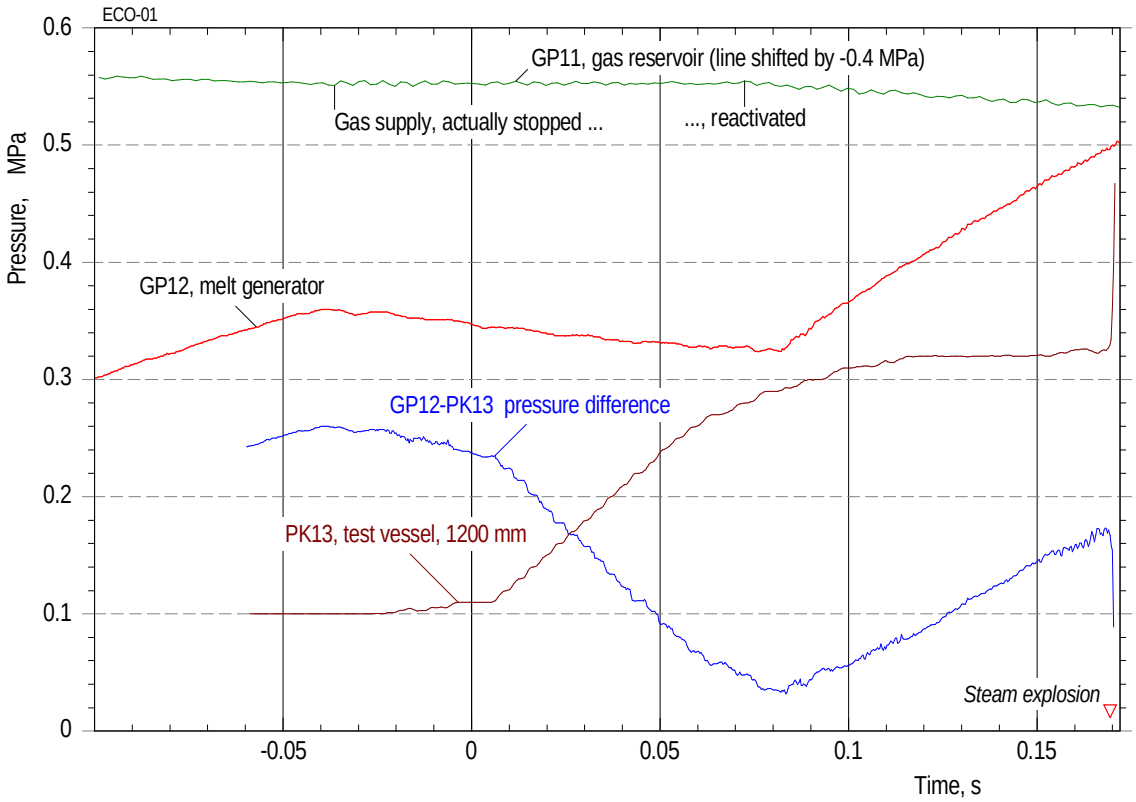

Fig. 5.1.1 ECO-01. Time history of pressures that determined the melt release.

In the calculation which was started at -0.05 s (Fig. 5.1.2), the melt front reached the water surface at 0.027 s. This is later than the measurements indicate. The maximum speed of the melt front in the calculation is 9.1 m/s. To be consistent with the measurements, the average speed should have been about 10 m/s. We assume that: (a) melting through of the steel foil took some time, about 15 ms (cf. Appendix A.4);

(b) at least some portion of melt must have moved faster than the average mass, within the release tube and also through the gas space. The larger speed of the melt front may be caused by the expansion of some gas within the melt.

The rate of melt penetration in the water, indicated by the void and temperature data, is lower than the above speeds, namely about 7 - 5 m/s (cf. Fig. 6.3). This reduction in speed is a general finding in our tests, namely that the speed of the leading edge of the melt is decelerated on penetration in the water.

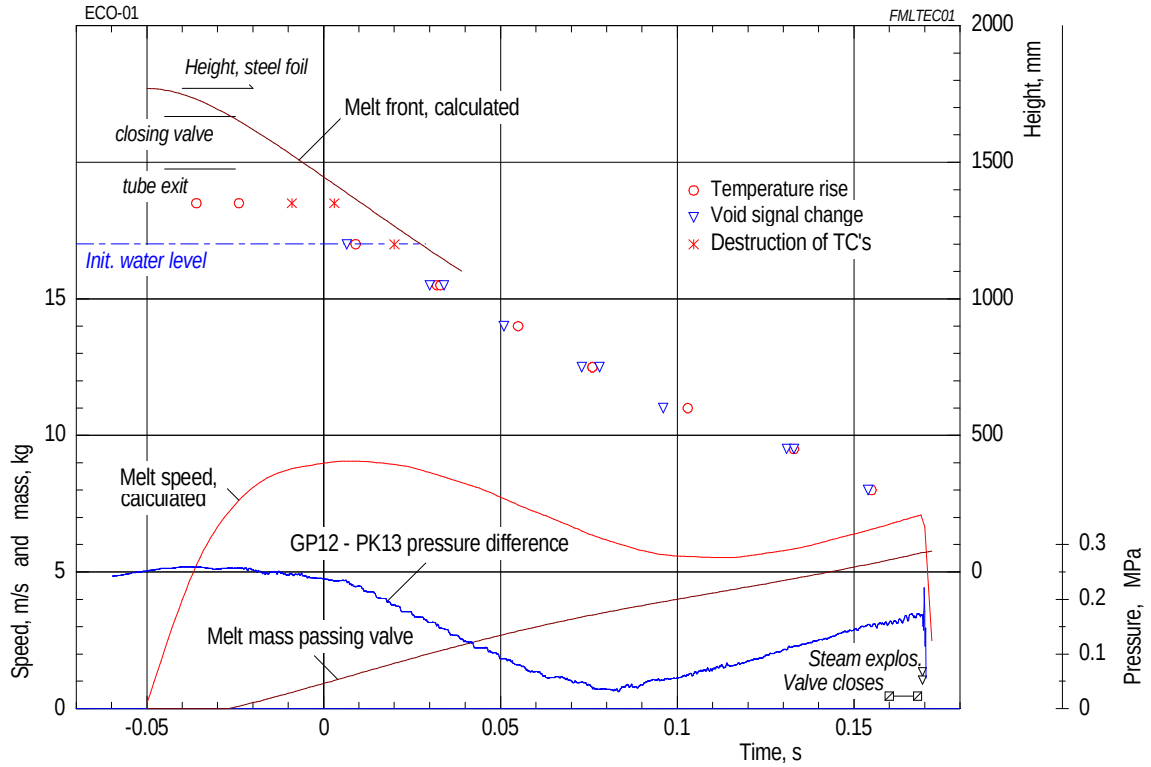

Fig. 5.1.2 ECO-01. Melt release and melt penetration, illustrated by calculated and measured data.

After the first melt/water contact, the pressure in the test vessel increased markedly over an interval of about 0.1 s. Feeding gas from the reservoir into the melt generator atmosphere prevented the pressure difference from becoming negative. The reason for the marked pressure increase is not yet clear. Instead, a rather small initial pressure increase had been anticipated since the steam production took place in highly subcooled water. (See also the Discussion section).

The melt release was terminated by closing the slide valve when the melt front had reached the lowermost measuring lance (criterion no 1). The slide valve was closed at 0.168 s. Immediately after that, the trigger capsule was ignited.

At the time of triggering, the pressure in the test vessel had reached a value of 0.325 MPa (Fig. 5.1.1) while a total mass of melt of 5.76 kg had been released. The latter value corresponds to an average rate of 31 kg/s.

Mixing period

The rate of melt penetration in the axial direction can well be followed by the times of temperature increases. More gentle increases indicate the approach of the mixing zone, whereas steep temperature increases are an indication of the destruction of the thermocouple by the melt. For the latter see, e.g., the T10 and T09 signals in

Fig. 5.1.3, (a) and (b). On the other hand, limited increases occur in the signals of two of the three thermocouples positioned in the lowermost part (see T03 and T02, same figure). It seems that both instruments have not been affected by melt attack.

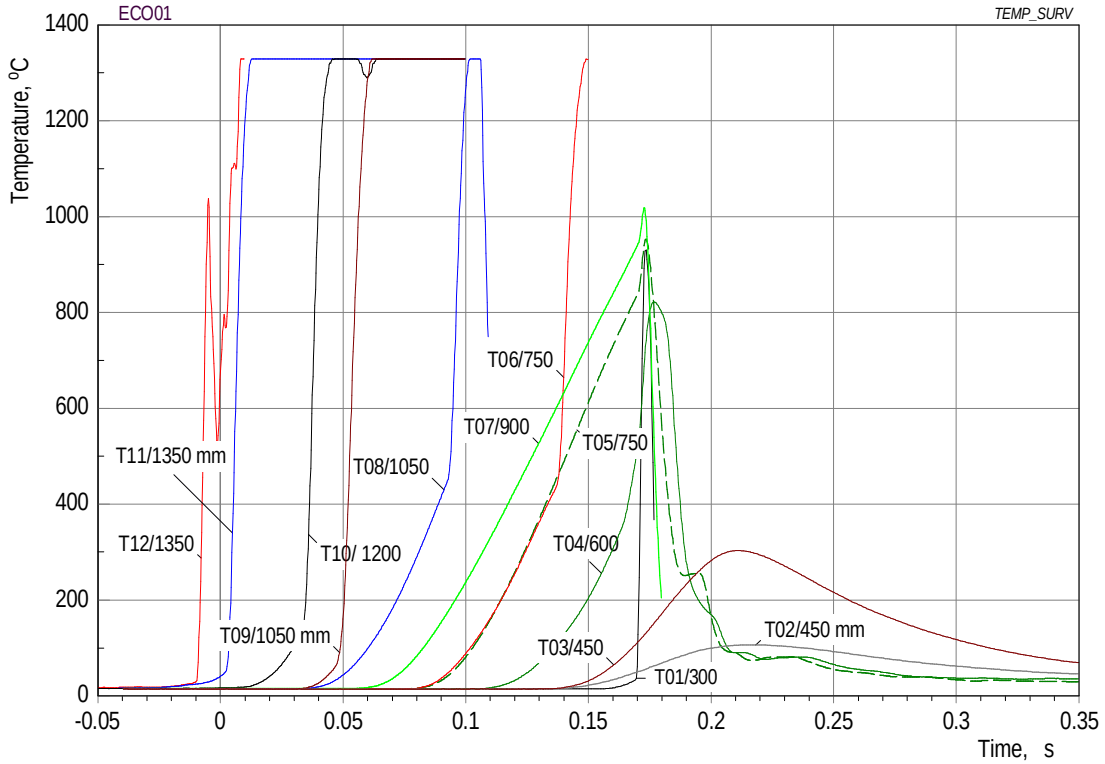

(a) Survey

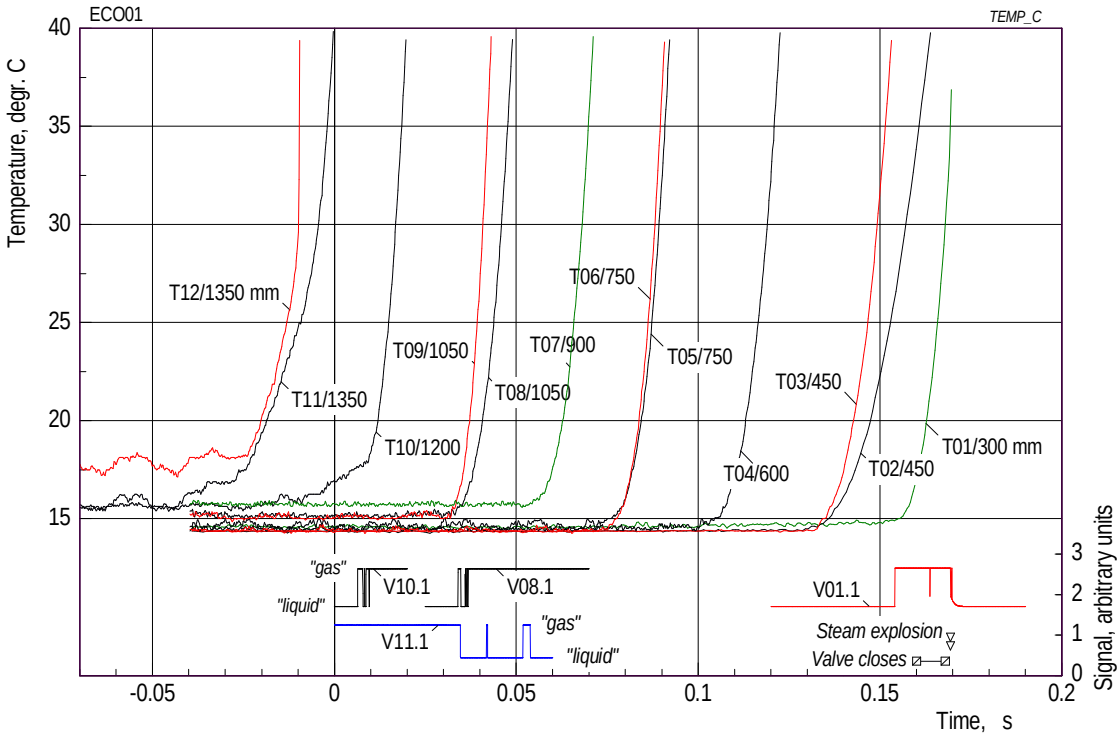

(b) Enlarged scales

Fig. 5.1.3 ECO-01. Time histories of the temperature measurements shown in different scales, complemented by a couple of void and event data.

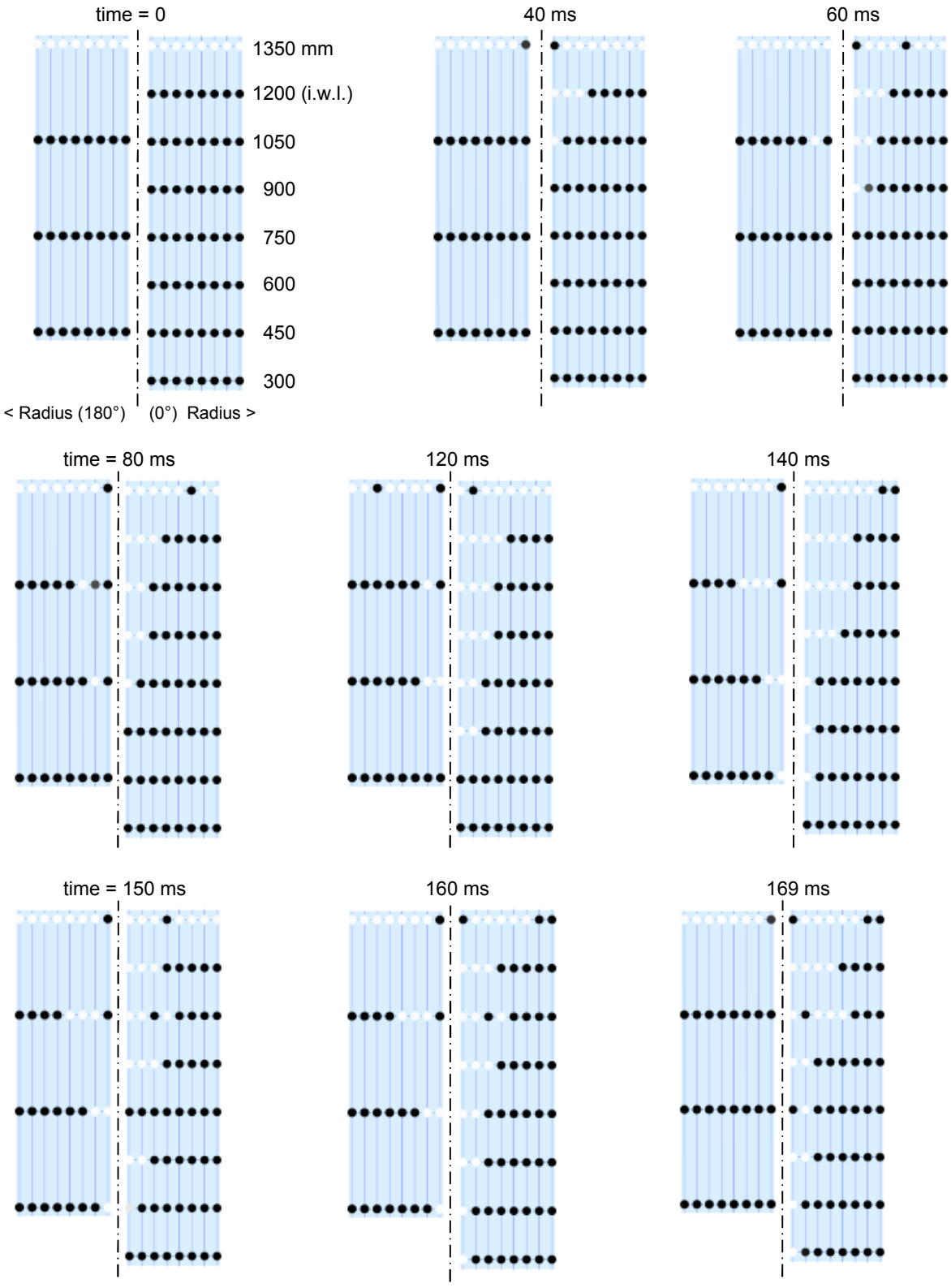

Fig. 5.1.4 ECO-01. Melt penetration mode illustrated by the local distribution of steam and water at increasing times.
The initial water level (i.w.l.) was at 1200 mm. The grid crossing points mark the locations of the void probes. Water is represented by dark points, steam by bright ones (see also caption of Fig. 5.1.9). The steam explosion started at 0.1693 s.

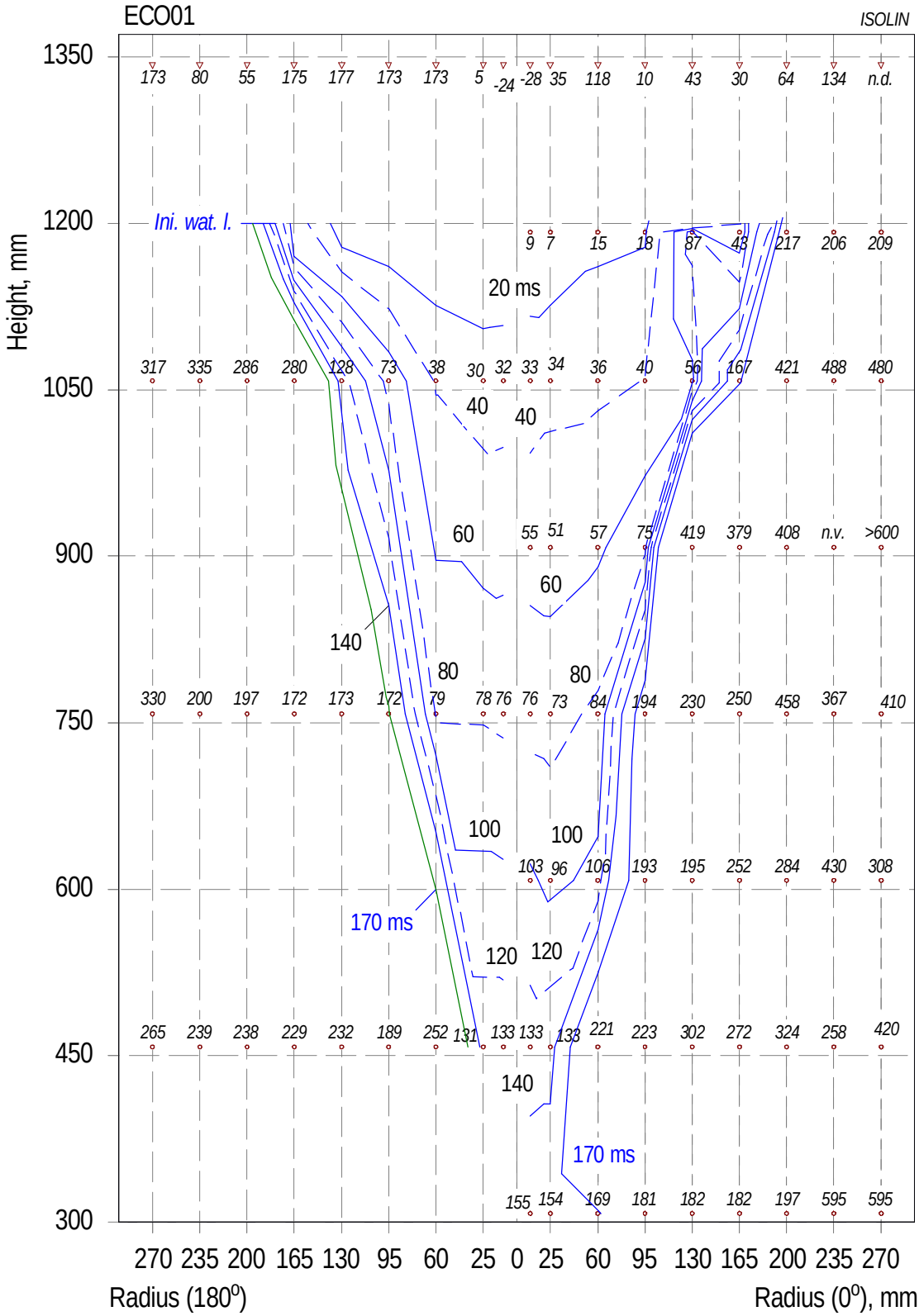

Fig. 5.1.5 ECO-01. Melt penetration in the water with the time as a parameter. Numbers in ms give the instants of first changes in the void signals. Temperature data (at 10 mm radius) denote the starting points of first steep increases. The lines represent the outmost boundaries of the mixing zone against the bulk of water. n.v. means: no void detected within 1.5 s; n.d.: no data available. The steam explosion started at 0.1693 s.

The progression of the mixing zone in the axial and radial directions can easily be followed in Figs. 5.1.4 and 5.1.5. The local distribution of steam and water in the pool at distinct times before and at the steam explosion is depicted in Fig. 5.1.4. The series of graphs gives, if one concentrates upon the bright points, an impression of the progression of the mixing zone in the axial and radial directions. Sporadic liquid points within the field of steam points give an approximate idea of how much liquid is within the interaction zone.

Another piece of information can be gained from the graphs in this figure: The bulk of water surrounding the mixing zone is relocated in the radial and axial directions by the steam production. This action results in an increase of the water level indicated by changes in the void data from steam to liquid (see Fig. 5.1.4, 1350 mm height, time = 140 to 169 ms).

Figure 5.1.5 shows the progression of the mixing zone with the time as a parameter. The lines, which were obtained by interpolation, give the boundaries of the multiphase mixing zone to the bulk of water. The family of lines shows the formation of a narrow mixing channel. Presumably, the slim shape is due to two conditions:

(1) The large amount of water subcooling. Generally, the steam produced under such conditions condenses largely in situ.

(2) The comparatively large speed of axial melt penetration. A value of 7 ... 5 m/s can be derived from the indications of steam drawn in Fig. 5.1.2.

The level, down to which melt penetrated in the water, is determined to be 200 mm. This value is obtained by extrapolating void signal and temperature characteristics (cf. Fig. 6.3). The effective volume of water available for mixing is 0.273 m^3. The melt-to-water mass ratio, based on a melt mass of 5.76 kg, is 0.021. This number has been listed in Table 6.2 and was used in the design of Fig. 6.2.

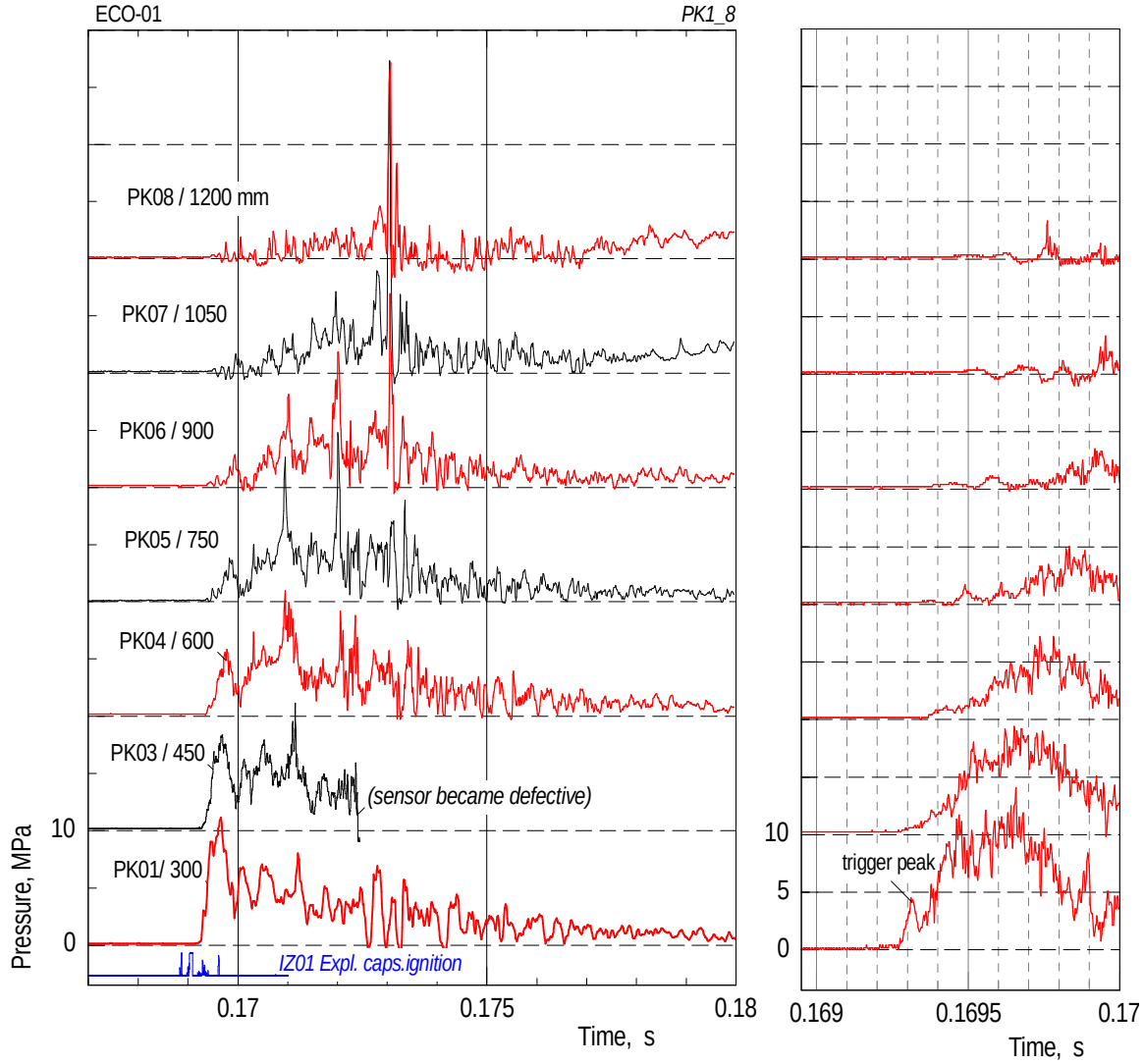

(a) Survey (b) Initial phase

Fig. 5.1.6 ECO-01. Signals of the piezo type pressure transducers located in the 60° azimuthal direction.
The labels give the axial height in mm. The data in graph (a) have been smoothed for a better visibility, those in graph (b) were plotted with the original sampling frequency of 500 kHz.

The steam explosion event

The steam explosion produced highly transient processes with peak pressures up to 12 MPa and a duration of one millisecond (Fig. 5.1.6). The figure shows in a survey the dynamic pressures measured at the inner surface of the test vessel. The steam explosion started in the bottom of the water pool, and the initial pressure peak propagated in the upward direction losing in magnitude.

At first sight, we state that no strong, coherently propagating steam explosion occurred in test 01 but a sequence of several pressure events. The pressures following the first peak pressure are attributed to smaller local steam explosion events resulting from energetic interactions of that part of the melt that later entered the mixing zone. Note that after closure of the slide valve, residual melt may have entered the mixing zone for another 0.020 s. The very sharp peaks at 0.173 s, amounting to 29 MPa in the PK07 signal, are ascribed to a water hammer taking place underneath

the bottom of the melt generator case. (As for the latter event compare the finding achieved below on discussing the water level rise.)

During the evaluation of test 01, more information was required about how the steam explosion was initiated. For this, calibration tests were performed to separate the trigger pressure (coming from the explosion capsule) from the actual pressure event. These tests showed (cf. Fig. 5.1.7) that only a very initial, narrow peak, generally amounting to 4 ... 7 MPa and lasting around 100 µs, was due to the trigger pressure. In test 01 (Fig. 5.1.6), this peak moved upwards, dying out with increasing distance from the bottom. A speed of 2500 m/s is obtained taking the maxima of the first peaks measured at the 300 ... 750 mm levels. This value corresponds better to the sonic speed in steel than to that in water.

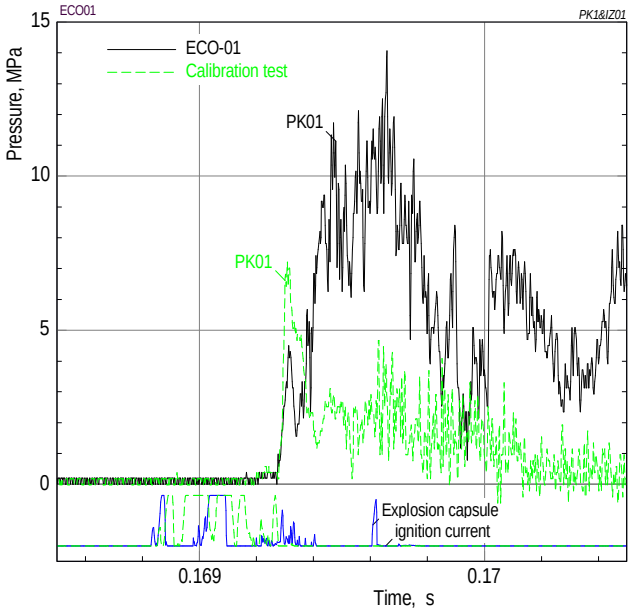

Fig. 5.1.7 ECO-01. Coherence between the ignition of the explosion capsule, the trigger pressure, and the start of the actual steam explosion.

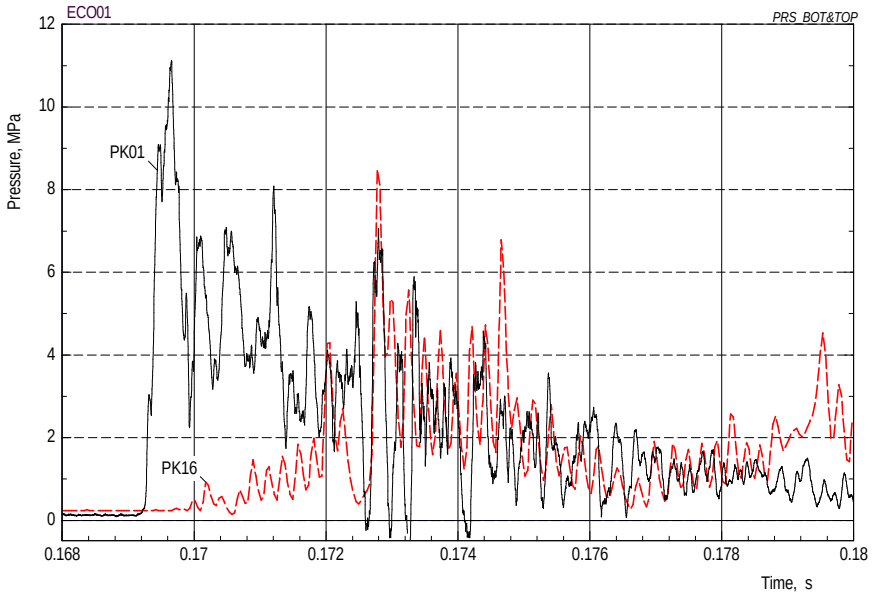

Fig. 5.1.8 ECO-01. Pressures measured at the bottom (PK01) and the top (PKu16) of the water pool.

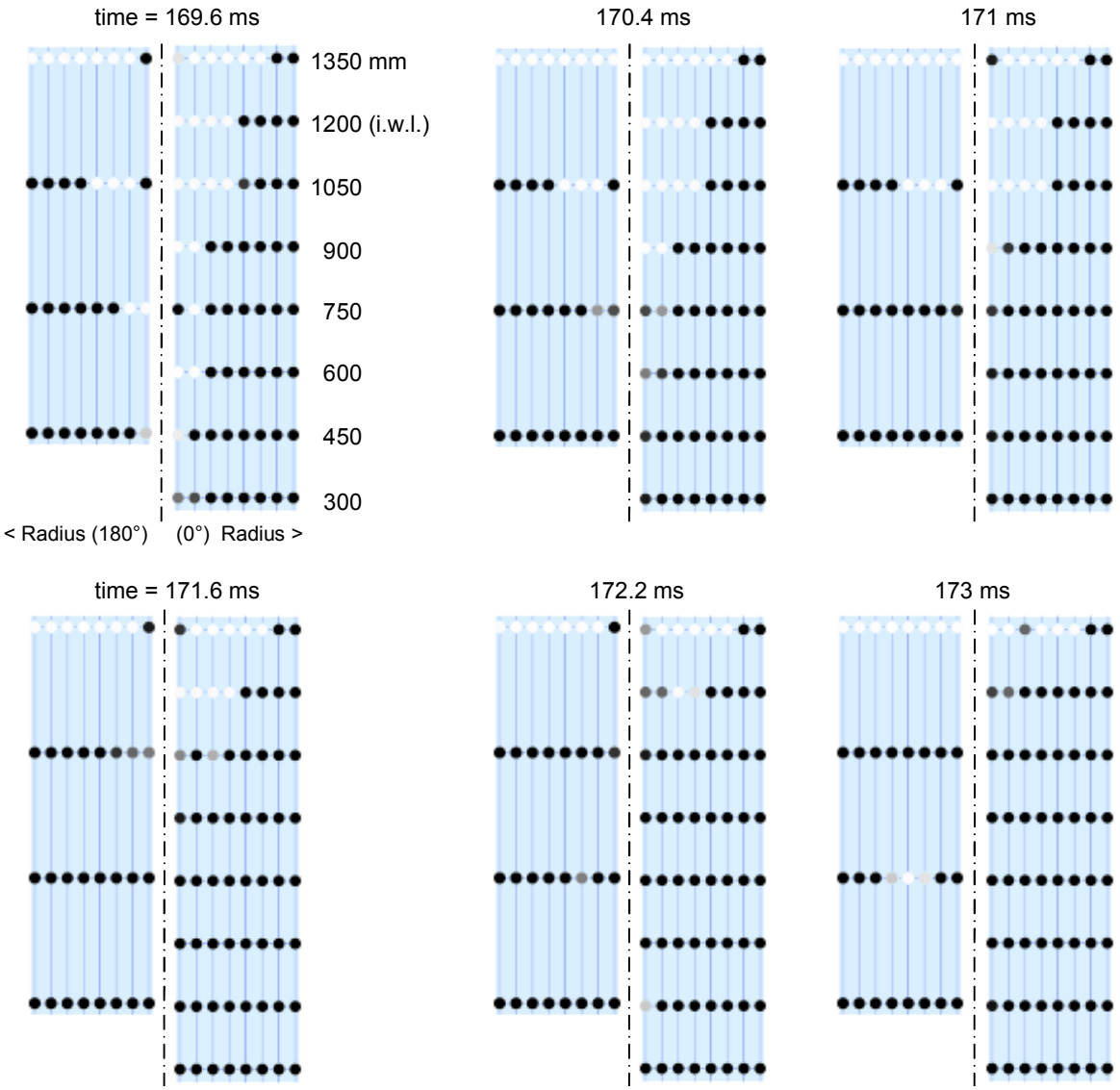

Fig. 5.1.9 ECO-01. Change of the steam/water distribution immediately after the steam explosion (169.3 ms).
Water and steam are represented by dark and bright points, respectively. Grey points indicate there was steam (respectively water) immediately before or after the point in time chosen (cf. Section 4.4).

Anticipating the evaluation of energy conversion (see below), pressures measured in the bottom and uppermost parts of the pool, respectively, have been plotted in a larger time scale in Fig. 5.1.8. The differences that can be seen in the times of first increase as well as in the magnitude of the peak pressures are attributed to the acceleration of part of the water in the upward direction.

An attempt was made to find the effect of the rapid vaporization and with it the movement of water in the graphs showing the distribution of void. For this, another six graphs are shown in Fig. 5.1.9 extending those in Fig. 5.1.4. In this presentation one has to consider, as discussed in Section 4.4, that some of the measuring lances and with them some of the void probes might have been displaced by the force of explosion.

As one can see, most of the void probes located in the centre show changes from steam to water within 2 ms (0.1696 to 0.1716 s), whereas a rise in the water level is

indicated by the changes in the signals of the four innermost probes, level 1200 mm, at 0.173 s.

Evaluation of the mechanical work and energy conversion

The mechanical work in test 01 (as well as in the later tests 02 and 03) and with it the energy conversion factor turned out to be very small. Nonetheless, as the measuring instruments worked well and the data are precise and consistent, it is worth while to analyse in this test the force and displacement time histories, respectively. Eventually, the mechanical work in all tests was calculated on basis of the displacement measurement as depicted in Fig. 5.1.10.

The piston began to move already during the premixing period, at 0.025 s. The pressure in the vessel had started to rise markedly 20 ms before (PK13 in Fig. 5.1.1). The displacement reached a value of one millimetre at the end of the premixing period. A first maximum of 5 mm was reached 11 ms after the start of explosion. After that, the deformation data oscillated ending with a permanent value of one millimetre.

The lower graph in Fig. 5.1.10 gives principal information about the time history of the essential forces resulting from the steam explosion. Complementing the statements made in Section 4.5, the discussion of the forces drawn in Fig. 5.1.10 (b) will show that the mechanical energy set free in ECO can be determined reliably only from the deformation of the crushing material.

The DMS forces were evaluated from the strain gauges mounted at the six supporting columns (Fig. 2.1). The PK01 and PK08 forces were obtained by multiplying the pressure data with the cross section area of the test vessel.

The shift in phase between F_{PK01} and F_{PK08} is due to the acceleration of the water above the level of 0.3 m (where the steam explosion probably started). There is another shift between two forces, namely between the F_{PK08} and F_{DMS} forces. The first one, F_{PK08}, is considered to be typical of the (areal) force which is passed into the "cylinder" via the bottom of the melt generator. The second one, F_{DMS}, which indicates the reaction force in the supporting columns, is delayed by about one millisecond.

These examples show that the steam explosion processes are both complex and highly transient. This means that the pressure and DMS forces, respectively, occur locally and temporally. Both forces can not be used for a proper calculation of the mechanical work.

The displacement measurement (Fig. 5.1.10 a) shows an oscillating behaviour. At the end of the mixing period, i.e. prior to the steam explosion, the deformation was one millimetre. The first maximum of the displacement, 5 mm, was reached 10 ms after the start of the explosion. The deformation of the crushing material obviously remained in the elastic range; no permanent deformation was measured.

Calibration tests with the crushing material (see Appendix B) showed that the plastic deformation starts after a limit of about 4 mm has been reached. This means that the force necessary to permanently deform layer 1 had just been reached in test 01 and the characteristic property value of 2.428 MN applies.

Considering the (elastic) deformation of 4 mm, the work is calculated by the equation $W = ½ \cdot F_1 \cdot L$ (cf. Section 4.5), or

$W = 0.5 \cdot 2.428\ \text{MN} \cdot 0.004\ \text{m} = 4.9 \cdot 10^{-3}\ \text{MJ}$.

The melt mass gives a thermal energy of $Q = 5.76\ \text{kg} \cdot 3.8\ \text{MJ/kg} = 21.9\ \text{MJ}$.

The energy conversion factor is $\eta = 0.022\ \%$.

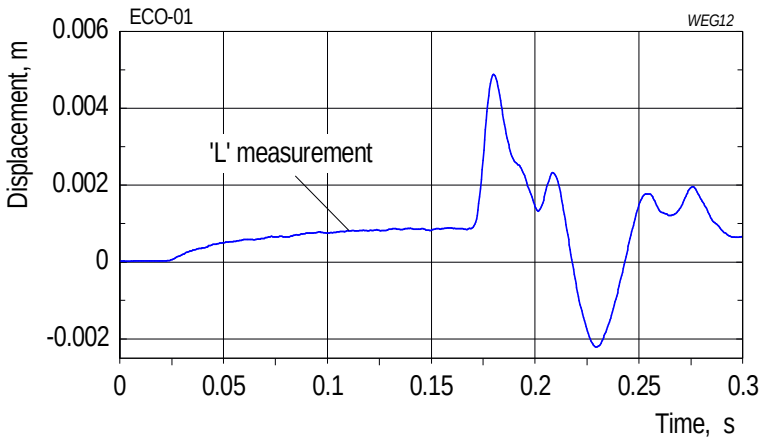

(a) Survey (long time)

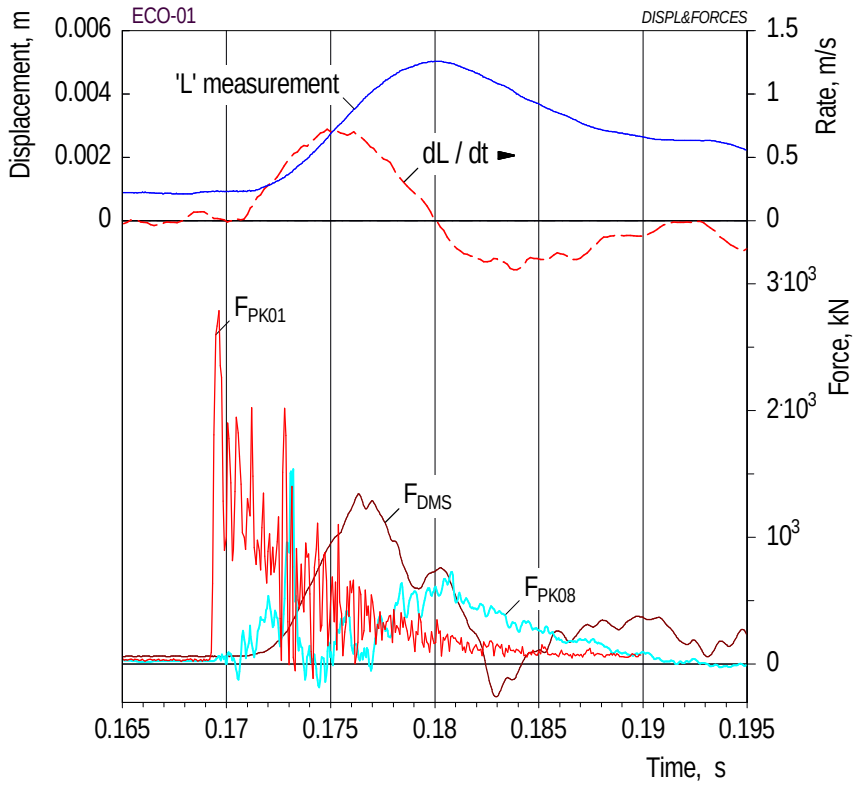

(b) Explosion phase

Fig. 5.1.10 ECO-01. Various measurements resulting from the steam explosion: The displacement of the piston, L, forces derived from the PK01 and PK08 pressures, and the DMS forces in the supporting columns.

Post test examinations

An important finding in test 01 is that the overwhelming portion of the injected mass was finely fragmented (Fig. 5.1.11). The largest portion of the mass was found in the particle size between 0.2 mm and 0.32 mm. This particle size distribution and the small amount of large particles are typical of a steam explosion.

The comparison shows larger particle sizes for the PREMIX test; these are typical of a long-term quenching process. (Note that the PM18 test was performed with a smaller amount of water subcooling and no explosion trigger was applied).

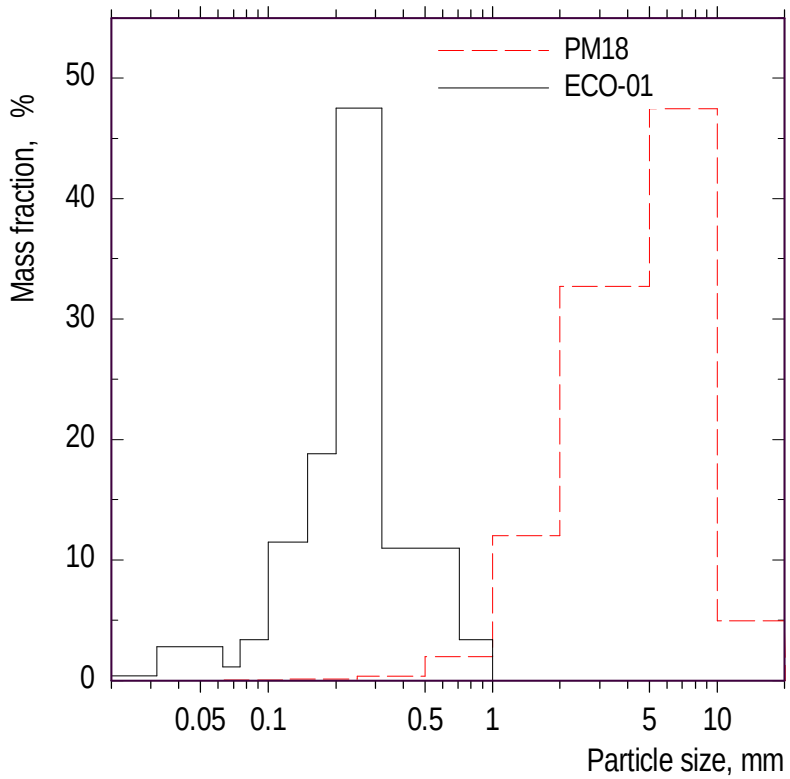

Fig. 5.1.11 ECO-01. Post-test particle size distribution. Comparison is made with the PM18 PREMIX experiment (without steam explosion).

5.2. Results of ECO-02

Objectives in brief

The major aim of test 02 was to obtain a larger amount of melt released into the water before the explosion was trigged. From there, the following conditions have been changed (see also the related comments in Section 3):

The 10-kg type melt generator was replaced by the 20-kg type one (cf. Fig. A2.1). The larger melt generator was able to supply up to 18 kg of melt; besides, it had a larger release tube diameter.

The gas space overlying the water pool was kept open to the environment during premixing. Its volume was increased by reducing the initial water level by 50 mm. To diminish the speed of the melt released, the driving pressure was reduced.

Course of events

On basis of the GP12 pressure time history (here: the first local maximum at about −0.180 s, see Fig. 5.2.1), we presume that melt-through of the steel foil started at the time of −0.180 s. The actual initial pressure difference was 0.1 MPa.

The reduced driving pressure resulted in a lower speed of melt and by it in a larger time interval between melt through of the steel foil and start of melt penetration. A melt speed of 6 m/s was obtained in the calculation (Fig. 5.2.2) which was started at the time of −0.120 s. To obtain the actual average melt release rate (11.2 kg/s, see Table 3), a smaller constant jet diameter of 30 mm was assumed in the calculation.

Because of the openings, the pressure in the test vessel did not increase during the mixing phase (Fig. 5.2.1). On the other side, the rate of pressure decrease in the melt generator was as low as anticipated (0.06 MPa/s), so that the gas supply was activated only once, at 0.181 s.

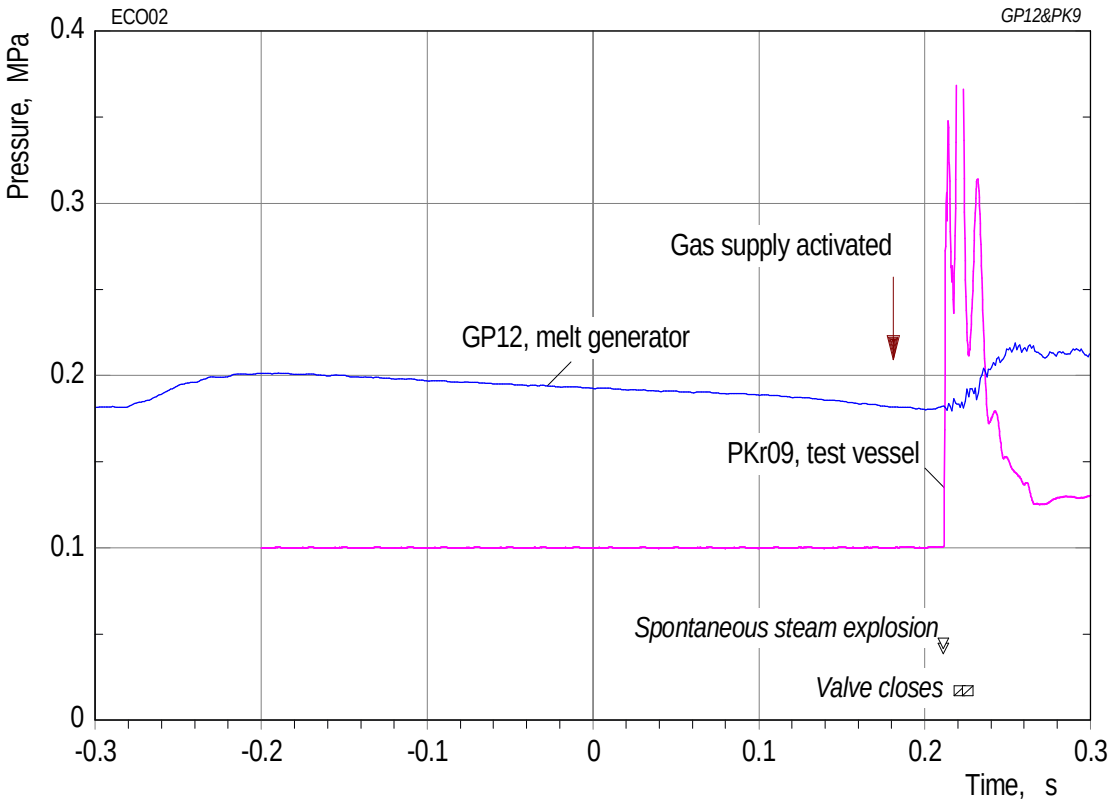

Fig. 5.2.1 ECO-02. Time history of pressures that determined the melt release.

Soon after that action, the premixing phase in test 02 was terminated by an unintended spontaneous steam explosion evidenced by a steep increase in the PKr09 pressure (Fig. 5.2.1, at 0.2117 s). By this, condition (2) of the operation control criteria (Section 2.2, page 8) was fulfilled. Consequently, the valves of melt release and test vessel venting, respectively, were closed with a delay of 10 – 15 milliseconds.

The melt had not penetrated far into the water until the instant of the explosion. For this see the void and temperature characteristics shown in Fig. 5.2.2. A total mass of melt of 2.87 kg had been released. This value gives an average release rate of 11.2 kg/s, compared to 28.5 kg/s in test 01.

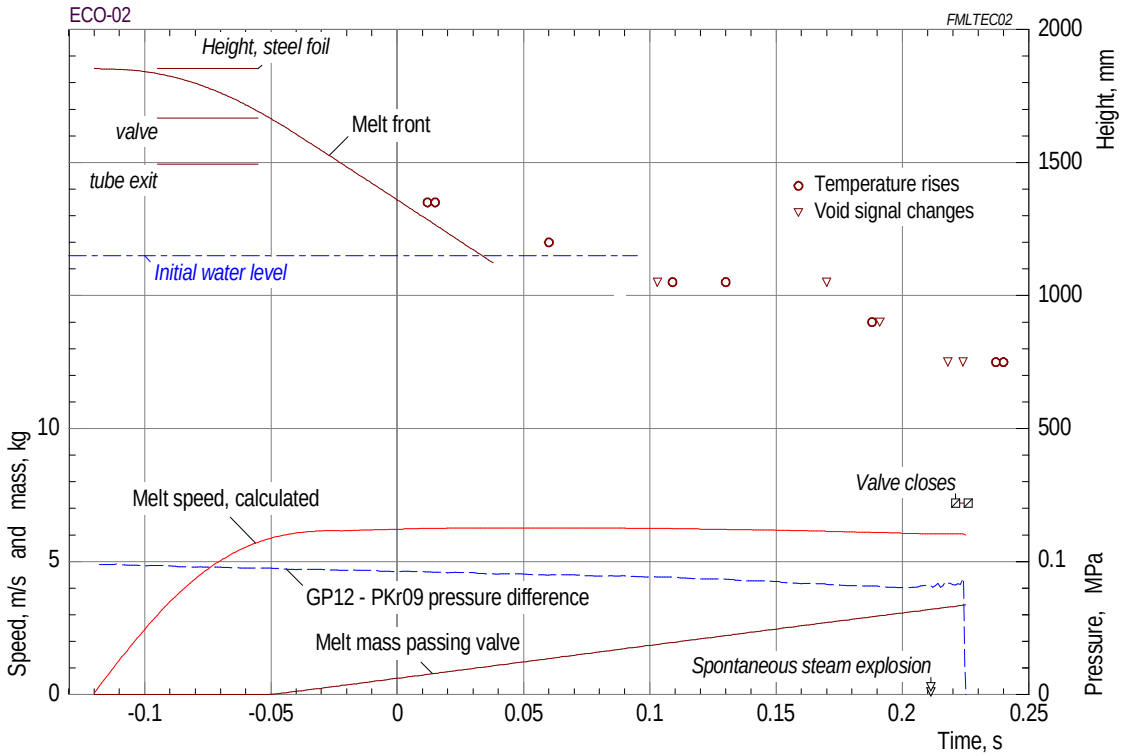

Fig. 5.2.2 ECO-02. Melt release and melt penetration, illustrated by calculated and measured data.

Mixing period

The time history of melt penetration in the axial direction can be followed by the times of temperature increases (Fig. 5.2.3). As mentioned, the distance of melt penetration into the water was small. A lower level of 800 mm was estimated by extrapolation (see Fig. 6.3 and Table 6.2).

Figure 5.2.4 shows local distributions of steam and water in the axial and radial directions at selected times up to and immediately after the steam explosion, respectively. Two interesting findings can be gained from these graphs:

1. Steam is indicated in the water only sporadically.

2. Small quantities of water are detected above the initial water level close to the vessel axis at 1200 and 1350 mm height, respectively. Larger quantities appear only after the steam explosion.

Figure 5.2.5 shows the progression of the mixing zone with the time as a parameter. The lines give the boundaries of the multiphase mixing zone to the bulk of water. Only a few lines can be drawn for times ≤ 211 ms, since the number of void probes concerned is small. This means that the mixing zone that had been formed at the

time of explosion is comparatively small. (The lines for times > 211 ms are discussed in the next section).

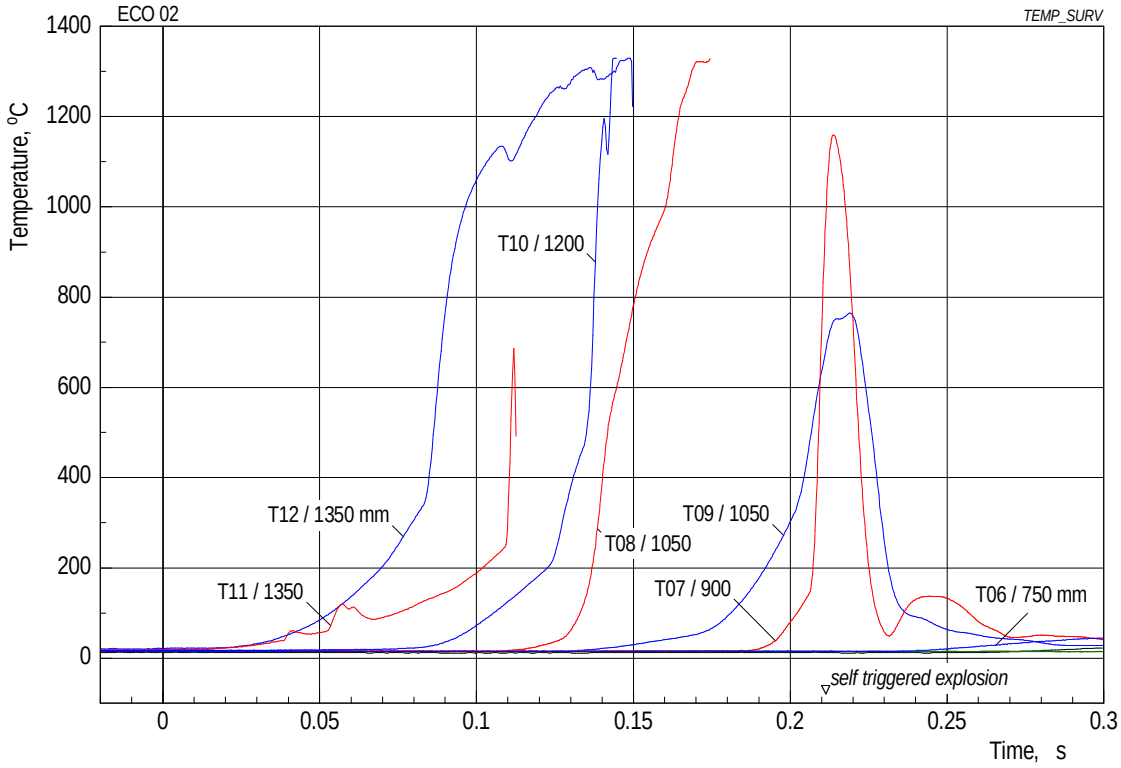

(a) Survey

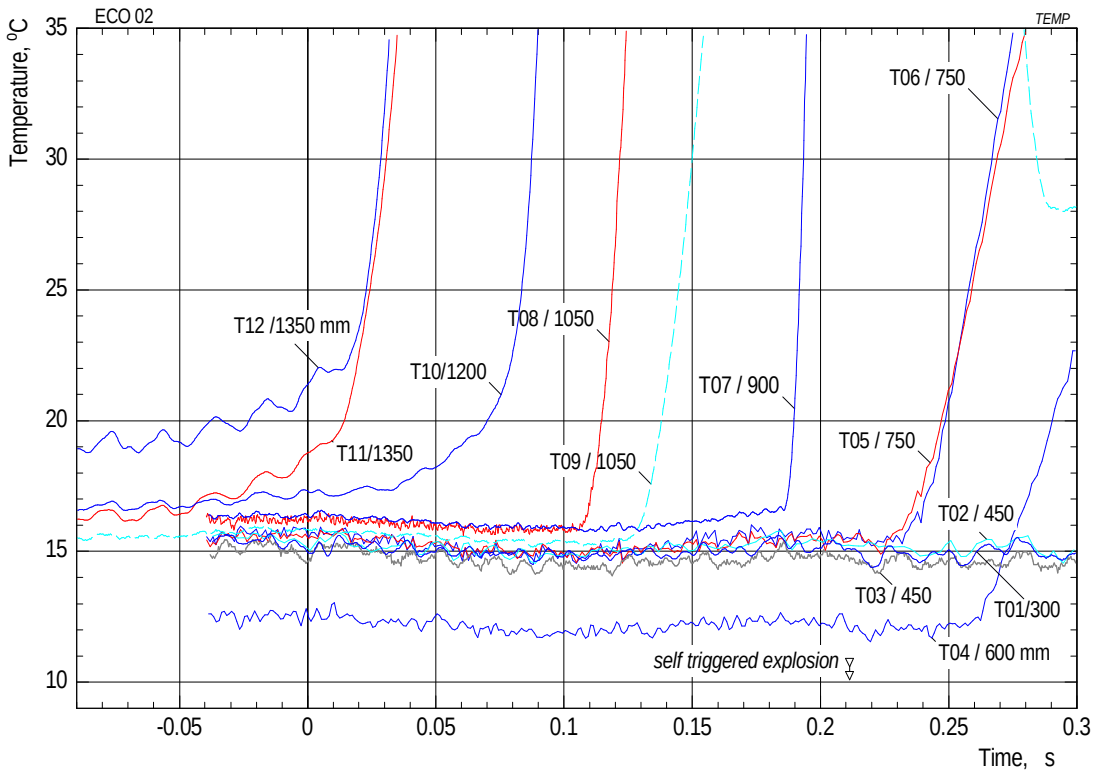

(b) Enlarged scales

Fig. 5.2.3 ECO-02. Time histories of the temperature measurements shown in different scales. The numbers in millimetres give the axial height.

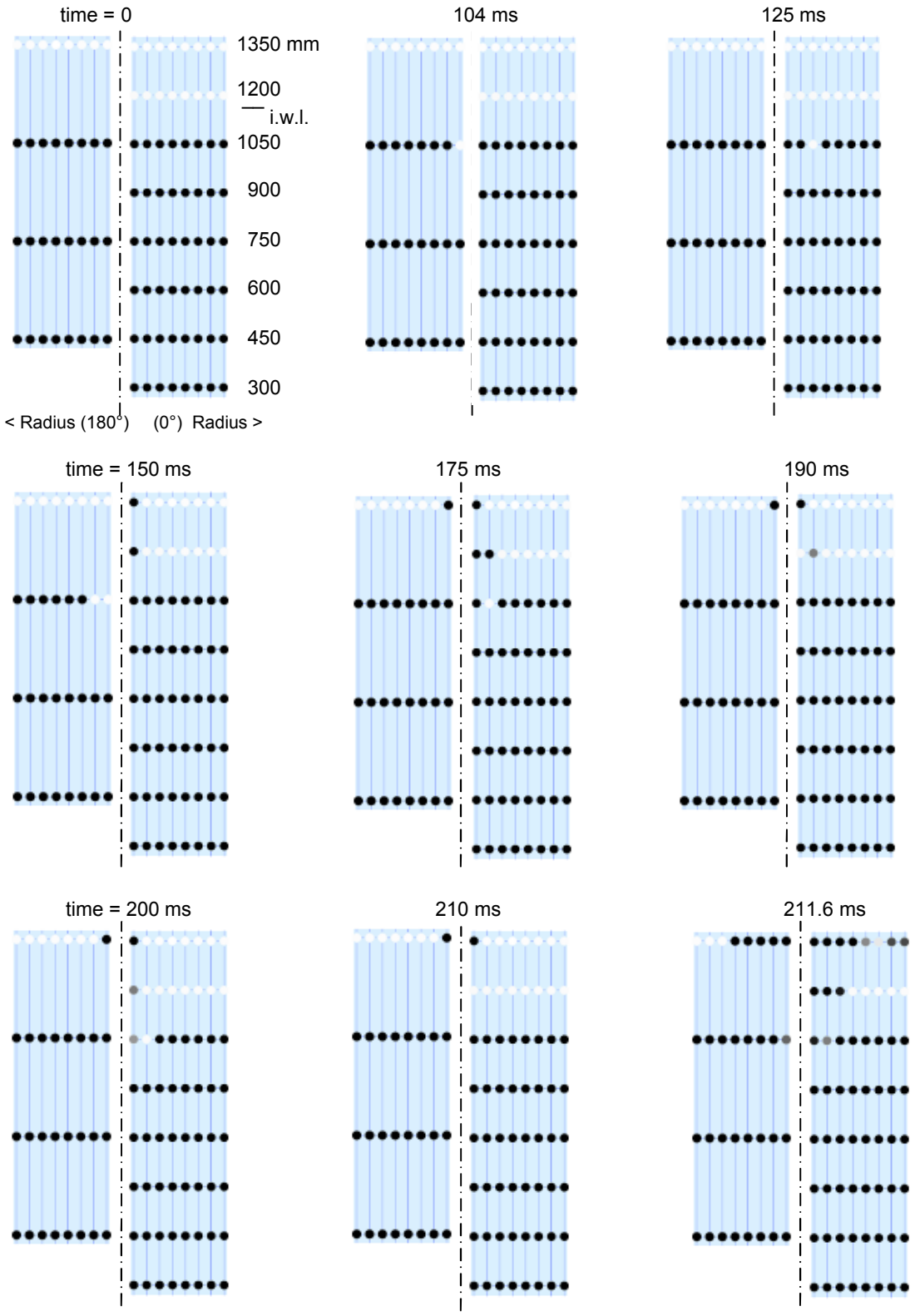

Fig. 5.2.4 ECO-02. Melt penetration mode illustrated by the local distribution of steam and water at increasing times.
Liquid and steam are represented by dark and bright points, respectively. Grey points indicate there was steam immediately before or after the point in time chosen. The initial water level (i.w.l.) was at 1150 mm, i.e. 50 mm less than in test 01. The steam explosion started at 0.2113 s.

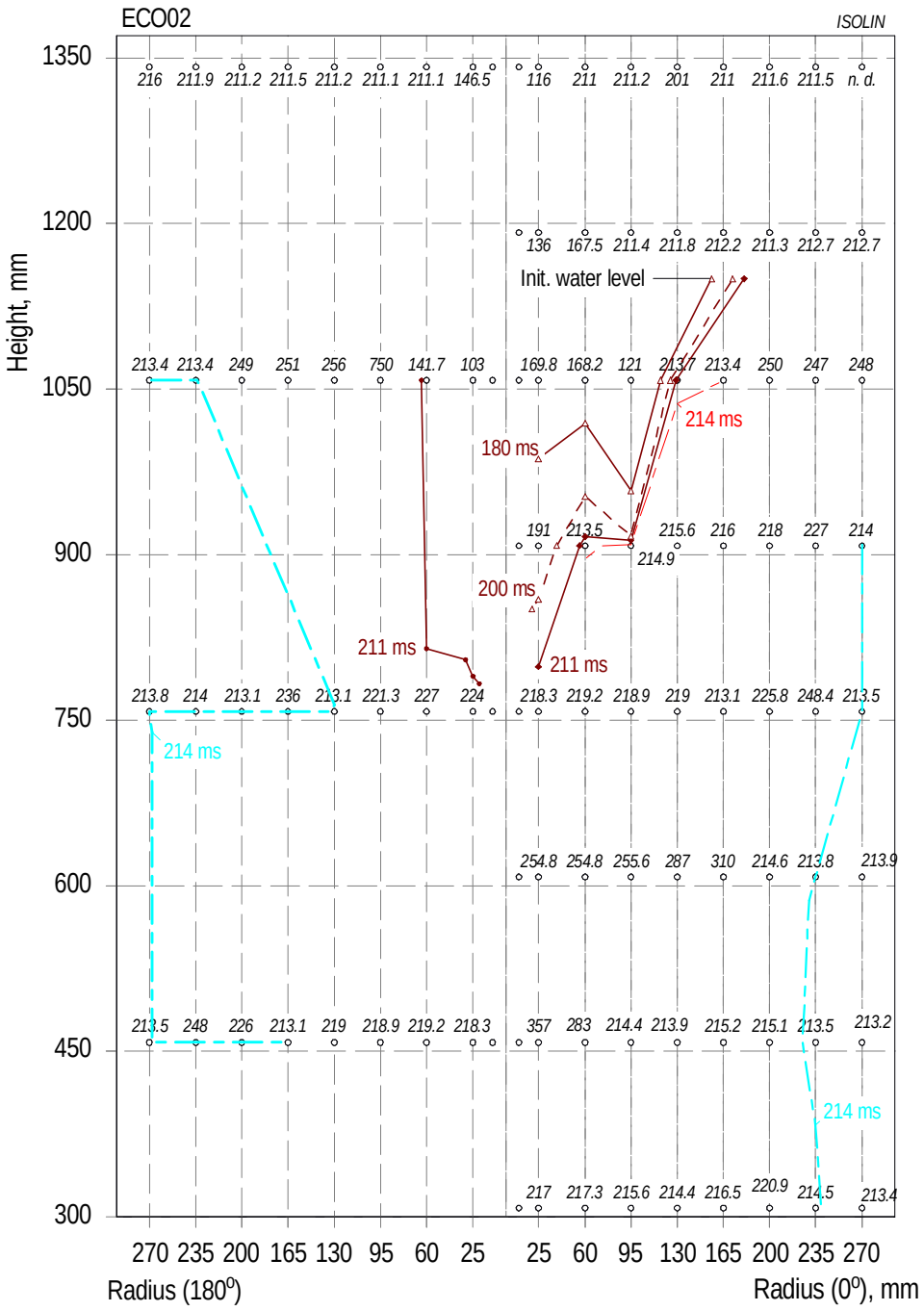

Fig. 5.2.5 ECO-02. Melt penetration in the water with the time as a parameter. Numbers in ms give the instants of first changes in the void signals. Temperature data (at 10 mm radius) denote the starting points of first steep increases. The lines represent outmost boundaries of the mixing zone to the bulk of water. Dash-dot lines connect a series of void data that indicate steam 2 ... 3 ms after the explosion. The initiation of steam explosion occurred at 0.2113 s.

In a first conclusion, one can state that the kind of mixing was different from that in test 01 in two major points:

Firstly, the melt release as well as the penetration occurred at smaller rates. Steam was indicated in the water not before 0.103 s (Fig. 5.2.2). The average speed

of melt penetration in the water was less than 2 m/s (compared to more than 6 m/s in test 01, cf. Fig. 5.1.2).

Secondly, no coherent zone of mixing, but single melt fragments (via steam) have been identified (Fig. 5.2.4). Moreover, the axial extension of the mixing zone was much smaller in test 02 than in test 01 at the instant of steam explosion (compare Figs. 5.2.5 and 5.1.5).

Significant portions of water above the water level were measured preferrably after the steam explosion (Fig. 5.2.4, 1200 and 1350 mm level). We presume that the open system facilitated the movement of water situated above the explosion level. On the other hand, steam with a very short life time (typically 4 ms) was measured in a large number of void signals. The location of the related probes was far from the place where the steam explosion started (see the lines connecting the 213 ... 214 ms labels in Fig. 5.2.5). The meaning of this appearance is not clear to us, yet. It might have been the effect of suppression behind a shock wave originating from the steam explosion and travelling through the bulk of water.

The level down to which melt penetrated in the water is assumed to be 800 mm. This number is obtained by extrapolation of void signal changes (see Fig. 6.3). The effective volume of water available for mixing is 0.0956 m^3, the melt-to-water mass ratio is 0.030 (cf. Table 6.2).

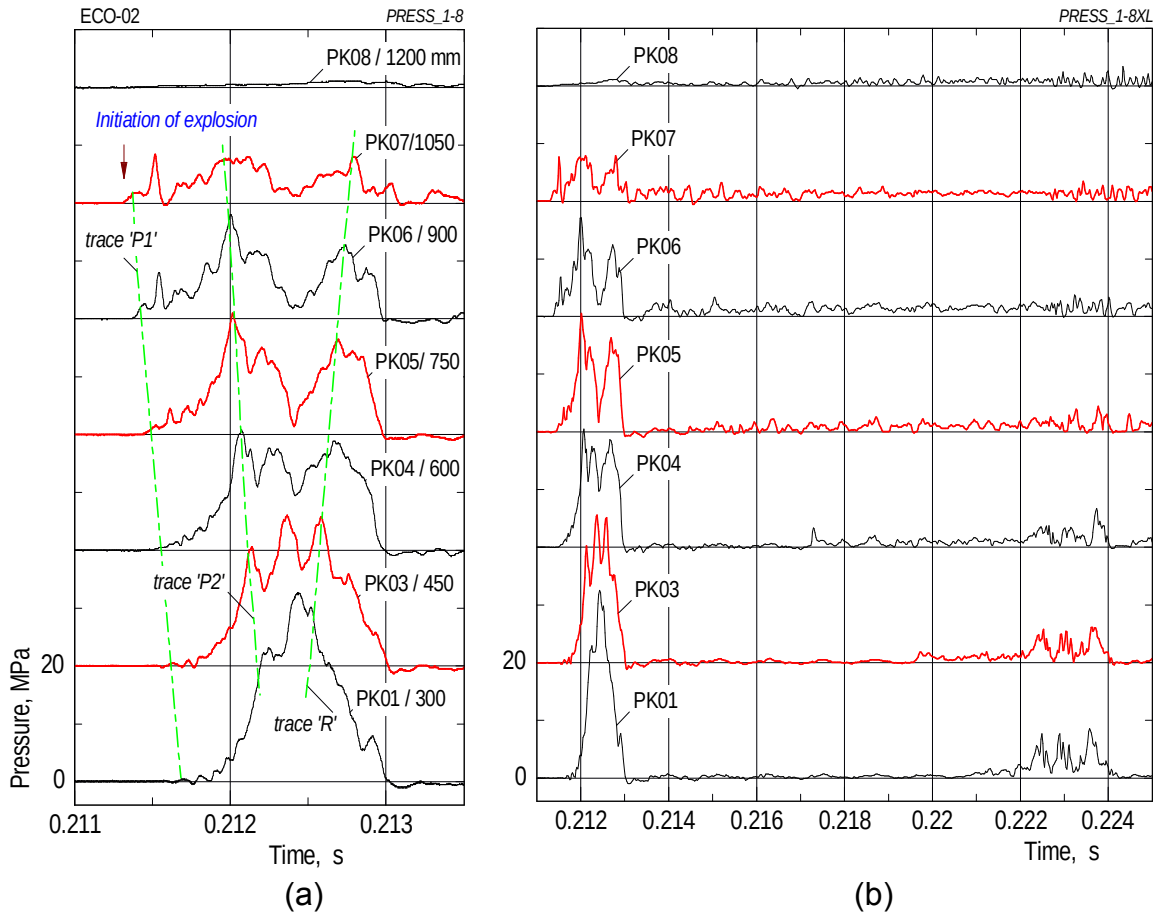

Fig. 5.2.6 ECO-02. Signals of piezo type pressure transducers shown in different time scales.
The labels give also the axial height. The dot - dashed lines help in identifying the directions and speeds of pressure propagation.

The steam explosion event

The pressure data (Fig. 5.2.6) show that the steam explosion started at 0.2113 s (see PK07) with gentle increases in the uppermost part of the water pool. The actual steam explosion was indicated by a steep increase in the PKr09 pressure at 0.2117 s. So far, no steam had been detected at the level of 750 mm. The initial pressure event propagated (cf. trace ‘P1’) from top to bottom dying out.

The rapid production of steam in the center caused the water to move into the radial and upward directions. The relocation of substantial portions of water in the upward direction obviously resulted in an impact of water on the bottom of the melt generator exerting a force to that part of the “cylinder”. This event is evidenced by the changes from steam to liquid in the void signals measured at the 1200 and 1350 mm levels at 0.2116 s (Fig. 5.2.4) as well as by the PK07 pressure (Fig. 5.2.6 (a), level 1050 mm) which reaches a second maximum at 0.2119 s.

This maximum is considered the start of the second pressure event which may originate, as mentioned, from the impact of water on the bottom of the melt generator as well as from melt that still had been released, i.e., before the slide valve was closed. The pressure peak propagated downward (cf. trace ‘P2’) increasing in amplitude and is lastly reflected (≈ 0.2123 s) at the bottom of the test vessel. The reflected pressure peak (trace ‘R’) moves up losing in magnitude.

With regard to the initial large pressure events, the steam explosion was essentially terminated at 0.213 s. The signals recorded in the lower part of the water pool (Fig. 5.2.6 (b)) show that there was another small pressure event later, at 0.222 s. This event may have induced the second maximum in the displacement time history (see Fig. 5.2.7 (a)).

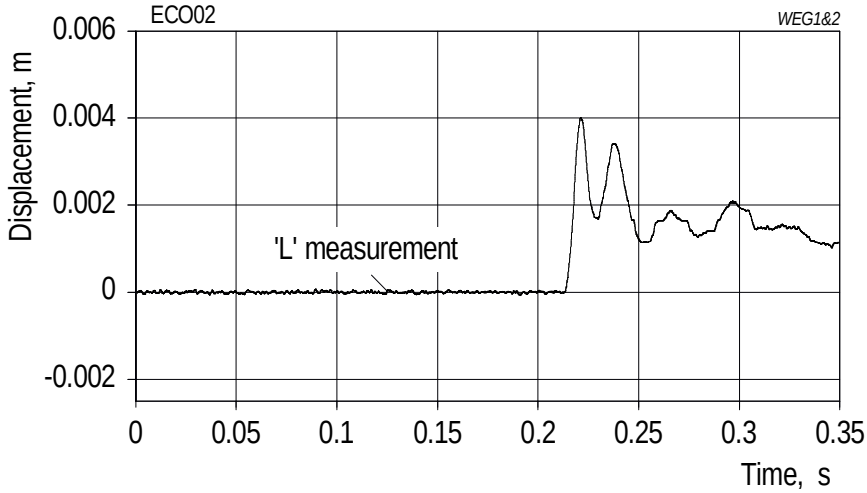

(a) Survey (long time)

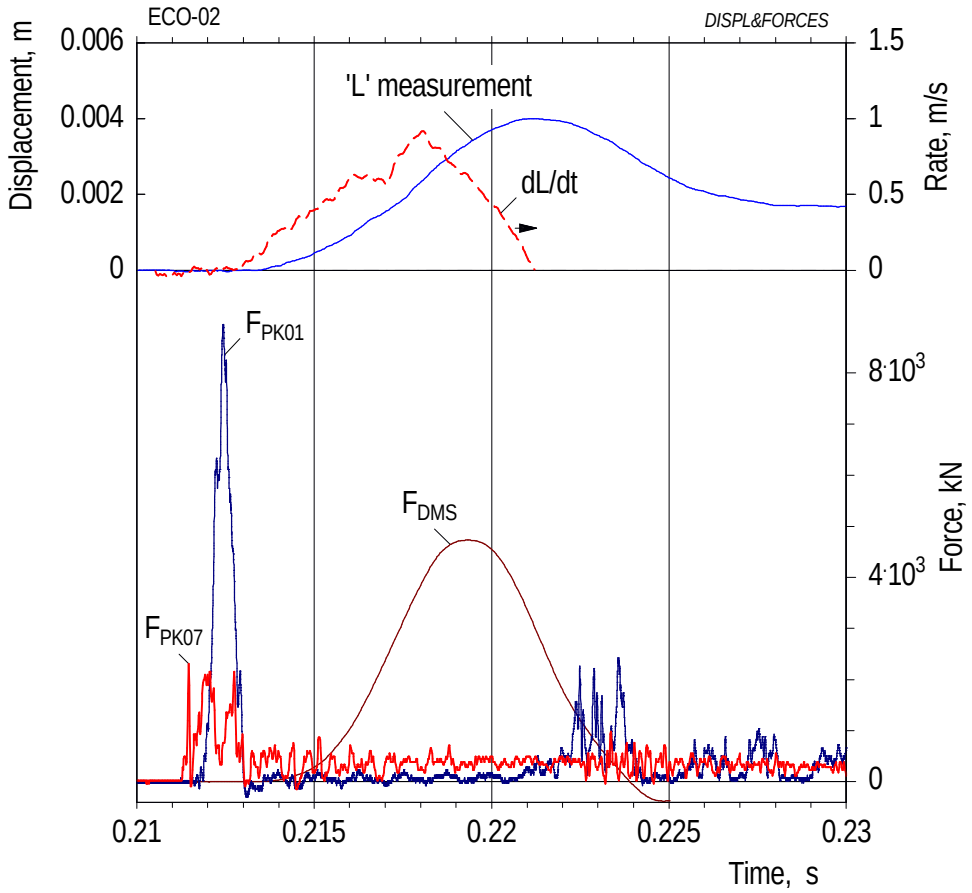

(b) Explosion phase

Fig. 5.2.7 ECO-02. Various measurements resulting from the steam explosion: The piston displacement, L, forces derived from the PK01 and PK07 pressure data, and the DMS forces in the supporting columns.

Evaluation of the energy conversion

Before the mechanical energy in test 02 is determined, a short excursion is undertaken with regard to its principal measurement (cf. Section 4.5), taking this test as an example. For this, we compare the time history of the forces acting within the test vessel (which result in the movement of the piston) with that of the forces measured outside of it, which are the DMS forces.

1. The 'piston' starts to move (see dL/dt in Fig. 5.2.7) at 0.2124 s. This is the time when the second pressure event is being reflected (in PK01) at the bottom of the water pool. The force is exerted on the test vessel bottom until the time 0.2180 s which is determined by the turning point of the 'L' curve (or the maximum in the dL/dt line). After that, the movement of the piston is determined by deceleration, i.e. the kinetic energy of the piston is converted to mechanic energy. Although the test vessel was open to the environment until 0.221 s, appreciable pressures (Fig. 5.2.6 (b)) were measured in the upper part of the test vessel all the time after the first pressure event. (The pressure data recorded in the lower part are comparatively low as the transducers' heads seem to suffer from a sudden change in temperature of the adjacent water).

2. The DMS force starts to increase at 0.2134 s. This is 1.0 ms after the start of piston movement and 1.5 ms after the postulated impact of water on the bottom of the melt generator. The maximum of the DMS force is delayed by 1.3 ms compared to that of the dL/dt function.

A conclusion from the before said is that, because of the shift in time of the DMS force compared the movement of the piston (which is found in all tests), the mechanical work done can be reliably determined only from the known force of the crushing material in conjunction with the deformation length.

The mechanical work in test 02, again, was very small. Because the system was open to the environment, the piston began to move not before the start of the steam explosion. A first maximum of 4 mm was reached 10 ms after the initiation of the explosion (Fig. 5.2.7 (b)). After that, the deformation oscillated. Eventually, a permanent deformation of one millimetre was stated in the uppermost layer of the crushing material. The elastic deformation was the same as in test 01.

Taking the above elastic deformation of 4 mm, the mechanical work is calculated with the equation $W = ½ \cdot F_1 \cdot L$, or

$W = 0.5 \cdot 2.428\ MN \cdot 0.004\ m = 4.9 \cdot 10^{-3}\ MJ$.

The melt mass gives a thermal energy of $Q = 2.87\ kg \cdot 3.8\ MJ/kg = 10.9\ MJ$.

The energy conversion factor amounts to $\eta = 0.045\%$. This number is twice as high as that in test 01.

Post test examinations

For a plot of the melt particle size distribution in test 02 see Fig. 5.4.8.

5.3. Results of ECO-03

Objectives in brief

To reduce the risk of a spontaneous steam explosion, two conditions were changed: 1. The venting conduits were closed again and the pressure in the test vessel was set to 0.25 MPa. To maintain a sufficiently high pressure difference, the pressure in the melt generator was raised, too. 2. The water temperature was raised to about 80 °C.

Additionally, a second explosion capsule was mounted in the edge of the vessel bottom to reduce the risk of a failure of triggering.

Course of events

We presume from the time history of the pressure in the test vessel (Fig. 5.3.1) that melting of the steel foil occurred around the time of -0.01s. From that time on, the pressure in the test vessel began to rise. The initial pressure difference was 0.13 MPa.

Unfortunately, because of the malfunction of a valve in the gas supply system, the pressure in the melt generator did not reach the forseen level. Backfeeding of gas after the start of melt release was not possible as well. As a result of this, the melt mass released was much too small (see discussion further below).

The trace of the melt front can be followed by means of thermocouples: Around zero time, the T12 - T10 thermocouples (Fig. 5.3.3) located in the gas space indicated the passage of melt. The T09 and T08 thermocouples situated below the water level started to increase at 0.1 s.

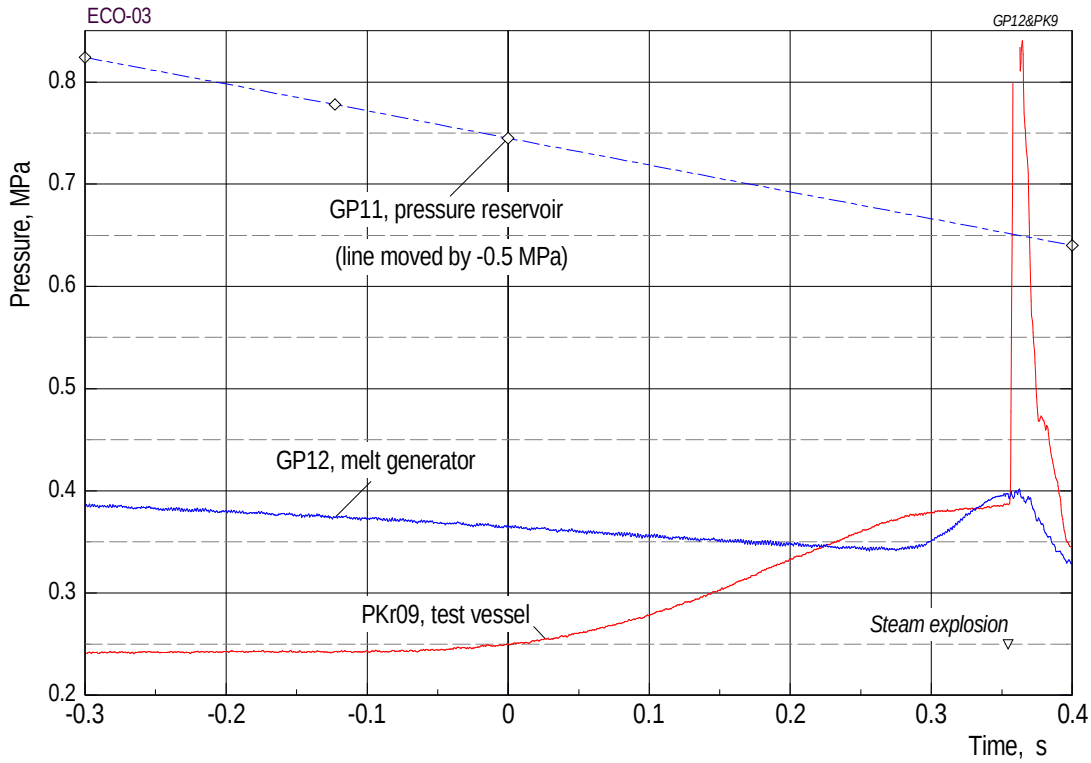

Fig. 5.3.1 ECO-03. Time history of pressures that determined the melt release.

The calculation (Fig. 5.3.2) gives an actual maximum melt speed of 7 m/s, while the melt front reaches the water at 0.03 s. This time obviously agrees with the measurements. Penetration of the melt into the water occurred at a much smaller rate,

≈1.8 m/s. Because of the pressure increase in the test vessel and due to the malfunction of the gas valve, the pressure difference became negative from 0.223 s on.

The melt slide valve was closed after the time interval set had been reached (0.343 s, criterion no 4). The pressure in the test vessel amounted to 0.39 MPa. The trigger capsule was ignited 11 ms after closure of the valve. The steam explosion was initiated by steep pressure increases in the bottom of the pool (see below).

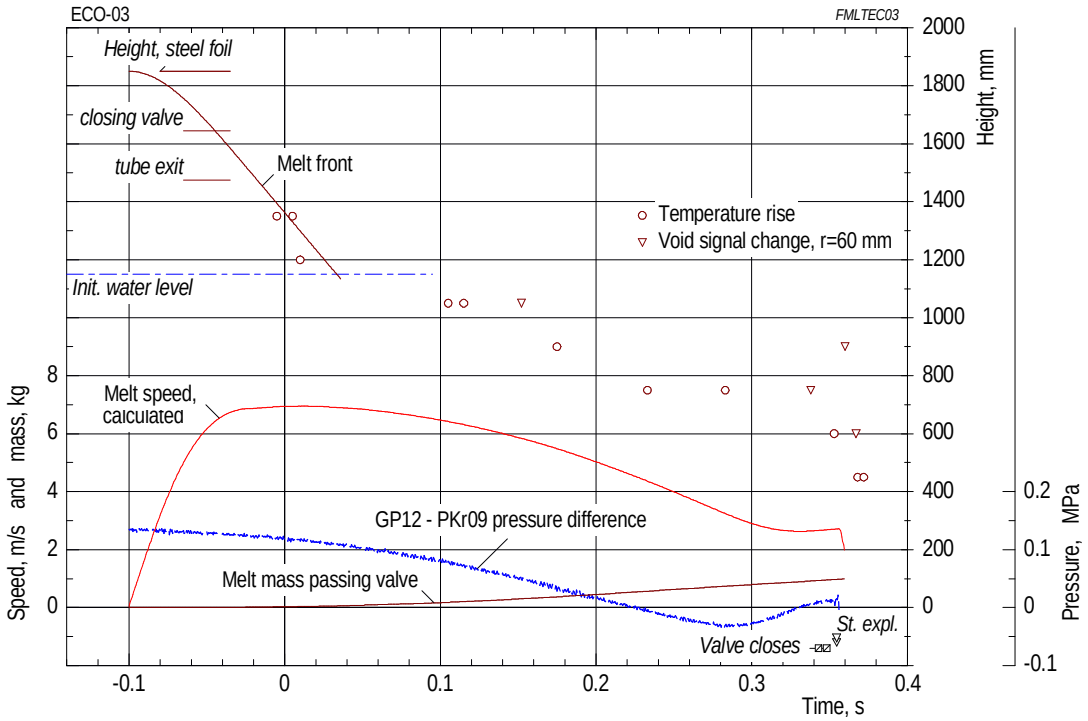

Fig. 5.3.2 ECO-03. Melt release illustrated by calculated and measured data.

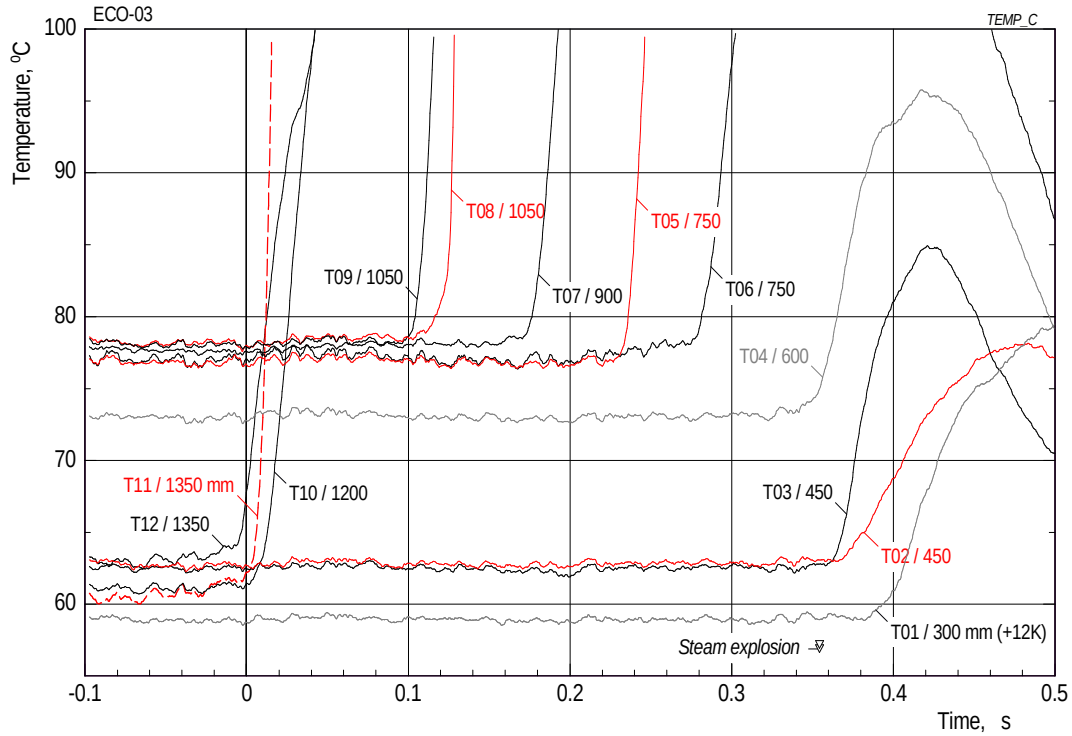

Fig. 5.3.3 ECO-03. Time histories of the temperature measurements.

A mass of melt of only 0.9 kg had been released. The average rate is 2.4 kg/s. The calculation gives rise to the assumption that melt through of the steel foil occurred at a rather low pace: The mass of melt released was calculated by assuming a jet whose diameter grew from 5 to 25 mm within 0.40 s (cf. Appendix A4).

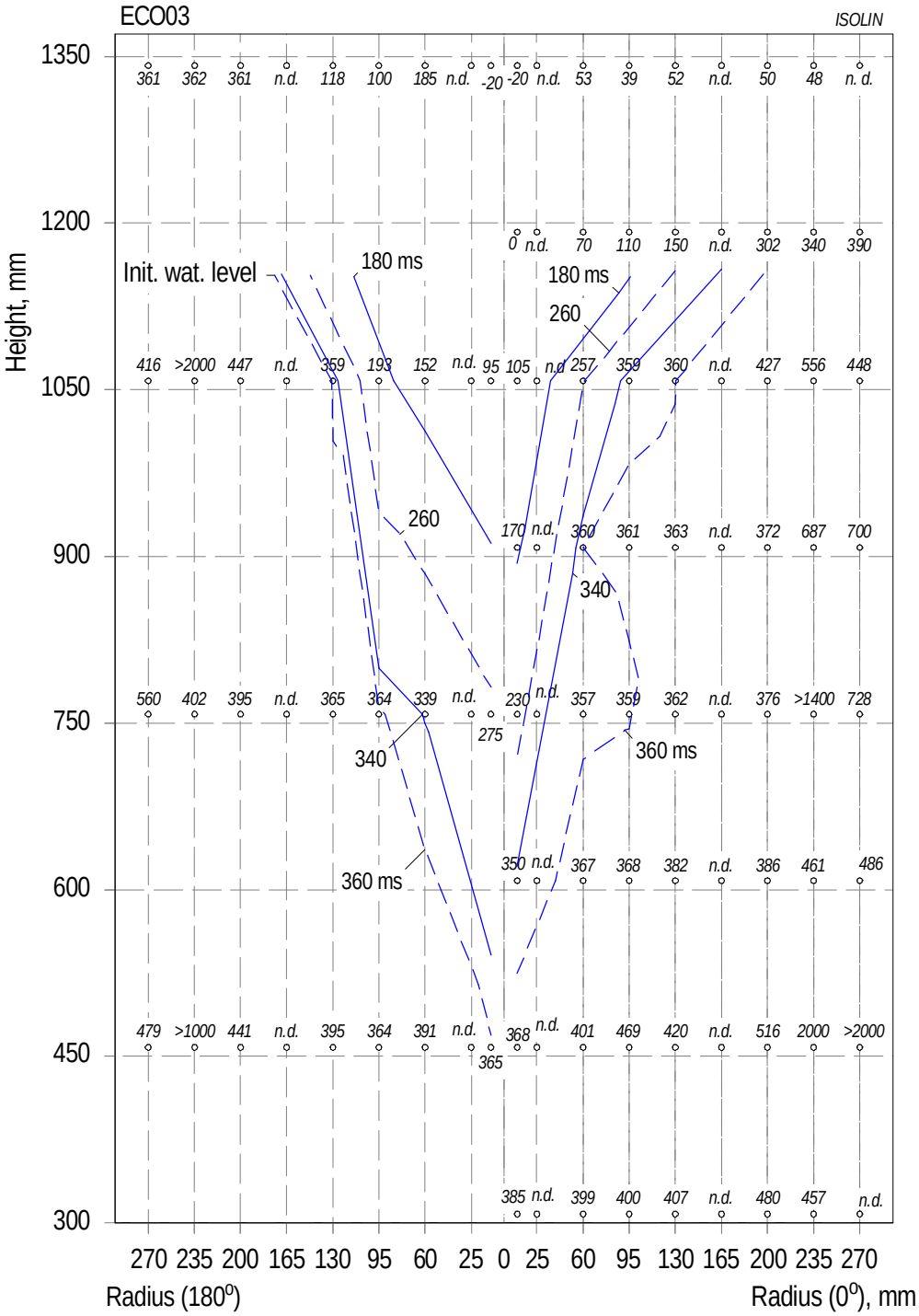

Fig. 5.3.4 ECO-03. Melt penetration in the water with the time as a parameter. Numbers in ms give the instants of first changes in the void signals. Temperature data (at 10 mm radius) denote the starting points of first steep increases. The lines represent outmost boundaries of the mixing zone to the bulk of water. “n.d.” means: no data available. The steam explosion was initiated at 0.3545 s.

Mixing period

The time history of melt penetration can be followed in Fig. 5.3.4. It should be noted here that no data are available from all those void probes positioned at r= 25 and 165 mm. The lines have been constructed on basis of the void and temperature data measured in the water. The family of lines shows, like in test 01, the formation of a narrow mixing channel. The void probes located above the initial water level indicate frequent changes of steam (gas) and liquid during the mixing period.

We assume that the slim shape of the mixing zone was only partly due to the water subcooling, although that was reduced compared to that in test 01 (Table 3). For the subcooling see the temperature data in Fig. 5.3.3 which show, in addition, a typical stratification.

Another reason for the slim shape of melt penetration may lie in the small jet diameter which resulted in a comparatively very small average melt release rate (cf. Table 3), although melt speeds of 7 to 3 m/s are calculated (Fig. 5.3.2). On penetrating, the small melt jet is expected to have fragmented easily. A pentration rate in the water of 1.8 m/s can be derived from the temperature data plotted in the figure.

As mentioned, the melt release was terminated when the time limit was reached (criterion no 4). Steam (i.e. melt) had been detected before by void probes down to the height of 750 mm only (though the interpolation lines for 340 ms suggest a deeper melt penetration). On the other hand, the T04 time history (Fig. 5.3.3) suggests that the lower boundary of melt penetration was close to 600 mm height at the time of steam explosion.

The steam explosion event

The very first pressure rises were measured in the bottom of the test vessel (PK17 and PK16, Fig. 5.3.5) at about 0.3545 s, i.e. 0.3 ms after the ignition of the explosion capsule. Based on the above discussion which results in the finding that temperature and void data available do not indicate the presence of melt below the level of 600 mm at the time of explosion, we assume that the first pressure increases mentioned above, measured at 200 mm height and amounting up to 9.8 MPa, were due to the trigger pressure coming from the explosion capsule. For this compare (Fig. 5.1.7) the first peaks in the PK01 pressure signals recorded in test 01 and in the calibration test, which amount to 4 and 7 MPa, respectively.

The actual steam explosion probably started at a level between 450 and 600 mm producing a first series of smaller pressure events. These travelled in the upward direction while increasing in magnitude, up to 10 MPa. Immediately after this first series, between 0.356 and 0.357 s, a second series of pressure events was measured whose magnitude increased in the downward direction.

The rapid production of steam due to the steam explosion forced the water to move in the radial direction (for this see the 360 ms line on the 0° side in Fig. 5.3.4). Relocation of water also occurred in the upward direction. After the steam explosion, almost continuous liquid was indicated in the signals of the void probes located above the initial water level.

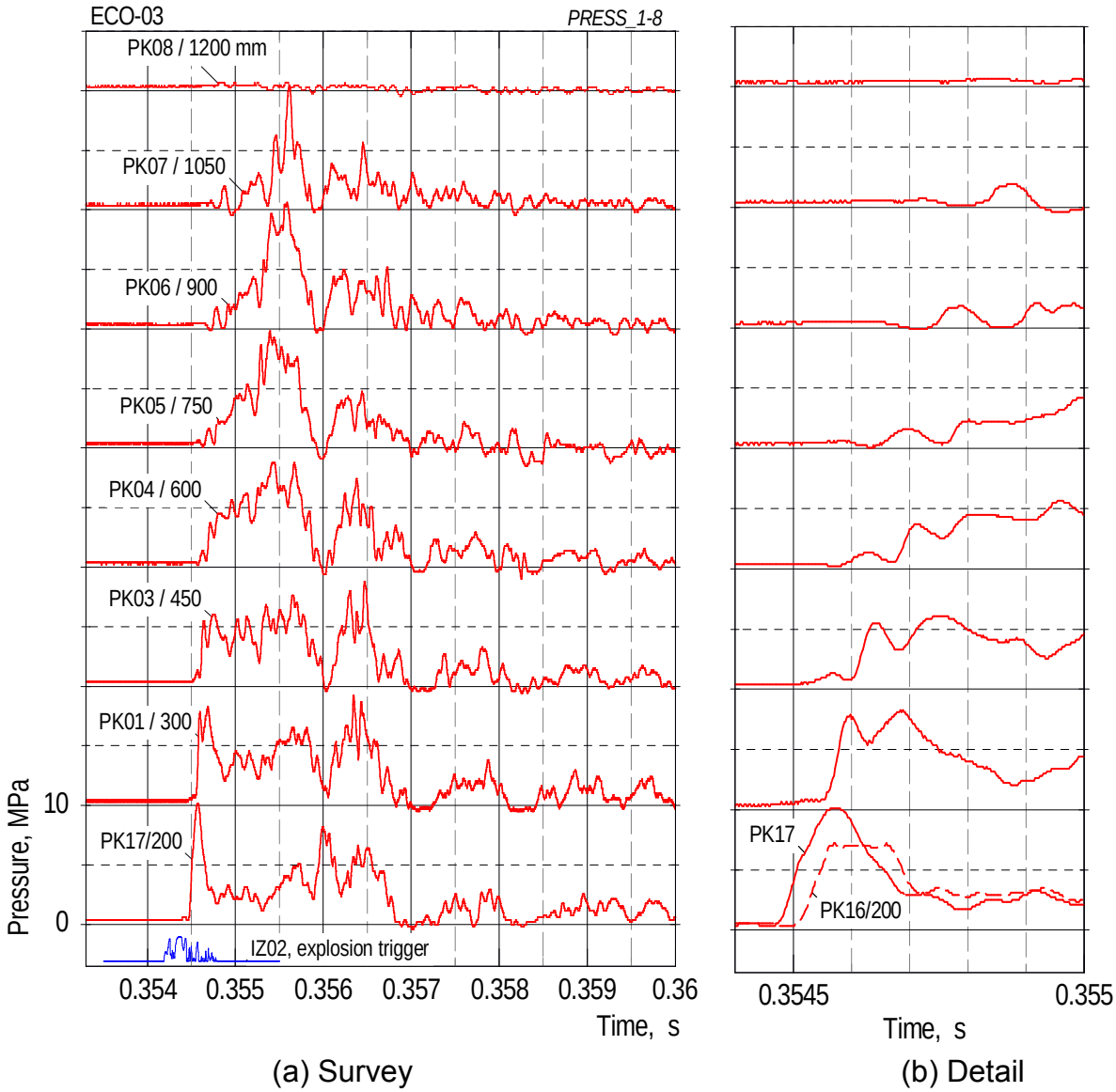

Fig. 5.3.5 ECO-03. Dynamic pressure data plotted in different time scales. The labels give also the height in mm. The IZ02 time history indicates the ignition of one of the explosion capsules.

Evaluation of the energy conversion

The displacement measurement (Fig. 5.3.6) gives evidence of an oscillating behaviour. The first maximum, 2.2 mm, was reached 10 ms after the start of explosion. The deformation of the crushing material lastly remained in the elastic range. With the above deformation of 2.2 mm, half of the force necessary to permanently deform layer 1 (the longer-time average is F_1 = 2.428 MN) had been reached.

The mechanical work is calculated using the equation: $W = ½ \cdot (0.5 \cdot F_1) \cdot L$, or $W = 0.5 \cdot 1.214\ MN \cdot 0.0022\ m = 1.34 \cdot 10^{-3}$ MJ.

The melt mass gives an energy of Q = 0.9 kg · 3.8 MJ/kg = 3.42 MJ.

The energy conversion ratio amounts to η = 0.04 %.

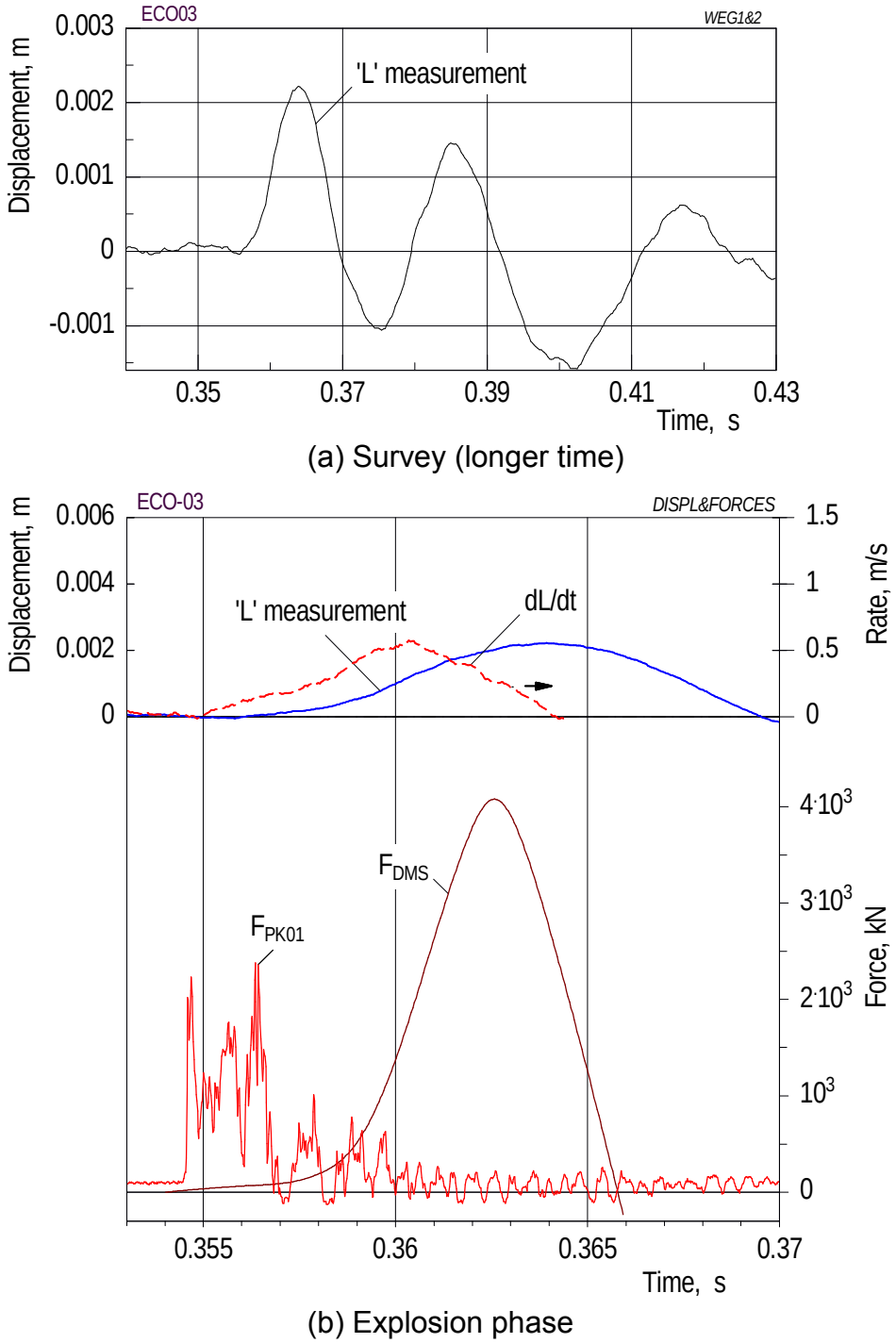

Fig. 5.3.6 ECO-03. Various measurements resulting from the steam explosion: The piston movement, L, the force derived from the PK01 pressure, and the DMS forces in the supporting columns.

Post test examinations

For a plot of the melt particle size distribution in test 03 see Fig. 5.4.8.

5.4. Results of ECO-04

Objectives in brief

The two essential aims of test 04 were to reach a larger melt mass released and to reduce the amount of water involved in the mixing and steam explosion processes. Therefore, the following conditions were changed:

(1) Melt release was no longer started with the uncontrolled melt-through of a steel membrane. The steel foil was maintained, to keep the crucible closed initially. The melt release now started by opening the upper fast slide valve, named valve 1, additionally mounted below the steel foil (see Fig. A2.1). The valve is opened when the steel foil is expected to have totally been molten.

(2) A larger driving pressure was applied.

(3) To reduce the amount of water, a restriction tube made of steel was mounted in the vessel having half the pool diameter (see Fig. 2.1).

Course of events

Melt release started at -0.024 s, i.e. when valve 1 was opened (Fig. 5.4.1). The pressure difference, 0.73 MPa, was 2.8 times larger than that in test 01. It resulted in a melt release rate that was twice of that in test 01. The pressure decrease in the melt generator was markedly stronger.

The pressure in the test vessel began to rise slowly, but at an increasing rate. Gas was fed into the crucible from 0.035 s on to compensate for the decrease in the pressure difference. At 0.03 s, the pressure rise in the test became very steep. We conclude that this steep pressure rise was caused by substantial penetration of melt into the water connected with an intense interaction of melt and water. For this see the steep increase in the signal of the T09 thermocouple (Fig. 5.4.3 at 0.035 s) which is located 100 mm below the initial water level.

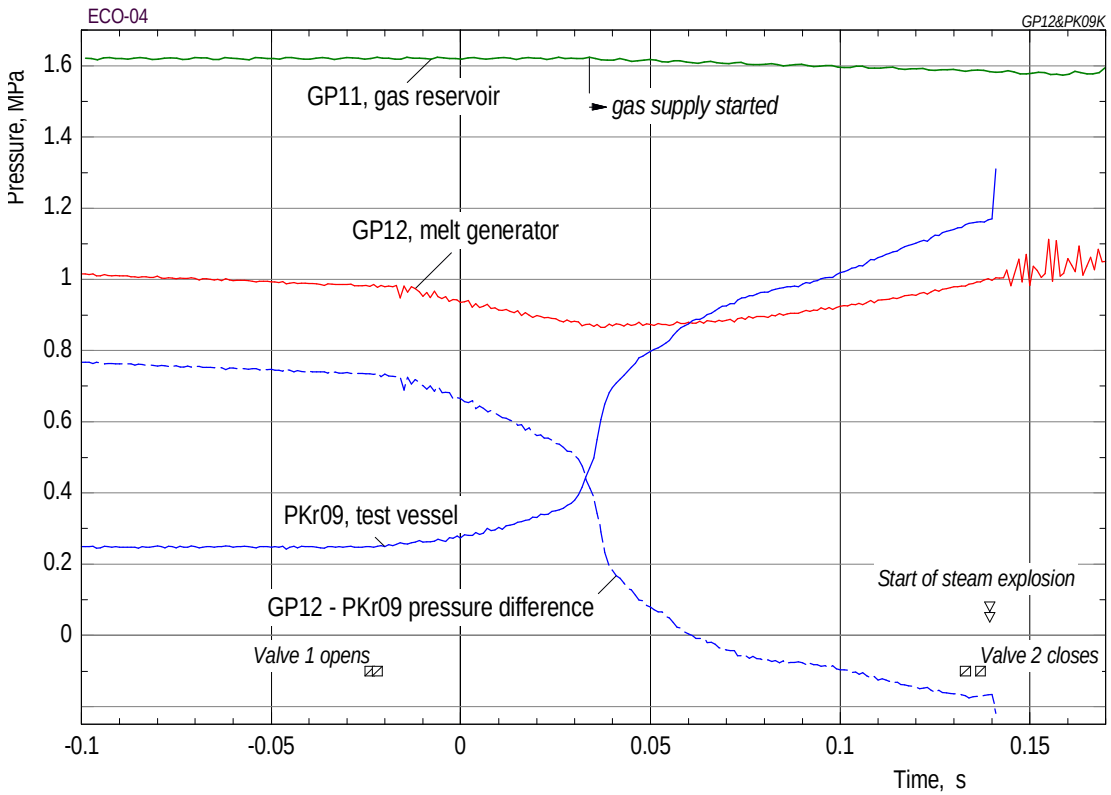

Fig. 5.4.1 ECO-04. Time history of pressures that determined the melt release.

In the calculation (Fig. 5.4.2), the progression of the melt front is delayed by about 10 ms compared to the measurements. The melt reaches the tube exit at 0.015 s and contacts the water at 0.037 s. We conclude that the melt front actually moved at a larger speed than obtained in the calculation. High speed frames later obtained in the ECO-06 test (see below) confirm a rather early melt/water contact.

Because of the strong pressure increase in the test vessel mentioned, the pressure difference dropped and became negative at 0.065 s. This condition, which lasted till the end of melt release, caused the speed of melt to decrease, too. A value of about 2.5 m/s was calculated for the time of steam explosion.

The melt release was terminated by closing valve 2 when steam (melt) was detected at the lowermost measuring lance (criterion no 1). For this see the V01.1 signal in Fig. 5.4.3. Valve 2 was closed at 0.137 s; the steam explosion was triggered two milliseconds later. At last, a total of 9.6 kg of melt had been released, while the pressure in the test vessel had reached a value of 1.17 MPa.

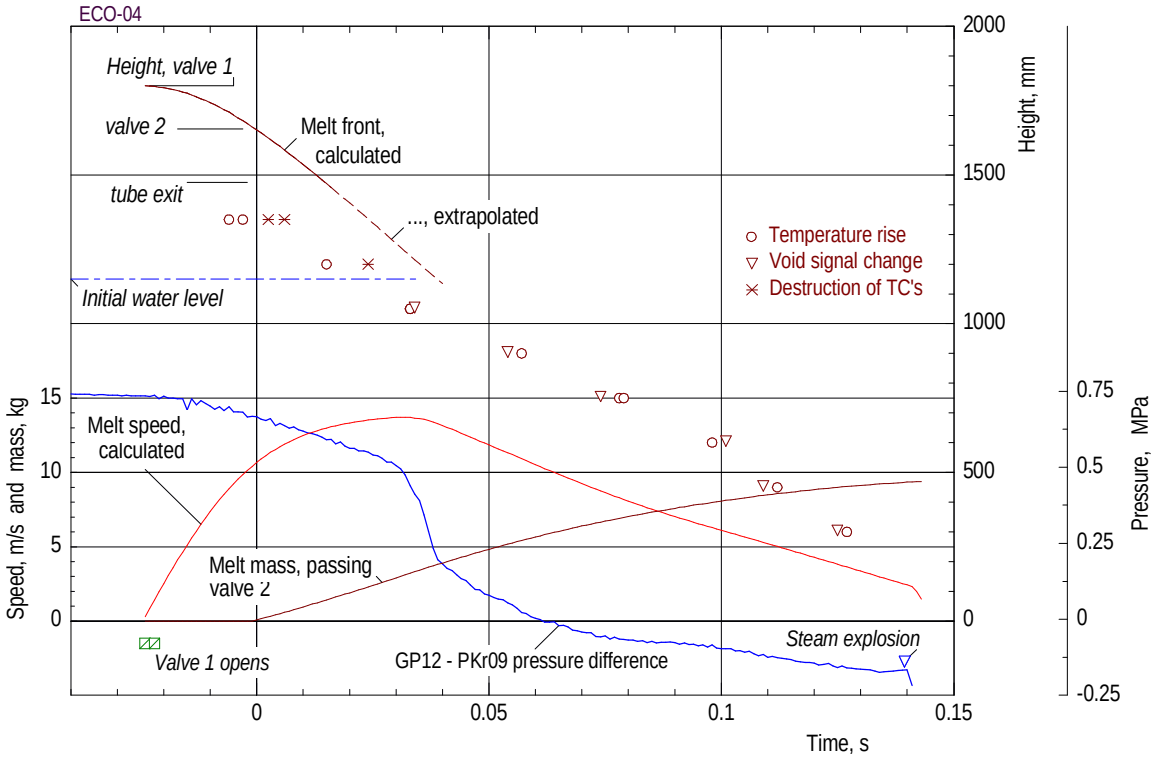

Fig. 5.4.2 ECO-04. Melt release and melt penetration, illustrated by calculated and measured data.

Mixing period

The rate of melt penetration in the axial direction turned out to be still rather large in test 04. An almost constant value of about 8 m/s can be derived along the trace line of the void and temperature data in Fig. 5.4.2. The scatter of the void and temperature data in the various levels is pretty small. This finding may be connected with the definition (Section 4.4) that the temperature data use to give the instants when the steep increases are going to start. Extrapolation of the line of the void data would end in a height of 200 mm (see further details below).

The temperature data are also noted in Fig. 5.4.5 at the respective coordinates near the centre line. The family of lines in this figure shows the formation of a narrow mixing channel whose shape appears symmetrical in the 0° - 180° measuring plane.

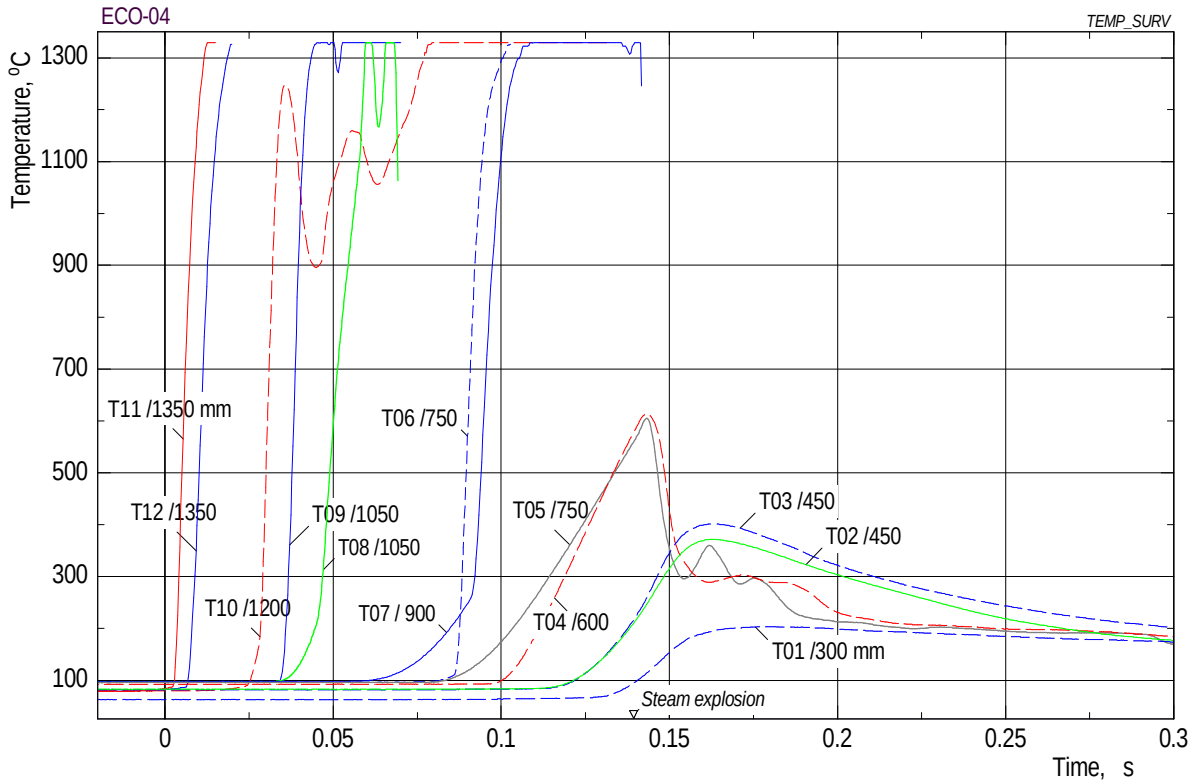

(a) Survey

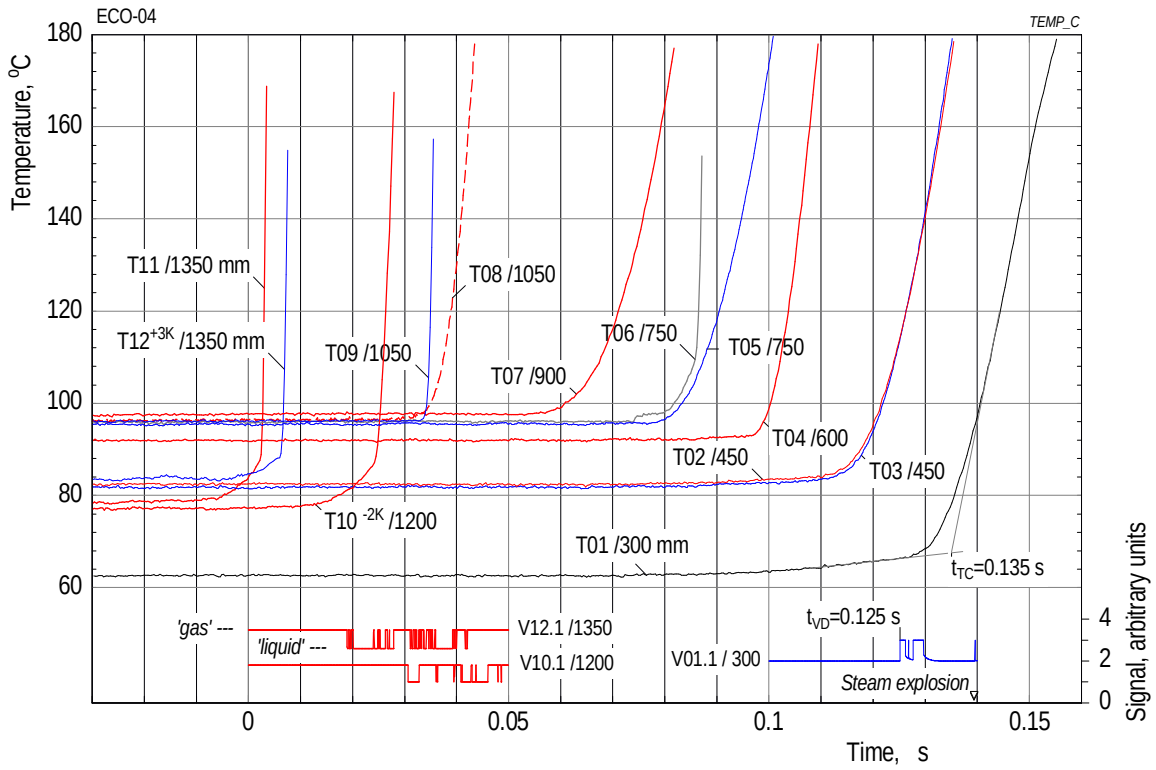

(b) Enlarged scales

Fig. 5.4.3 ECO-04. Time histories of the temperature measurements shown in different scales.
The data have been complemented by a couple of void signals. The subsidiary lines in the lower graph are explained in Section 4.4.

The radial extension of mixing was essentially confined by the restriction tube also drawn in the graph. With two exceptions, steam was detected beyond the restriction tube only after the steam explosion. For this see the numbers at 1050 mm height both at 165 mm radius.

The result of a narrow mixing channel is also visible in Fig. 5.4.4. Two other essential results can be taken from this figure: 1. Water is present within the mixing zone at all times. 2. The rise in the water level, within and outside the restriction tube, is indicated by changes in the signals of the void probes located at 1200 and 1350 mm. The last two pictures (139 ms and 142.4 ms) give the conditions immediately before and 3 ms after the steam explosion, respectively.

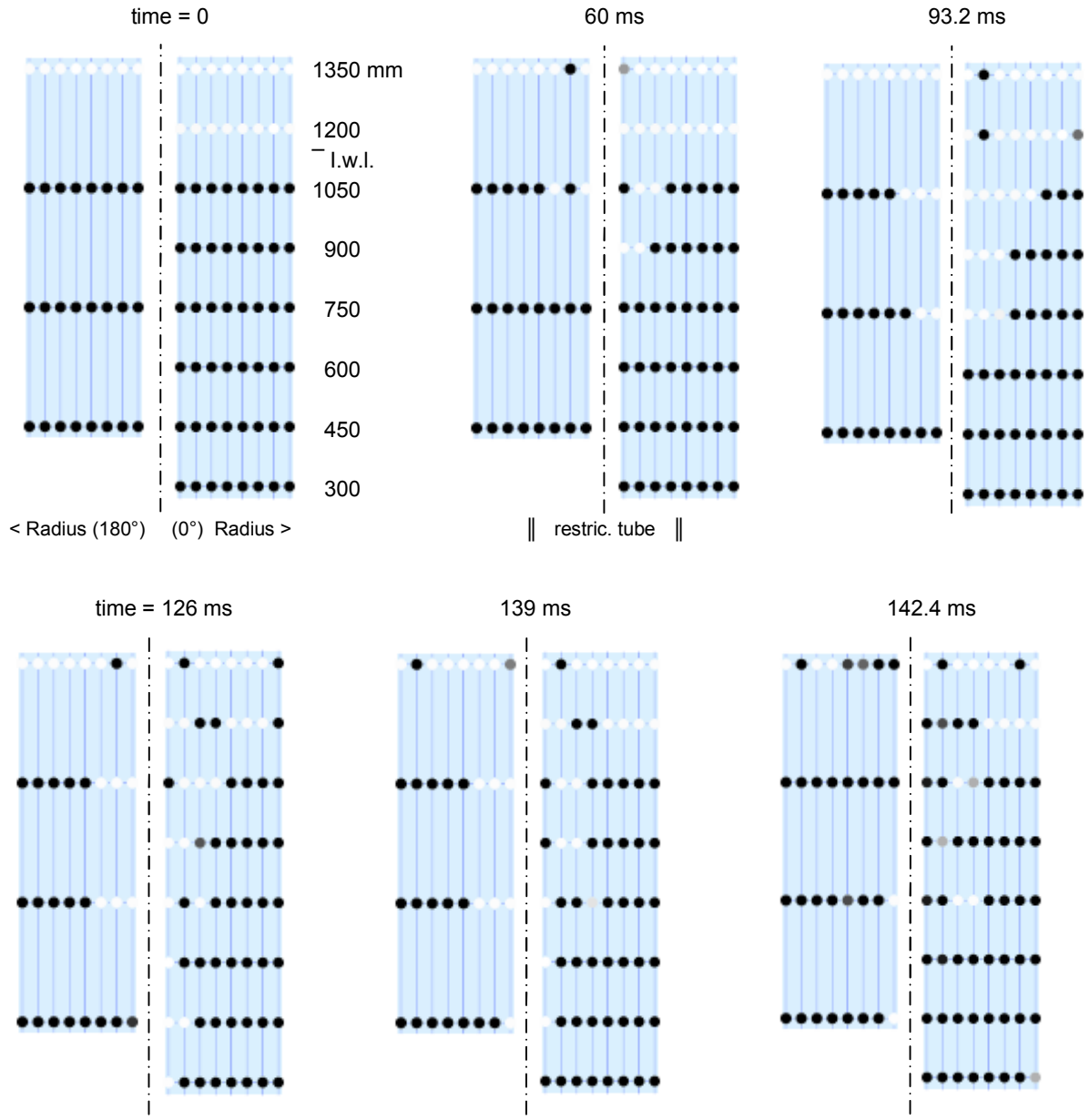

Fig. 5.4.4 ECO-04. Melt penetration mode illustrated by the local distribution of steam and water at increasing times.
For the location of the restriction tube see the sub-line in the 60 ms picture. For the meaning of the dots see Figure 5.2.4. The initial water level was at 1150 mm height. The steam explosion started at 0.1394 s.

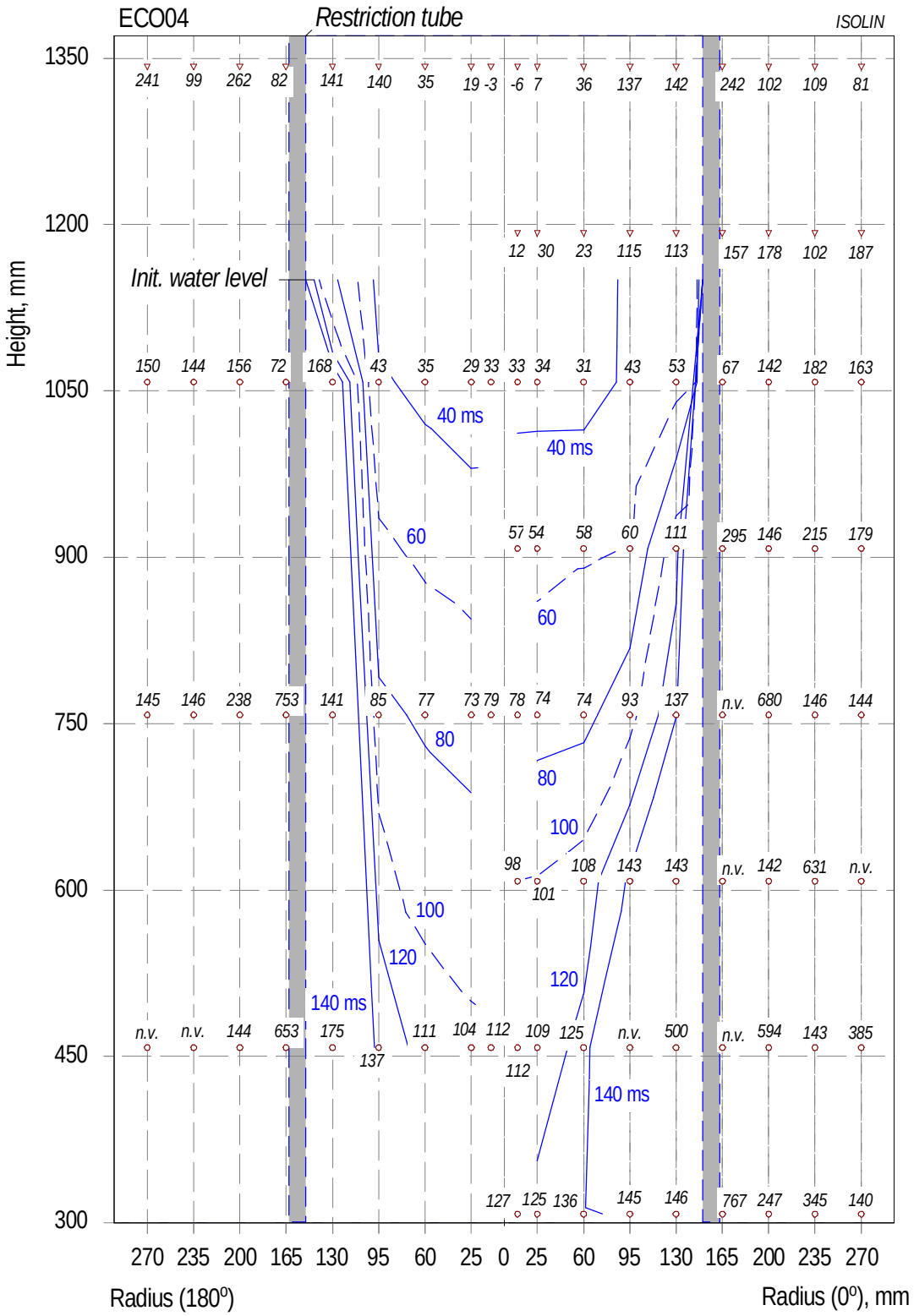

Fig. 5.4.5 ECO-04. Melt penetration in the water with the time as a parameter. Numbers in ms give the instants of first changes in the void signals. Temperature data (at 10 mm radius) denote the starting points of first steep increases. The lines represent outmost boundaries of the mixing zone to the bulk of water. Data outside the restriction tube were not considered in the interpolation. “n.v.” means: no void detected within one second. The steam explosion started at 0.1394 s.

The level down to which melt penetrated in the water is determined by extrapolation (Fig. 6.3) to be 200 mm. This number is confirmed by the axial height of the PK17 pressure transducer whose signal indicates, at the same time as that of PK01, the first steep pressure increase (Fig. 5.4.6). The effective volume of water available for mixing is 0.0665 m^3, the melt-to-water mass ratio is 0.144 (cf. Table 6.2).

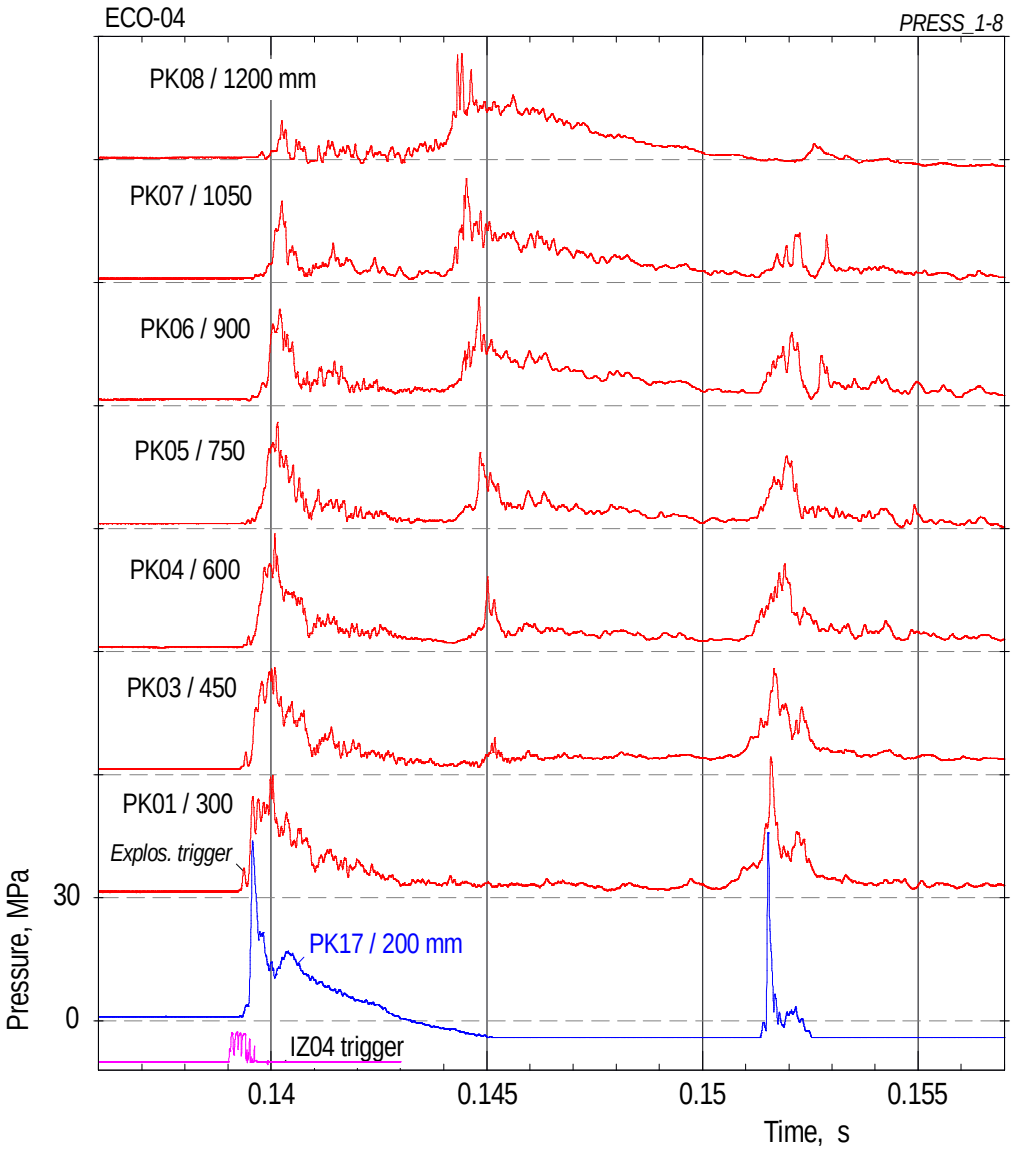

Fig. 5.4.6 ECO-04. Dynamic pressures measured during the steam explosion.

The steam explosion event

A sequence of three major pressure events (Fig. 5.4.6) occurred in test 04, lasting a total time of 16 ms. The first event started in the lowermost part of the pool, recorded by the PK01 and PK17 transducers almost at the same time, 0.1394 s. We attribute the first needle shaped peak to the trigger pulse which amounts to 7 MPa and appears most clearly in the PK01 reading. The explosion event proper in PK01 has a maximum of about 28 MPa and a duration of 3 - 4 ms. In PK17, the maximum is larger but the width is less than in PK01. The pressure event propagates upwards at a large speed, typically 1500 m/s, but loses in magnitude; i.e., no pressure escalation occurs. The fall of the PK17 signal below zero after 0.143 s is a thermal effect exerted on the transducer by a fast change in temperature of the adjacent water.

The second pressure event started in the upper part of the test vessel, 4.5 ms after the first one. The pressure peak may be caused by the impact of water on the bottom of the melt generator as well as by a local steam explosion. As mentioned before, an increase occurred in the fraction of water in the gas volume prior to this event (Fig. 5.4.4). The second event propagated downward losing its magnitude.

The third pressure event, probably due to another local steam explosion, started in the bottom of the pool (cf. the PK01 signal at 0.151 s). It propagated upward losing its magnitude.

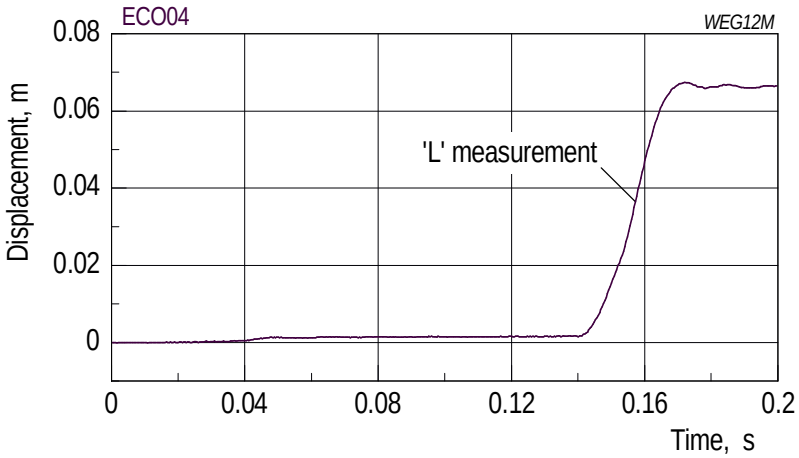

(a) Survey (long-term)

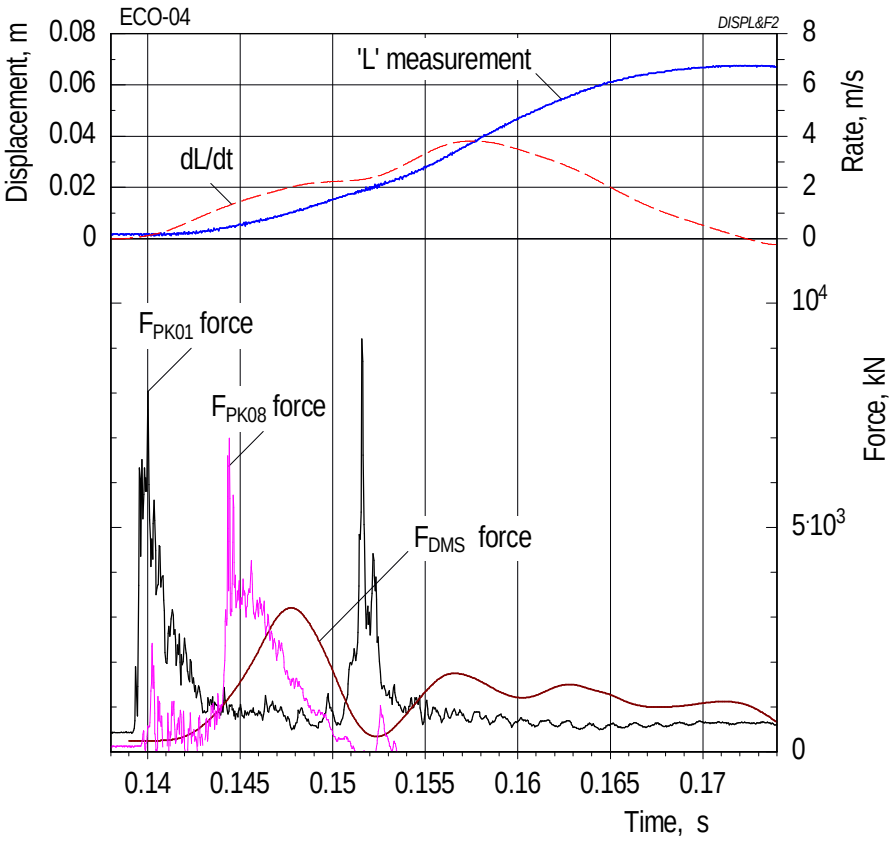

(b) Explosion phase

Fig. 5.4.7 ECO-04. Various measurements resulting from the steam explosion: The movement of the piston, L, forces derived from the PK01 and PK08 pressure data, and the summed DMS forces in the supporting columns.

The various signals plotted in Fig. 5.4.7 help in understanding the sequence of events.

1. The first pressure event (F_{PK01}, bottom) causes the piston to move down. As a reaction, the overlying water column is accelerated in the upward direction at the same time.

2. The second pressure event (F_{PK08}, top) acts onto the bottom of the melt generator. This action becomes visible in the DMS force whose first maximum falls into the decline period of the F_{PK08} force.

3. The third pressure event (F_{PK01} at 0.151 s) causes the second acceleration period in the piston movement (dL/dt). After 0.157 s, the movement of the piston is mainly determined by the absorption of kinetic energy.

In the end, the crushing material is permanently compressed in the uppermost layer by 64 mm.

Evaluation of the energy conversion

In test 04, the energy conversion was much larger than in the preceding tests and, for the first time, clearly measurable. This result is probably due to the presence of the restriction tube in the water pool in combination with a considerably enlarged mass of melt released. The compression of the crushing material gives a work of W = 0.155 MJ.

The heat content of the melt, based on a mass of 9.6 kg, amounts to Q = 36.5 MJ. This gives an energy conversion factor of η = 0.42 %.

The kinetic energy put into the acceleration of water is calculated using the difference in the PK01 and PK08 pressures and a water column of 0.7 m height. We obtain a value of 0.033 MJ, which adds another 0.08 % to the energy conversion factor.

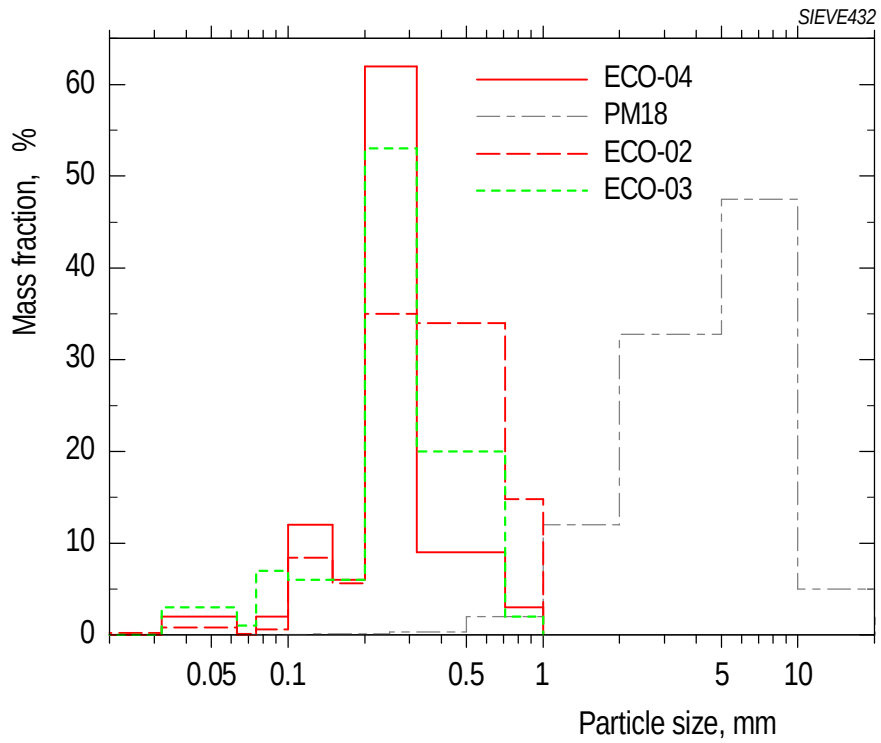

Fig. 5.4.8 ECO-04. Post-test particle size distribution.
Comparison is made with tests 02 and 03 and the PM18 PREMIX test (without steam explosion).

Post test examinations

In test 04, as well as in tests 02 and 03, the overwhelming part of the injected mass was found to be finely fragmented (Fig. 5.4.8). The largest fraction in tests 03 and 04 was in the size between 0.2 mm and 0.32 mm. In the test with a spontaneous steam explosion, test 02, the maximum includes the next larger particle size, up to 0.71 mm. Presumably, the result in test 02 can be attributed to the condition, that part of the melt had not yet penetrated into the water, when the spontaneous steam explosion occurred.

As already shown in test 01 (Fig. 5.1.11), the maximum mass fraction in PM18 is shifted to larger particle sizes. This result is typical of a long-term quenching process.

5.5. Results of ECO-05

Objectives in brief

Trying again to improve the experimental conditions, a melt dispersion device (also called melt flow divider) was mounted at the exit of the melt release tube. This was to achieve a wider spread of the melt jet (cf. Fig. A3.1) and, by that, to reduce the average melt penetration speed in the water. Both effects were expected to increase the portion of the melt involved in premixing. The other experimental conditions remained unchanged compared to those in test 04.

Course of events

The melt release was started at a pressure difference of 0.76 MPa at -0.035 s, i.e., when slide valve 1 was opened. The initial development of the pressure in the test vessel (Fig. 5.5.1) was similar to that in test 04: A slow initial pressure increase was followed by a steep increase that was caused by the start of melt penetration into the water. Considering the void data obtained in the water (Fig. 5.5.2) as well as the instant of the steep pressure rise, the first melt/water contact should have been at 0.010 s. In the calculation, this event is delayed a bit; so it was in test 04.

The steep pressure rise in the test vessel resulted in a decrease in the pressure difference which caused, in turn, the melt speed to decrease as well. Gas was fed into the melt generator from about 0.025 s on. The pressure difference became even negative for a short period of time. Nevertheless, due to the kinetic energy of the melt flow, the melt speed remained always positive.

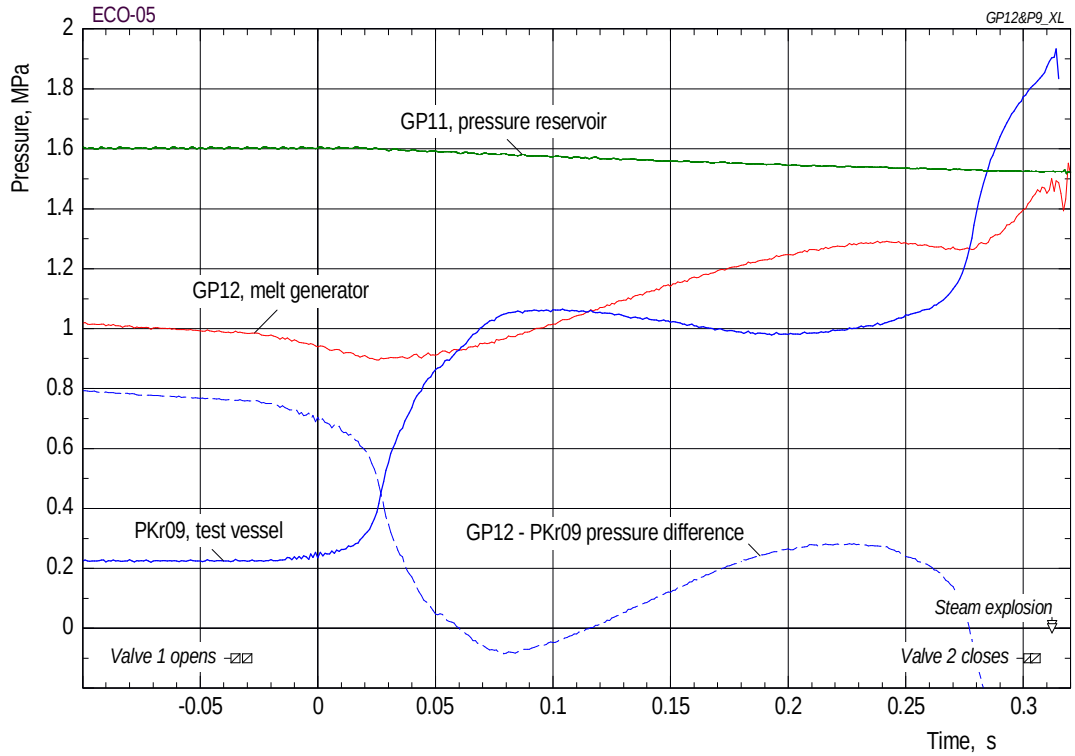

Fig. 5.5.1 ECO-05. Time history of pressures that determined the melt release.

The pressure in the test vessel oscillated slightly. After its first maximum (just above one MPa) it declined a bit (not found in test 04!) before another steep rise occurred at 0.27 s. A pressure of 1.9 MPa was measured when the steam explosion started.

The pressure in the melt generator decreased again between 0.240 and 0.275 s though feeding of gas continued. We conclude that during that time melt and gas were released. For this mind the bend in the (calculated) melt surface line at 0.26 s in Fig. 5.5.2. The faster gas flow entrained the residual melt which is highly accelerated and fragments easily on merging with uprising water (cf. the details given below at the end of the next section). The resulting violent vaporisation is expected to have caused the last steep pressure rise in the test vessel prior to the steam explosion. We further conclude that the last increase in the melt generator pressure was due to gas or steam coming from the test vessel (mind the lines' intersection at 0.275 s!).

The melt release was terminated by closing valve 2 at the time of 0.305 s. Probably, the time limit (criterion no 4) was reached before. At about the same time, the pressure difference fell below the limit set (-0.2 MPa) giving rise to criterion no 3. No steam was indicated so far by the innermost void probes, V02.1 and V01.1.

The steam explosion was triggered a few milliseconds after valve closure. Its enormous strength is indicated by both the pressure records (Fig. 5.5.6) and the large compression of the crushing material, 319 mm. The forces were such that the test facility including the base plate was lifted by about 0.1 m.

A total mass of 16.4 kg of melt had been released (this value is close to the maximum that could be released) while the pressure in the test vessel had reached a value of 1.9 MPa. The calculation of the melt mass released (Fig. 5.5.2) agrees well with the experimental finding. The final position of the melt surface in the crucible acknowledges that essentially all melt was released.

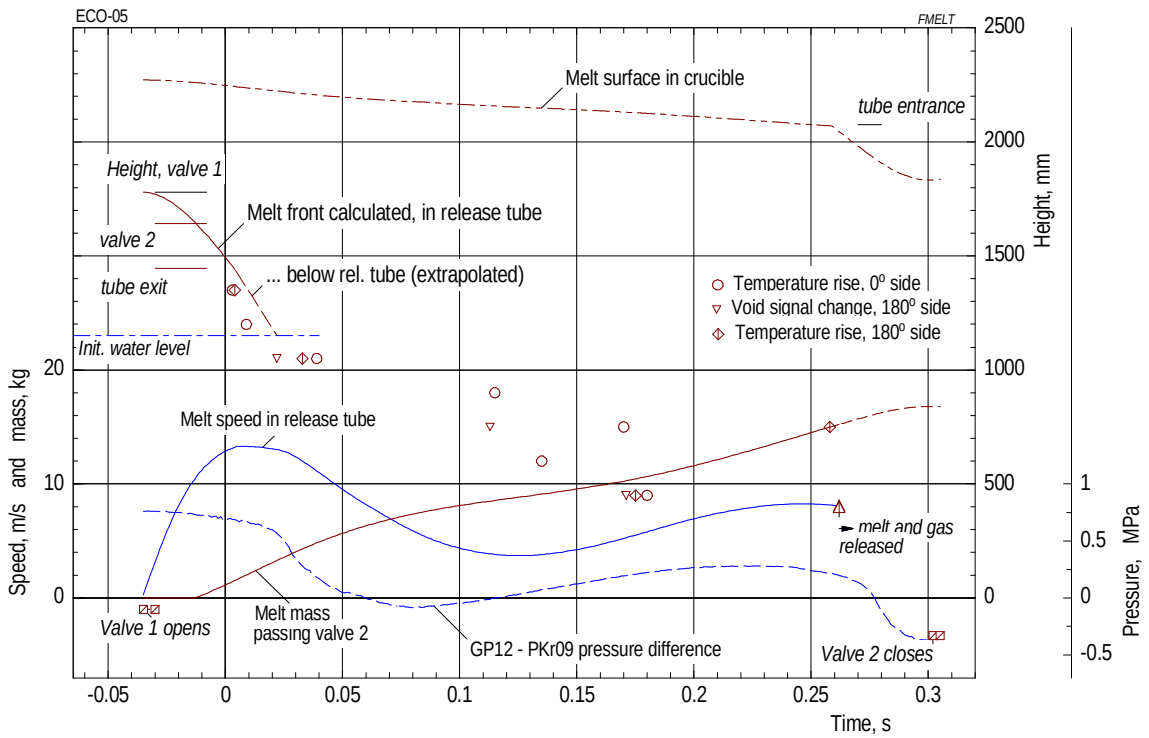

Fig. 5.5.2 ECO-05. Melt release illustrated by calculated and measured data.

Mixing period

The release of melt and mixing took place well inside the restriction tube. Short-term peaks indicating steam appeared in a few void signals that were recorded outside the restriction tube. For this see the numbers in parentheses in Fig. 5.5.5.

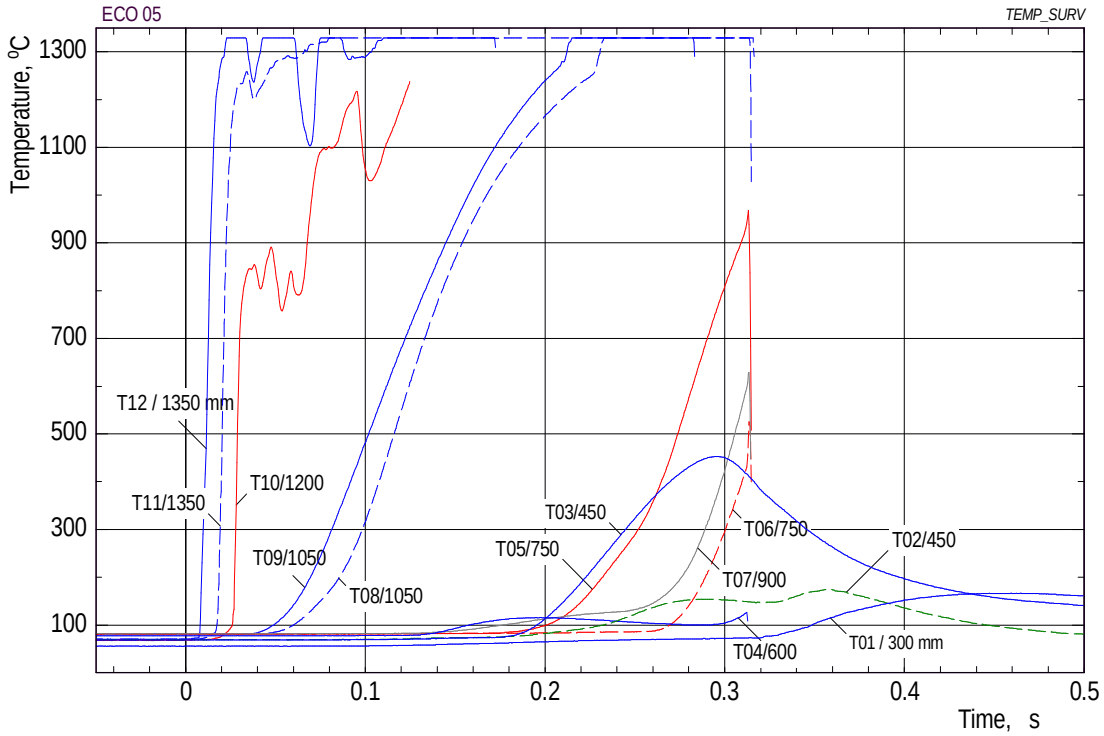

(a) Survey

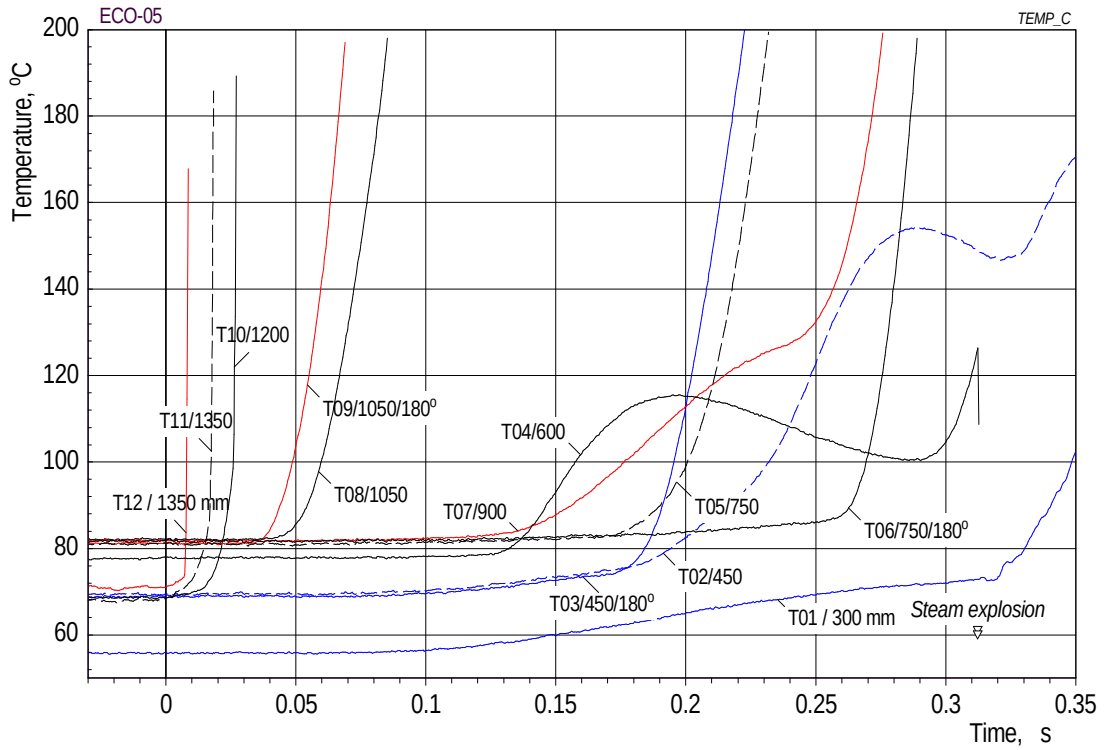

(b) Enlarged scales

Fig. 5.5.3 ECO-05. Time histories of the temperature measurements shown in different scales.

The most important consequence of the melt flow divider is that the melt penetration in the water occurred in a wider radial area, i.e. no more chiefly along the axis as observed in the tests before. By the latter condition, steam was detected by the lowermost inner void probes late, i.e. at the same time when the end of release time was

reached. This enabled utilization of the full release time set and, consequently, the large melt mass released.

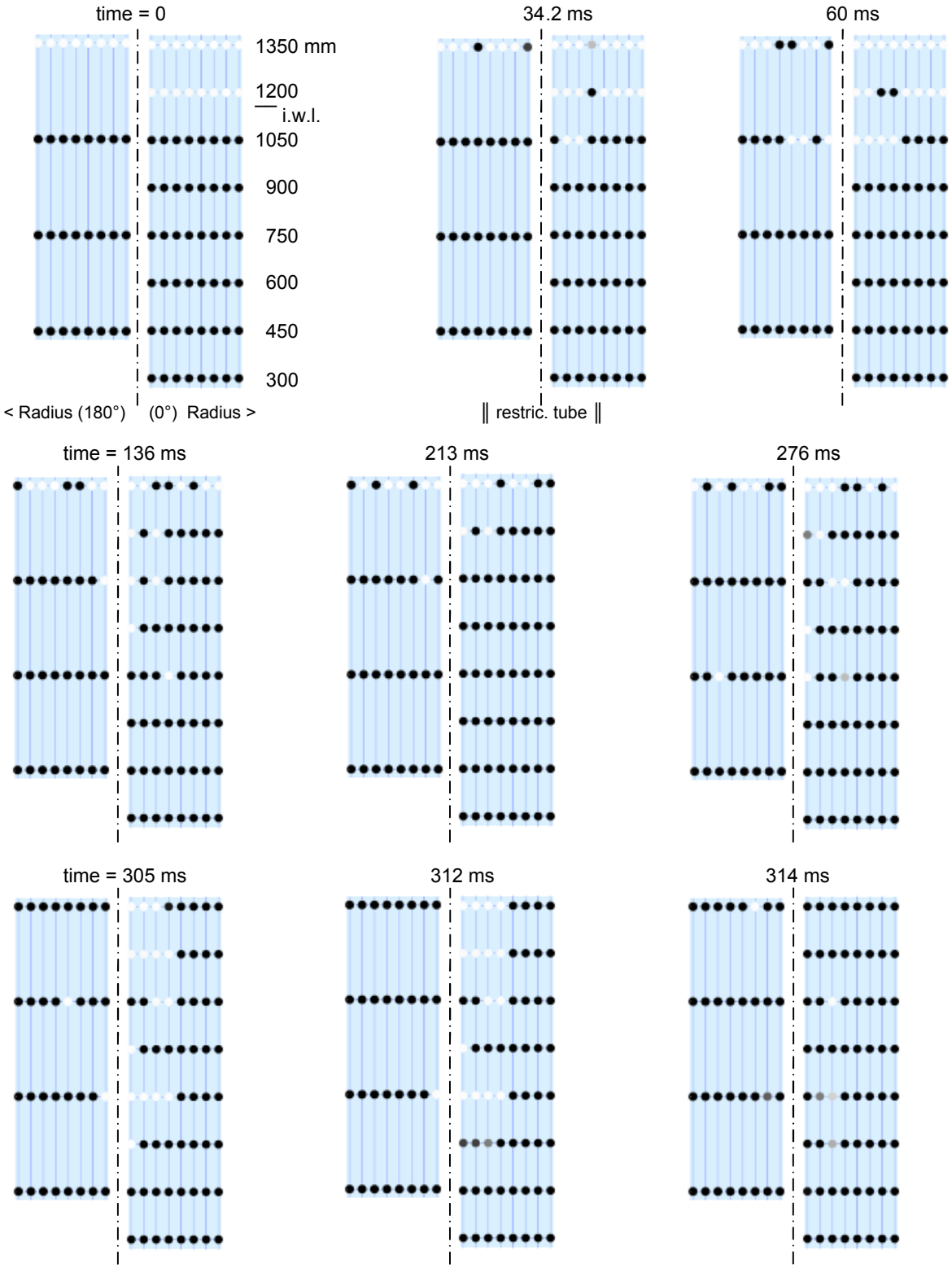

Fig. 5.5.4 ECO-05. Melt penetration mode illustrated by the local distribution of steam and water at increasing times.
For the location of the restriction tube see the sub-line in the 34.2 ms picture. For the meaning of the dots see Figure 5.2.4. The steam explosion started at 0.3124 s.

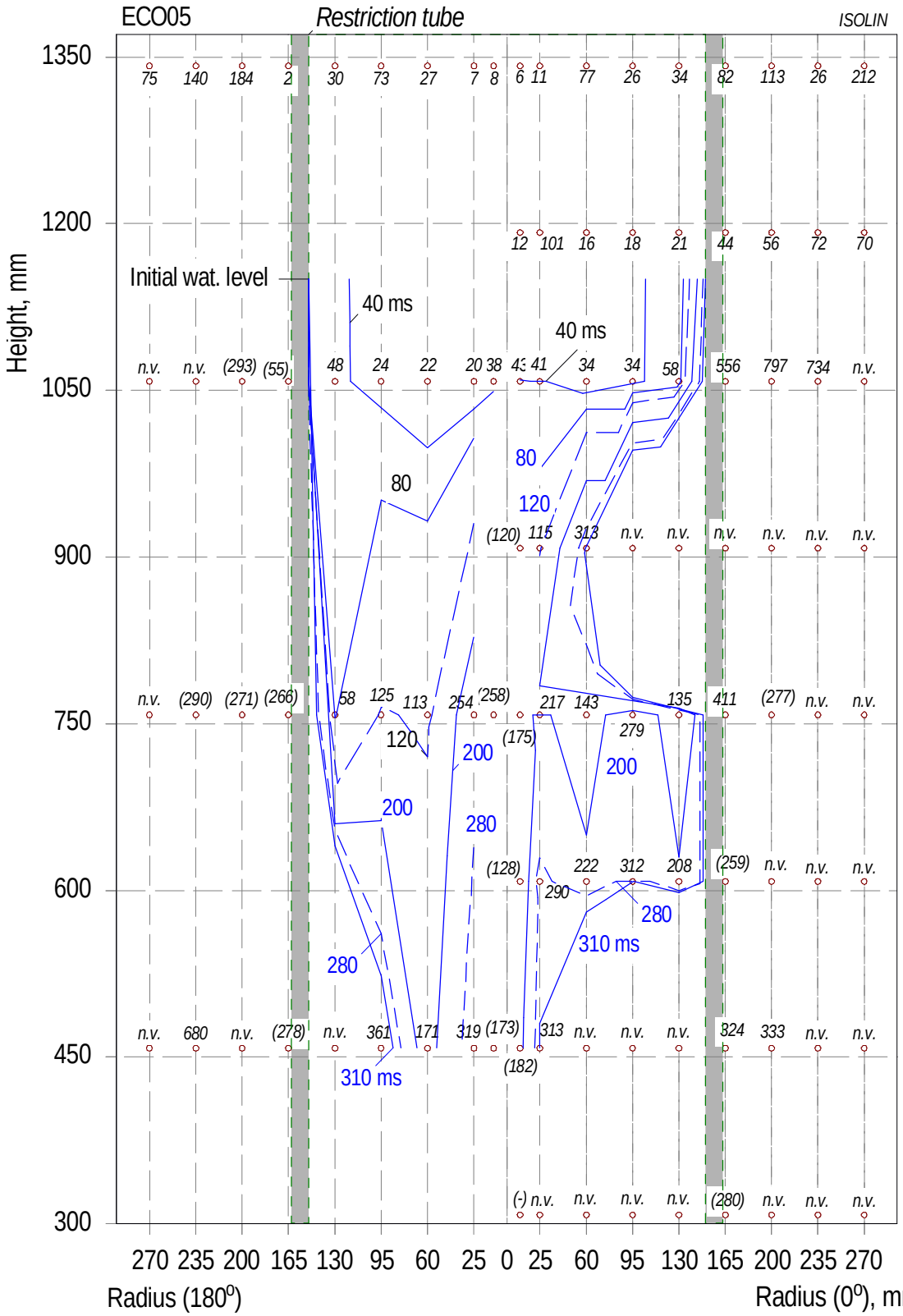

Fig. 5.5.5 ECO-05. Melt penetration in the water with the time as a parameter. The numbers in ms give the instants of first void signal changes (at 25 ... 130 (270) mm radius) and of first temperature rises (at 10 mm radius). Numbers outside the restriction tube have not been considered in the interpolation. "n.v." means: no void detected within one second. The steam explosion started at 0.3124 s.

Another effect of the melt flow divider seems to consist in a rather unsymmetrical melt penetration and distribution of melt fragments during mixing. This impression is conveyed by the scatter of the void and temperature data in one height (Fig. 5.5.2) as well as by the (seemingly random) numbers in milliseconds in Fig. 5.5.5.

The unclear kind of melt penetration makes a calculation of the axial penetration rate difficult. Nonetheless, estimations of the axial penetration rate and of the lower limit of melt penetration are made in the following on basis of the void data noted in Fig. 5.5.5.

1. A trace of melt is identified on the 180° side marked by the void detected at 60 mm radius at the 1050, 750, and 450 mm levels at 22, 113, and 171 ms, respectively. Along this line, speeds of 3.3 ... 5.2 m/s were derived (see also Fig. 6.3). On the other side, no penetration rate can reliably be determined in the centre of the test vessel, neither from void nor from temperature data. Taking the above penetration rate, one can state that it is only about half of that found in test 04.

2. No exact value can be given in test 05 (as in all the following tests performed with the flow divider) for the axial level down to which melt had been penetrated when the steam explosion started. Instead, a level range has been estimated (cf. Section 4.6) on basis of the void and temperature data as well as of dynamic pressure data.

- Extrapolation of the above 22, 113 and 171 ms void numbers obtained at the 180° side (Fig. 5.5.5) would result in the conclusion that part of the melt had reached the bottom of the test vessel, i.e., about 200 mm height (see also Fig. 6.3), before the steam explosion was initiated.
- The increase in the T03 thermocouple signal (Fig. 5.5.3 (b)) starting at 173 ms indicates the immediate lateral approach of the mixing zone. The increase confirms the above 171 ms void number obtained at the same level, 450 mm, at a radial distance of 50 mm. No such evidence of an approach of the mixing zone can be derived for the 300 mm level in the T01 temperature signal.
- The first steep pressure rises well above the trigger amplitude occurred in the PK17 and PK01 signals measured at 200 and 300 mm height, respectively, within a very short time (see below).

Taking these findings into account, we determined the level range, down to which melt had penetrated, to 300 ... 200 mm.

To better understand the above findings in the void and temperature data, let us remind the actual changes in the melt release mode brought about by the dispersion device:

Firstly, the device produced four single dispersed jets while the melt was depleted in the central area.

Secondly, the axes of the measuring lances formed an angle of 20° with one of the two continuous ribs of the dispersion device (cf. Fig. A3.2). The latter condition means that the eight void probes were situated on a secant line that crossed the rim area of one of the four jet flow cross sections. This means that the void probes did not observe the area where the density of melt fragment flow was maximum.

A more integral result is obtained from the void data recorded above the initial water level: The dispersed nature of the melt jet resulted in an enlarged surface and, hence, a larger steam production rate so that the water level was raised stronger than in test 04. Especially outside the restriction tube, the water rose above the 1350 mm level (see Fig. 5.5.4, the graph at 305 ms).

The steam explosion event

The explosion trigger firstly appeared in the PK17 signal (Fig. 5.5.6). It moved upwards at a speed of about 600 m/s dying out. The family of lines in this figure indicates two major pressure events.

The interaction started in the lower part of the pool with a delay of 2.5 ms to the trigger. The first pressure rise was recorded at elevation 200 mm (again in PK17) at 0.3122 s The signals of the pressure transducers positioned at heights up to 750 mm followed within a very short time (to be exact, within 0.1 ms).

From elevation 750 mm on, the first pressure event proceeded upwards at a speed of about 850 m/s, again not escalating but loosing strength. The peak pressures of this event are way above the measuring range chosen for this test, i.e. 45 MPa. They probably reach above 60 to 70 MPa which is about twice as high as in test 04. The duration was little more than one ms; this is similar to that in test 04.

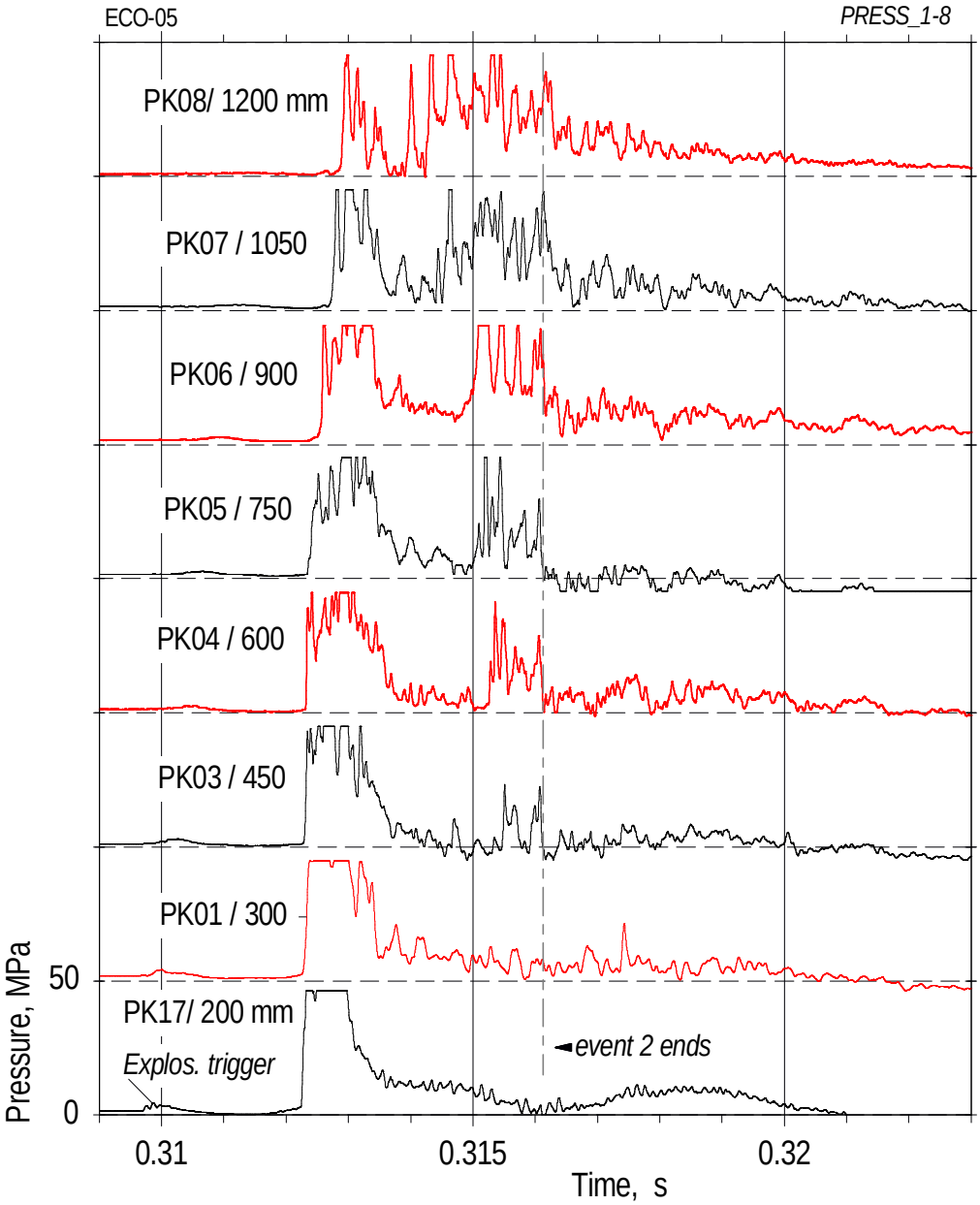

Fig. 5.5.6 ECO-05. Dynamic pressures measured during the steam explosion.

The second pressure event might consist of several interactions which started in the upper part of the test vessel (PK08) just before 0.314 s. At that time, the void probes (Fig. 5.5.4) indicate that, in contrast with the conditions at 0.312 s, the upper (originally free) volume inside the restriction tube was completely filled with water; this remained so for several milliseconds. The above interactions went on for about 2 ms. There might have been some escalation on the way down, but below the level of 900 mm, the pressure wave died out quickly.

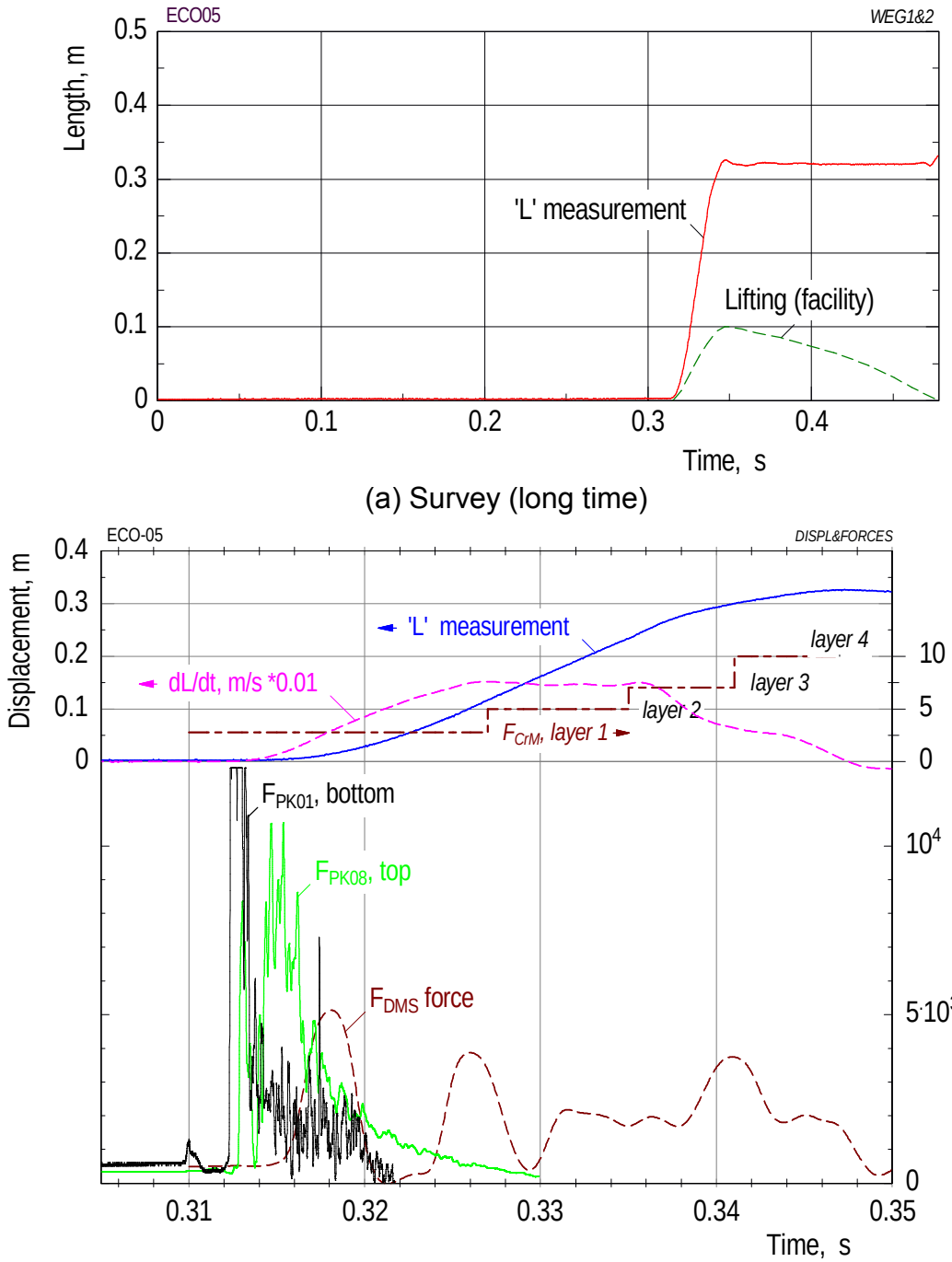

Fig. 5.5.7 ECO-05. Measurements quantifying the extent of the steam explosion: The piston and facility movements; forces derived from pressure and DMS data. The F_{CrM} forces impressed to the layers of the crushing material are drawn in chronological order of their probable responses.

The overall course of events is similar to that in test 04: The first pressure event (F_{PK01} in Fig. 5.5.7) caused the piston to move, accelerating the overlying water at the same time.

The second pressure event was predominant in the uppermost part of the test vessel. It lasted essentially from 0.314 to 0.316 s, ending abruptly in all signals (see the auxiliary line in Fig. 5.5.6). It acted on the bottom of the melt generator base (i.e. the roof of the interaction zone) as a kind of water hammer. The impact of water caused the test facility including the base plate to move up. The time history of this movement (Fig. 5.5.8) has been taken from high-speed film frames, the start being at 0.315 s.

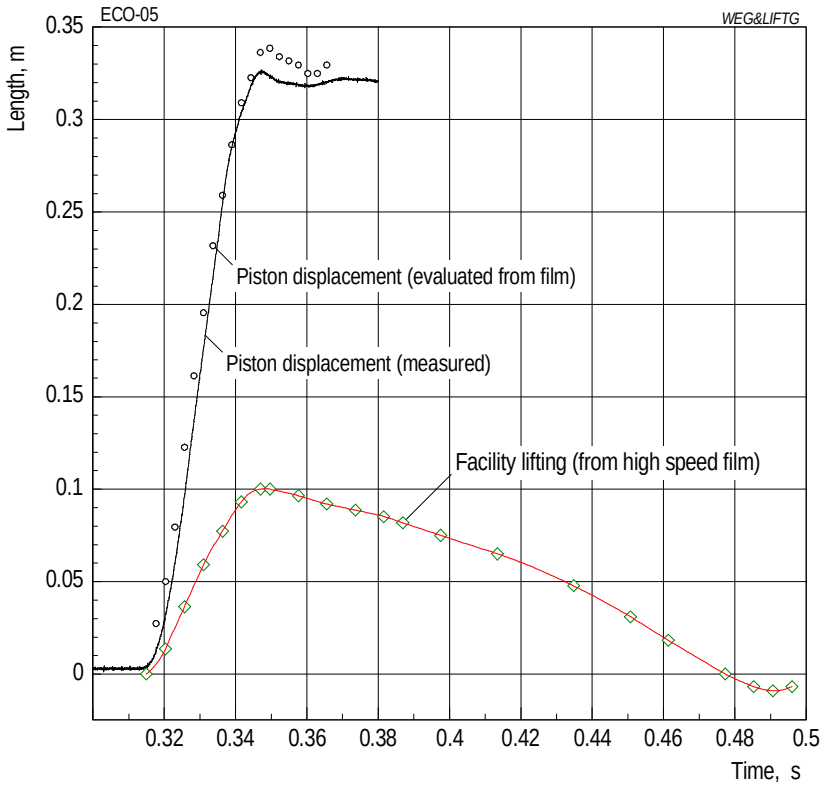

Fig. 5.5.8 ECO-05. Lifting-up of the test facility. The time history of the piston displacement is shown for comparison.

The photographs in Figs. 5.5.9 and 5.5.10 give an impression of the strength of the steam explosion in test 05. The two uppermost layers of crushing material were maximally compressed, i.e. by around 118 mm each, the third by 80 mm, and the remaining two by only a few millimeters each.

The restriction tube (Fig. 5.5.10, right photograph) was locally widened in diameter by several millimetres; the maximum of the bump is situated at about 500 mm height, i.e. the approximate axial location where the steam explosion started. The photograph on the left shows in the foreground the bottom side of the tube. Three sections had been cut out at the lower end of the restriction tube to allow the water to escape into the large radial space between tube and vessel wall during the mixing and steam explosion periods. The deformation at this end is clearly to be seen. Three small blocks mounted to the lower end of the tube served as spacers within the bottom design of the test vessel.

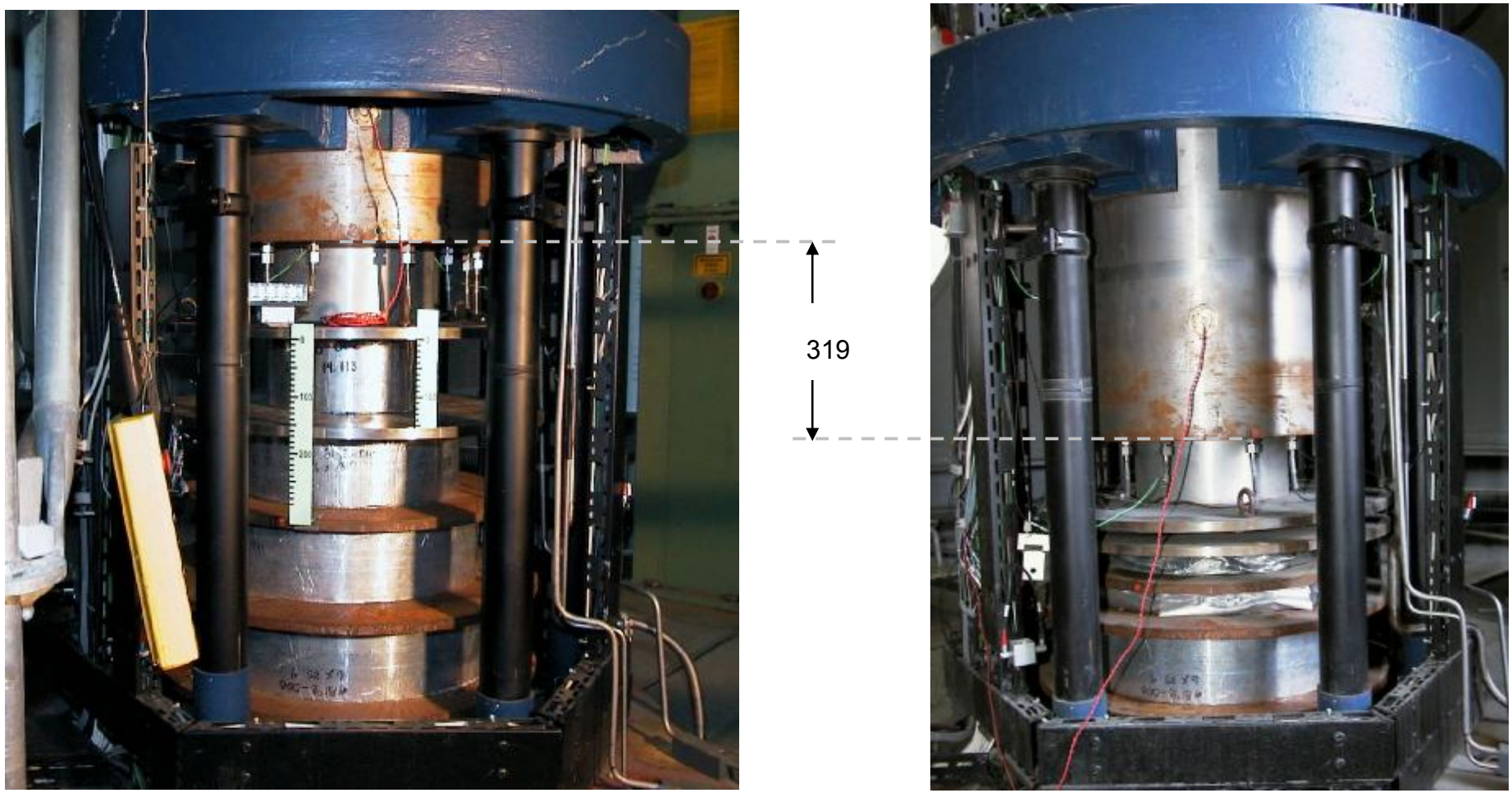

Before ...

... after the test

Fig. 5.5.9 ECO-05. Compression of the stack of crushing material.

Fig. 5.5.10 ECO-05. Plastic deformations of the restriction tube caused by the steam explosion.

Evaluation of the energy conversion

The total deformation of 319 mm gives a work of W = 1.49 MJ. The heat content of the melt is estimated to be Q = 62.3 MJ, based on a melt mass of 16.4 kg. So one obtains an energy conversion factor of η = 2.39 %.

The strong pressure imbalance existing between the lowermost part of the interaction region and the top (Fig. 5.5.7) accelerated, as mentioned, part of the water (and melt) towards the bottom of the melt generator. Using eqs. (6) to (9), page 21, the difference in the PK03 and PK08 pressures, and a water height of 0.7 m, a value for the kinetic energy of 0.28 MJ is found. This would add 0.4 % to the energy conversion factor.

The movement of the whole facility (Fig. 5.5.8) started at the same time as the second pressure event did. This movement, which largely comes from the kinetic energy of the water that hit the bottom of the melt generator, involved another about 0.1 % of the thermal energy.

Post test examinations

No recovery of the melt fragments was possible in test 05 due to a leak that occurred in the bottom of the vessel at the end of the explosion period. The water inventory including the suspended melt fragments drained off almost completely through the leak.

5.6. Results of ECO-06

Objectives in brief

The main purpose of the test was a repetition of test 05 to test the reproducibility (compare Table 3). The measuring range of the pressure transducers was raised to 90 MPa and an endoscopic high-speed video system was installed to observe the melt stream on its way from the tube outlet to the water surface.

Course of events

The pressure time histories in test 06 (Fig. 5.6.1) are quite similar to those in test 05. The slow increase in the test vessel pressure after opening of valve 1 was followed by a steep rise ending in a first maximum. This steep rise started at 0.01 s.

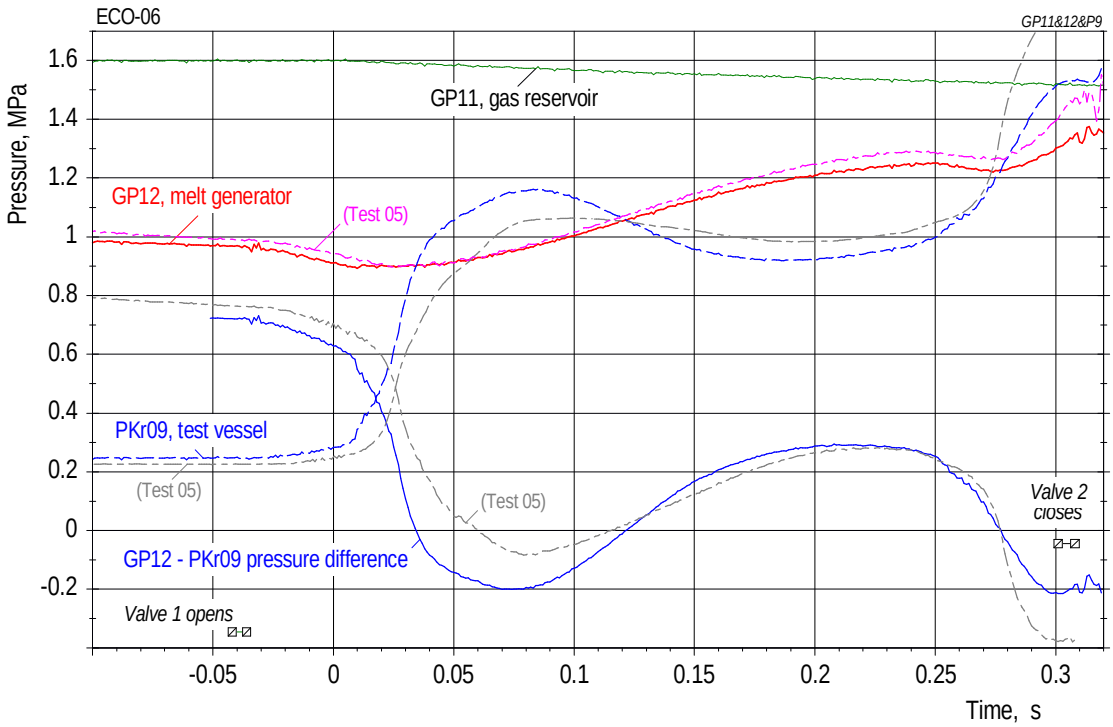

Fig. 5.6.1 ECO-06. Time history of pressures that determined the melt release. Comparison is made with results of test 05.

As a consequence of this, the pressure difference became negative. Gas was fed into the crucible from 0.01 seconds on to compensate the decrease in pressure difference. Nonetheless, the latter became negative for a time of 90 ms which is markedly longer than that in test 05. Still, the melt speed remained always positive (see Fig. 5.6.2) owing to the kinetic energy of the melt. Back in the positive range, the pressure differences in both tests behaved in a similar way. So did the pressures in the melt generator: Towards the end of the mixing period, both curves decreased a bit due to the release of gas (together with residual melt), and then rose again after the intersection with test vessel pressure lines. Melt release was terminated, as in test 05, by closing valve 2 when the end of the time interval (criterion no 4) was reached. In the end, the pressure in the test vessel attained a value of 1.53 MPa.

The steam explosion was triggered a few milliseconds after closure of valve 2. Its strength is indicated by the pressures (Fig. 5.6.5) and the compression of the crushing material by 151 mm. The latter value is only half of that in test 05. The forces were such that the facility was lifted by 0.04 m. This is less than half of that in test 05.

A mass of melt of 15.2 kg had been released, i.e. 7% less than that in test 05. The smaller mass in test 06 is ascribed to the longer period of time in which the pressure difference was negative. The calculated melt mass (Fig. 5.6.2) agrees with the experimental finding, while the calculated level of the melt surface in the crucible (uppermost curve) had just reached the upper end of the release tube.

In test 06, for the first time, an endoscope high-speed video system was employed in the test vessel. With that system, melt was observed to arrive at the tube exit at −0.019 s already and the leading edge of the melt to contact the water surface at −0.007 s. This information has been included in Fig. 5.6.2.

Examples of the film pictures have been reproduced in Appendix A, Fig. A5.1. On basis of the information gained from the film and regarding the actual (finite) valve opening time of 5 ms, we presume that, initially, part of the melt travelled at a larger speed than estimated in the calculation.

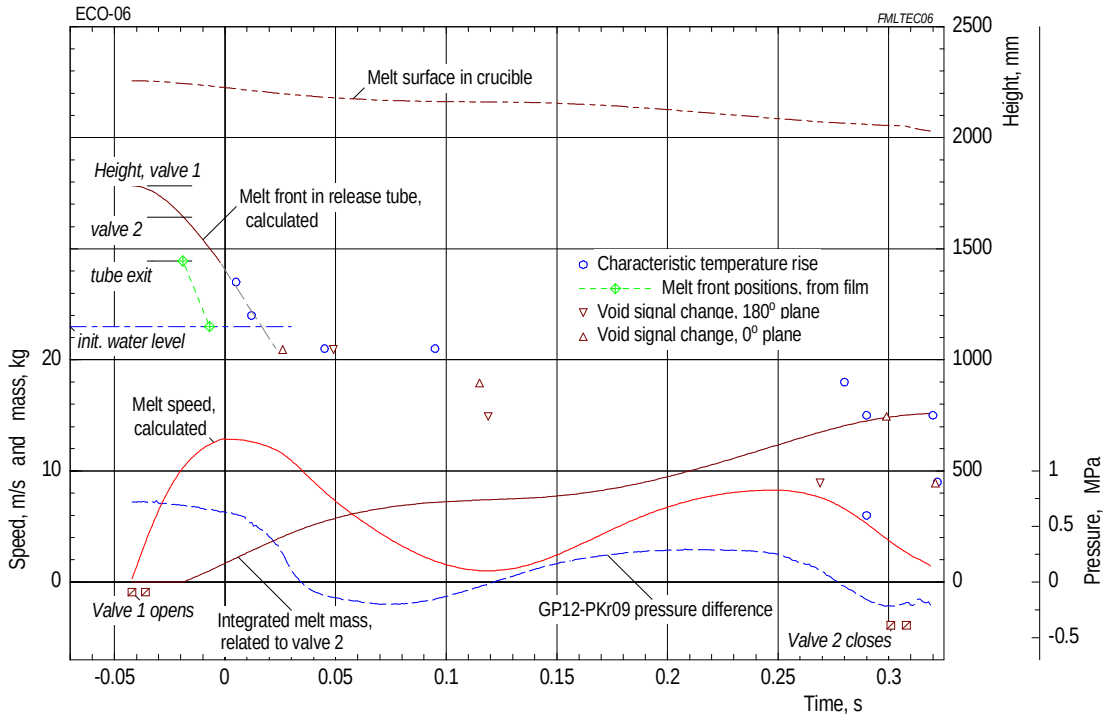

Fig. 5.6.2 ECO-06. Melt release illustrated by calculated and measured data.

Mixing period

Penetration of melt into the water as well as mixing took place, as in test 05, inside the restriction tube. However, the mode of melt penetration in test 06 is found to be partly different from that in test 05 (compare Figs. 5.6.5 and 5.5.5), though the starting conditions were largely the same. It should be mentioned here that the partition wall of the flow dispersion device was mounted in test 06 at a smaller (absolute) angle (-10° instead of 20°, cf. Fig. A3.2) relative to the axes of the measuring lances. The changed condition moved, in principle, the maximum density of melt fragment flow a bit further away from the void measuring lances.

One could conclude from the lines in Fig. 5.6.5 that the mixing zone remained, up to the time of 0.30 s, essentially above the 600 mm level. For this see the time history of the T04 signal (same level, Fig. 5.6.3 (b)) which increases steeply only after the steam explosion. However, the steep rise in the T03 signal and the data obtained at the 450 mm level / 180° side (see the 269 and 317 ms numbers, Fig. 5.6.5) show that

melt had been at, respectively below, this level at the instant of steam explosion.

As for the additional thermocouples mounted in test 06 in the pool: the T13 and T15 time histories agree with those measured at the same levels, 900 and 450 mm. The two sensors located outside the restriction tube, T14 and T16, show small changes and little reactions during the mixing and explosion periods, respectively.

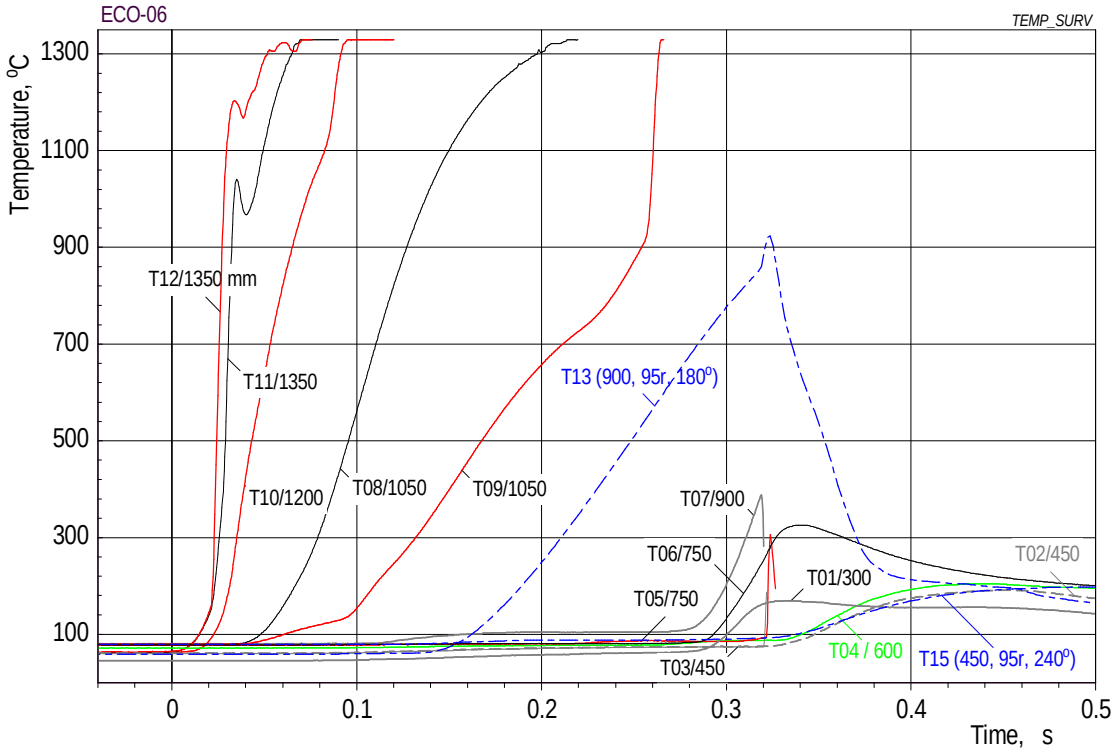

(a) Survey

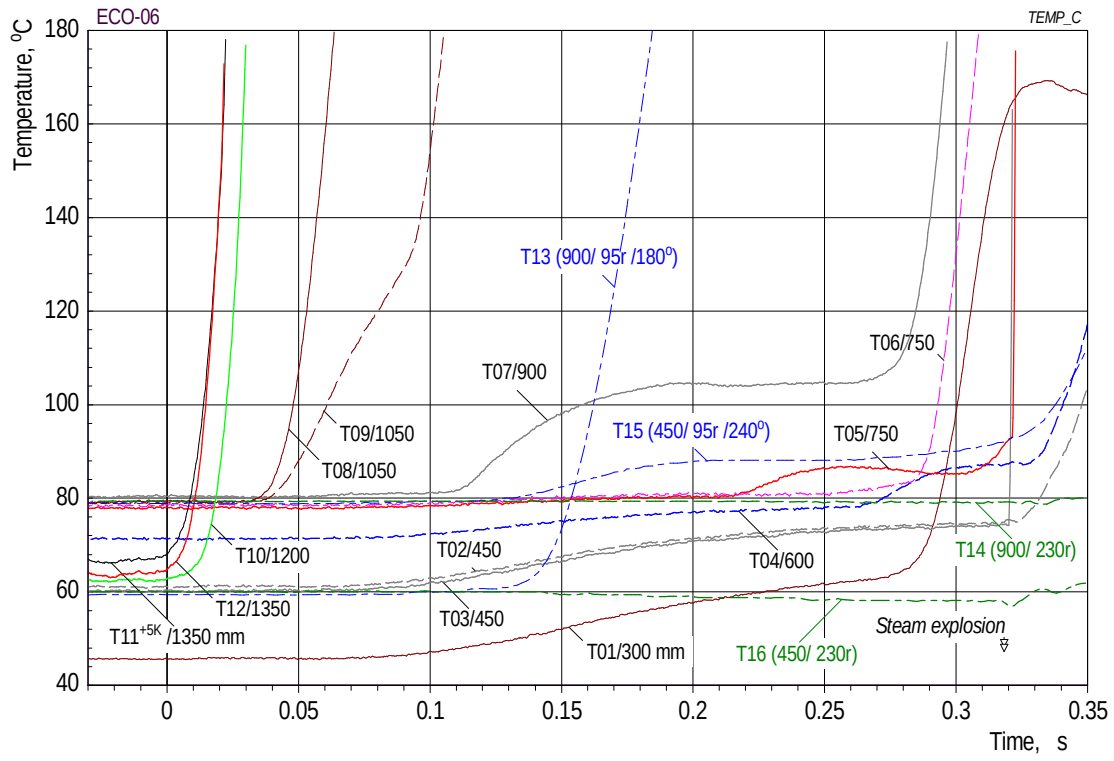

(b) Enlarged scales

Fig. 5.6.3 ECO-06. Time histories of the temperatures shown in different scales.

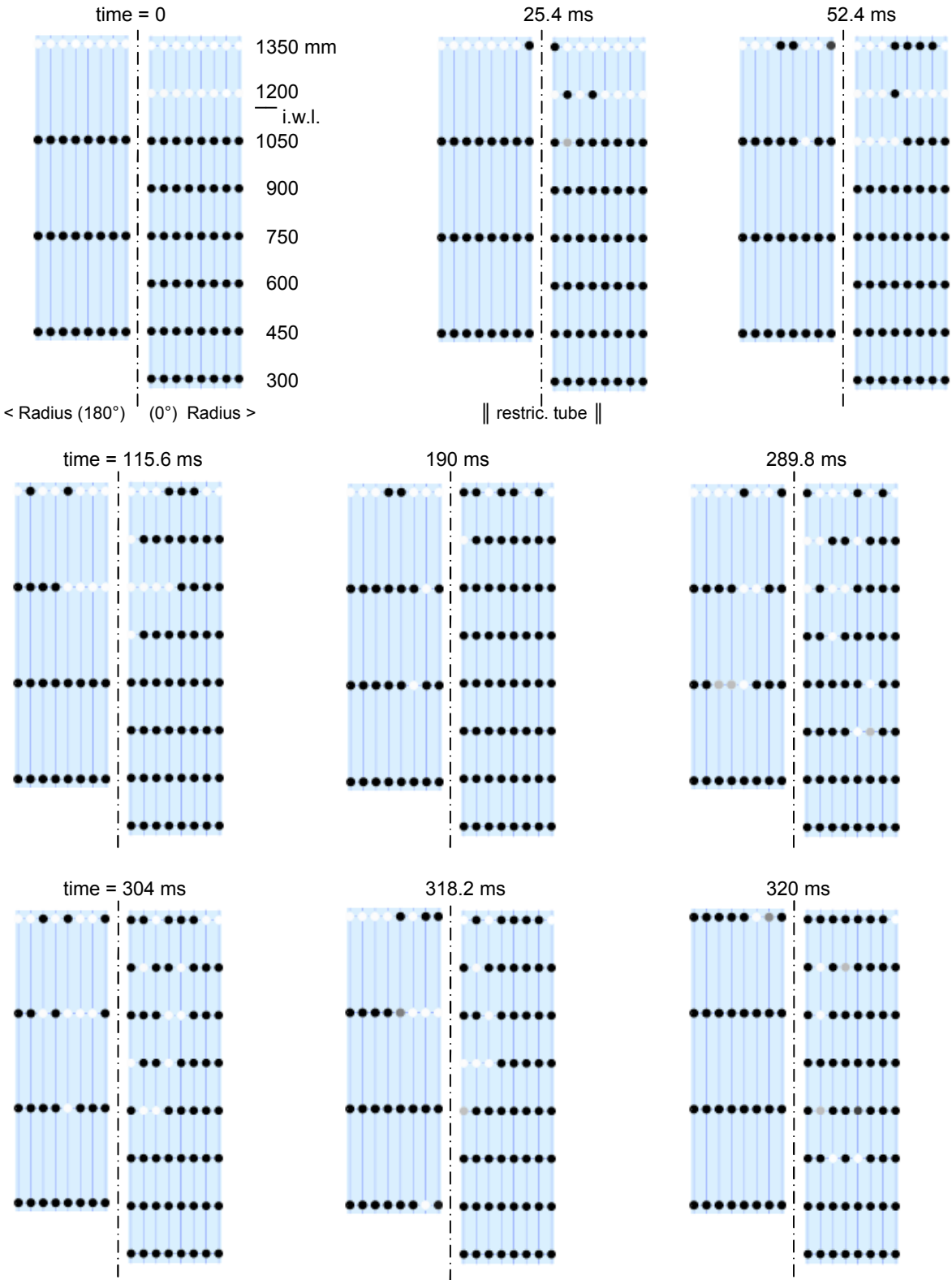

Fig. 5.6.4 ECO-06. Melt penetration mode illustrated by the local distribution of steam and water at increasing times.
The steam explosion started at 0.3184 s.

The rate of melt penetration in the water was estimated using the 49, 119, and 269 void numbers measured at the 180° side (Fig. 5.6.5). From top to bottom, rates of 4.3 and 2.0 m/s were calculated (compare also the rates depicted in Fig. 6.3). These rates are similar to those obtained in test 05.

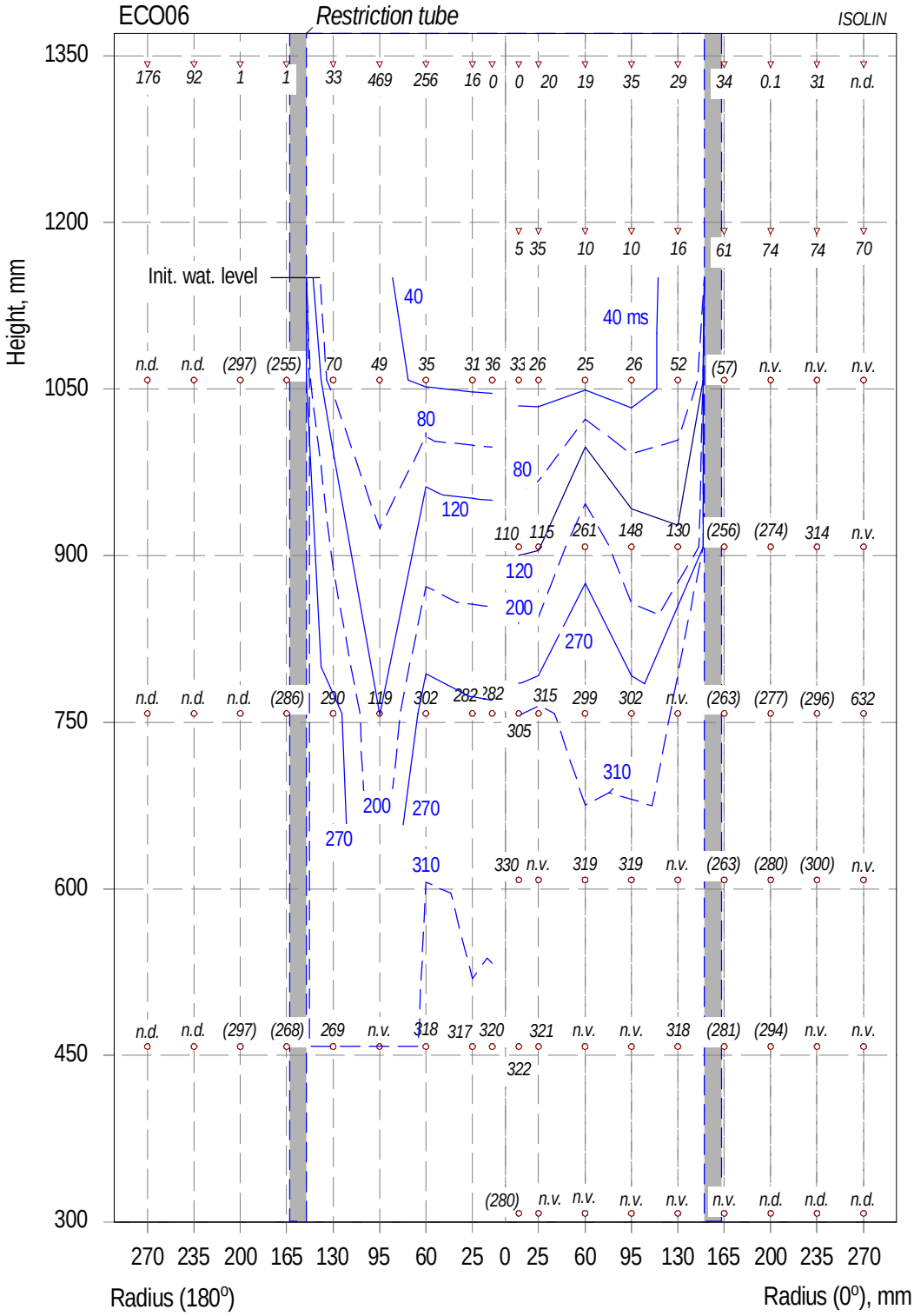

Fig. 5.6.5 ECO-06. Melt penetration in the water with the time as a parameter. Numbers in ms give the instants of first changes in the void signals. Temperature data (noted at 10 mm radius) denote the instants of first marked increases. The lines represent outmost boundaries of the mixing zone to the bulk of water. Data outside the restriction tube were not considered in the interpolation. n.v. means: no void detected within one second; n.d.: no data available. The steam explosion started at 0.3183 s.

The level down to which melt penetrated prior to the start of the steam explosion, is estimated to be between 450 and 400 mm. The first number is identical with the level where the first pressure rise was measured (Fig. 5.6.6), the second was determined by extrapolating the void data (Fig. 6.3). The melt-to-water mass ratio amounts to 0.310 ... 0.290.

The steam explosion event

In this test, the interaction clearly started at the 450 mm level at 0.3183 s, i.e., 3.5 ms after the explosion trigger appeared in the PK17 signal (Fig. 5.6.6). The steam explosion in test 06 was weaker than in test 05, although some peak pressures exceeded the measuring range of 90 MPa, the highest range which has been applied so far. The interaction propagated upward and downward at a speed of about 1500 m/s which corresponds to the sonic speed in water but is too fast for a pressure wave propagation in a multi-phase zone.

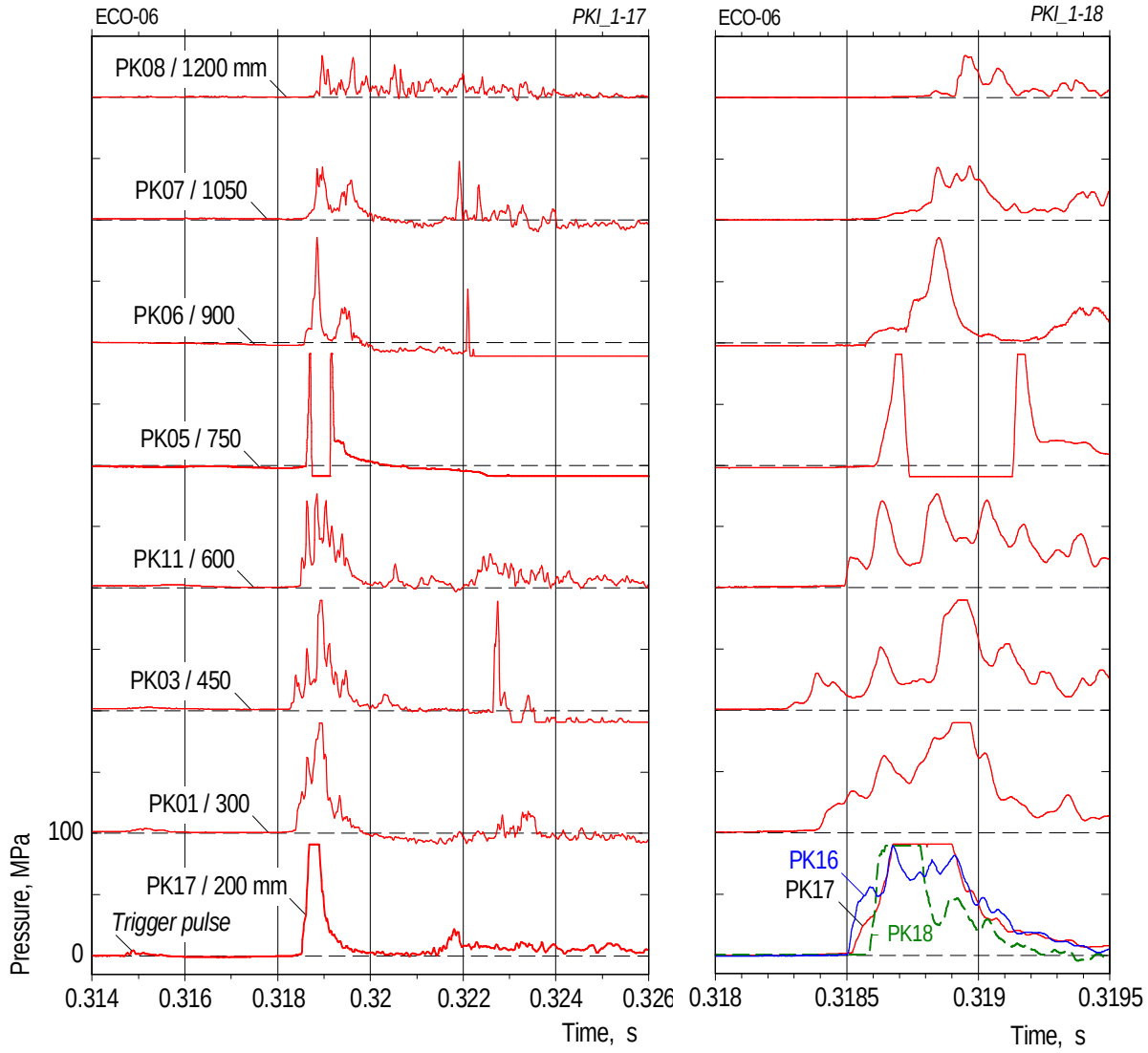

Fig. 5.6.6 ECO-06. Dynamic pressures shown in different time scales.

There was a second pressure event in test 06 as well, but it was weaker, too, and started at the 1050 mm level with a delay of about 3 ms to the first one. We conclude from the start position of the steam explosion (450 mm) that there was no melt below

that level. Hence, the pressure signals recorded there indicate pure pressure wave progagation in the water. On the other side, the pressures recorded above that position are attributed to a progressive triggering of the steam explosion at increasingly higher elevations.

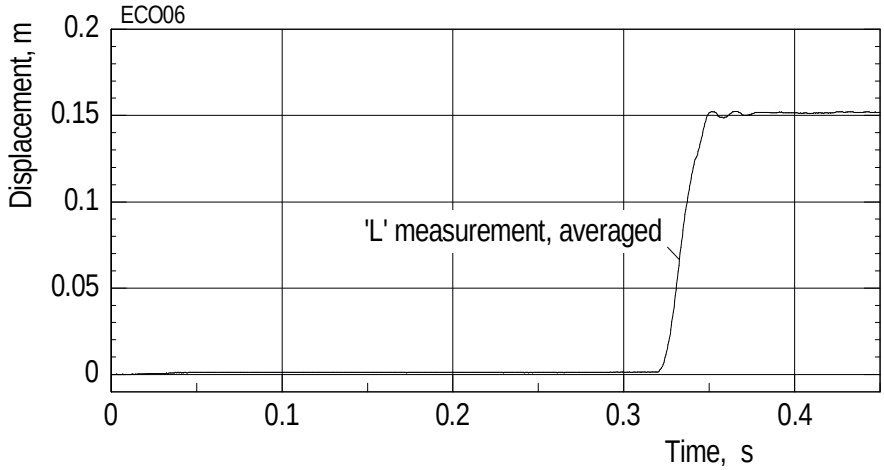

(a) Survey (long time)

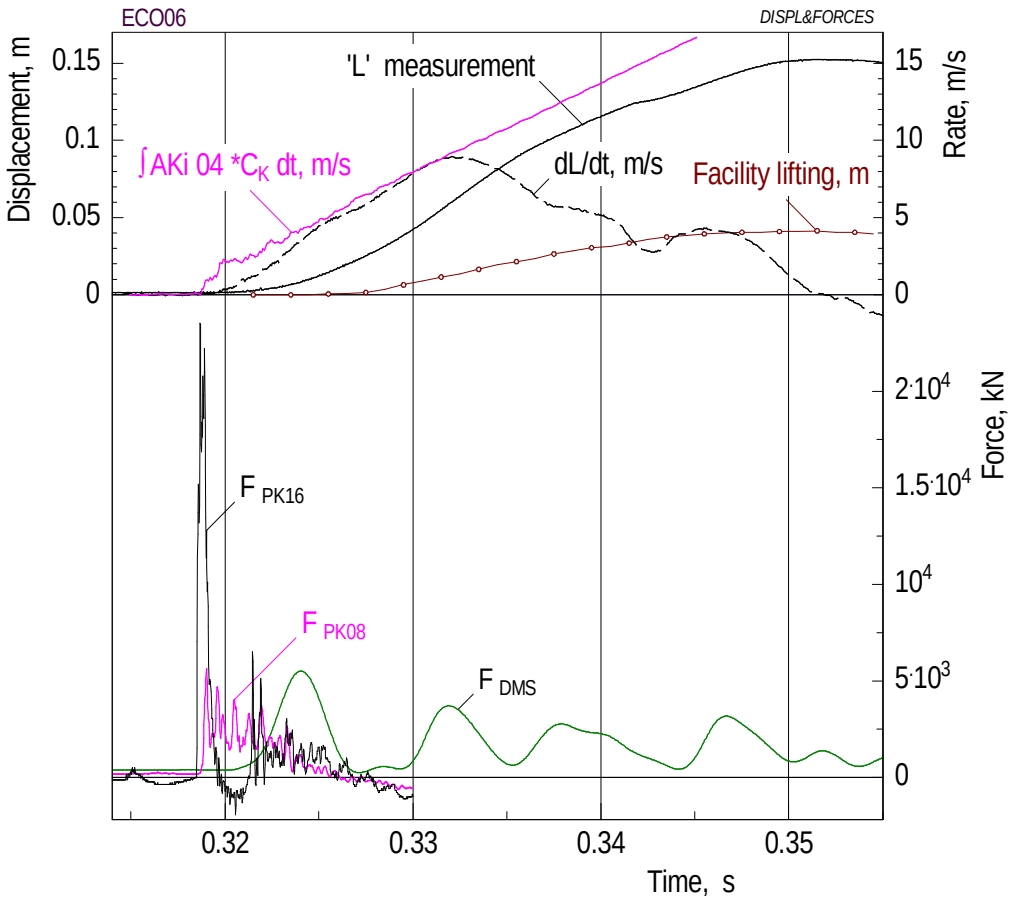

(b) Steam explosion

Fig. 5.6.7 ECO-06. Measurements quantifying the extent of the steam explosion: The piston movement, L, and its differential function, the lifting of the faciliy, and forces derived from pressure and strain gauge data. C_K is a constant used to calibrate the AK04 acceleration signal.

The piston moved down by 151 mm (Fig. 5.6.7), with the first and second layers being compressed by 101 and 50 mm, respectively. The facility was lifted by 0.04 m. The integrated AKi04 acceleration signal, also drawn in the graph, gives the rate of the piston movement. It is in an approximate qualitative agreement with the derivative of the 'L' measurement, dL/dt, as long as the acceleration of the piston in the downward direction, d^2L/dt^2, is positive.

Evaluation of the energy conversion

The compression of the crushing material of 151 mm gives a work of

W = 0.461 MJ.

The heat content of the melt, based on a melt mass of 15.2 kg, amounts to 57.8 MJ. So one obtains an energy conversion factor of η = 0.80 %. This is only one third compared to that in test 05.

5.7. Results of ECO-07

Objectives in brief

The purpose of the test was to investigate the effect of the restriction tube (which was omitted in this test), in conjunction with the melt flow divider, on the mixing process and on the steam explosion. The other test conditions (cf. Table 3) were the same as in test 05.

Course of events

Melt release started at a pressure difference of 0.76 MPa at -0.028 s, i.e., when valve 1 was opened (Fig. 5.7.1). This event caused, besides the well-known pressure decrease in the melt generator, a slight pressure increase in the test vessel. A comparison shows that the increase was steeper than in test 05 (as well as in tests 06 and 04).

We conclude from the endoscope pictures, that the first melt-water contact took place at 0.007 s (Fig. 5.7.2). From that time on, the pressure in the test vessel rose, slightly oscillating, more steeply to a first maximum of 1.04 MPa. The following oscillation was more pronounced than in the two tests before: The pressure dropped to 0.7 MPa before reaching its first maximum again. This large pressure drop is thought to be an effect of the missing restriction tube (see below). The pressure declined again, more gently, to 0.98 MPa at the time of triggering.

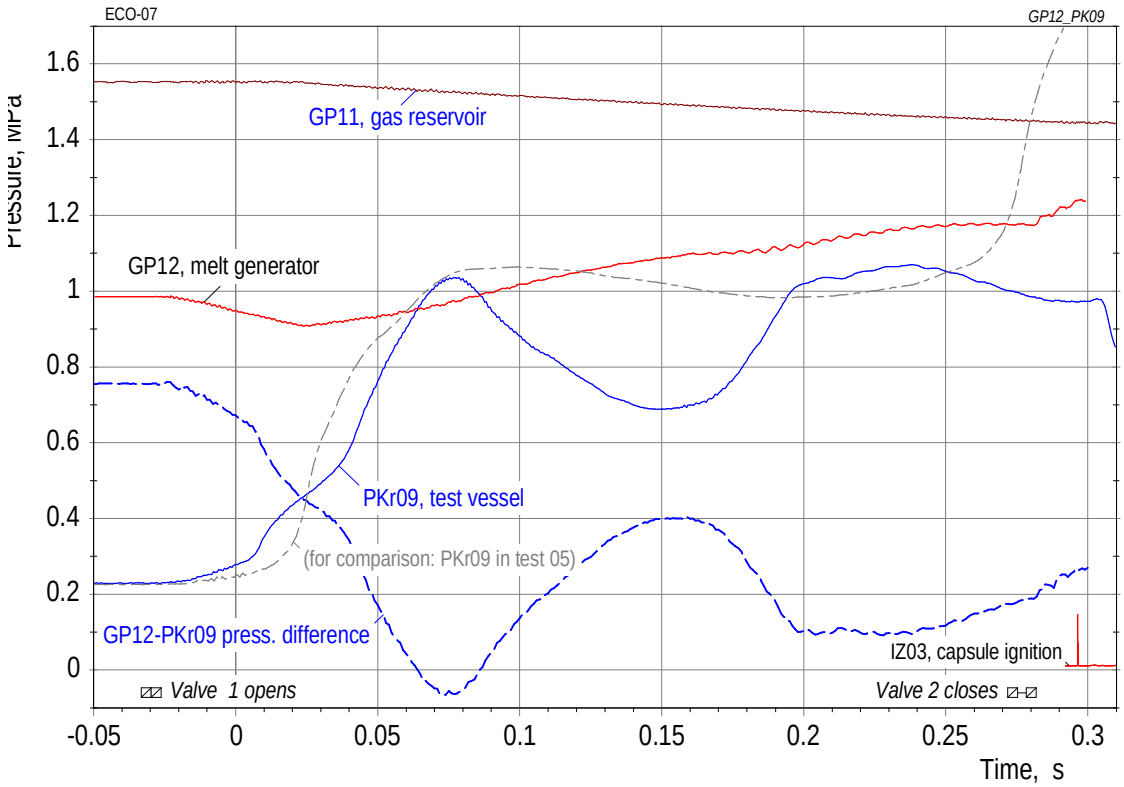

Fig. 5.7.1 ECO-07. Time history of pressures that determined the melt release. The IZ03 signal indicates the time when the explosion capsules were ignited. Comparison is made with the test vessel pressure in test 05.

We recognize in test 07, as in the tests before, the interdependence of subsequent events, such as the first pressure increase, the decline in the pressure difference, melt release rate, and vapour production, respectively, followed by a recovery

of the pressure difference, melt release rate, vapour production, and pressure in the test vessel, respectively, and so on. The more pronounced oscillation in the test vessel pressure is attributed to a larger condensation rate (heat sink) due to the missing restriction tube (see next section but one).

Gas was fed into the crucible from about 0.025 s until the end of melt release. The pressure in the crucible remained constant after 0.250 s. We presume that gas was released together with the melt from that time on.

Melt release was terminated by closing valve 2 at 0.280 s. A total of 15.2 kg of melt had been released, i.e., the same amount as in test 06. The calculation – performed with the standard friction and loss coefficients as listed in Table A4.1 – predicts a larger melt mass released (18 kg, cf. Fig. 5.7.2). Agreement in the masses is obtained with friction and loss coefficients that are increased by around 60% each.

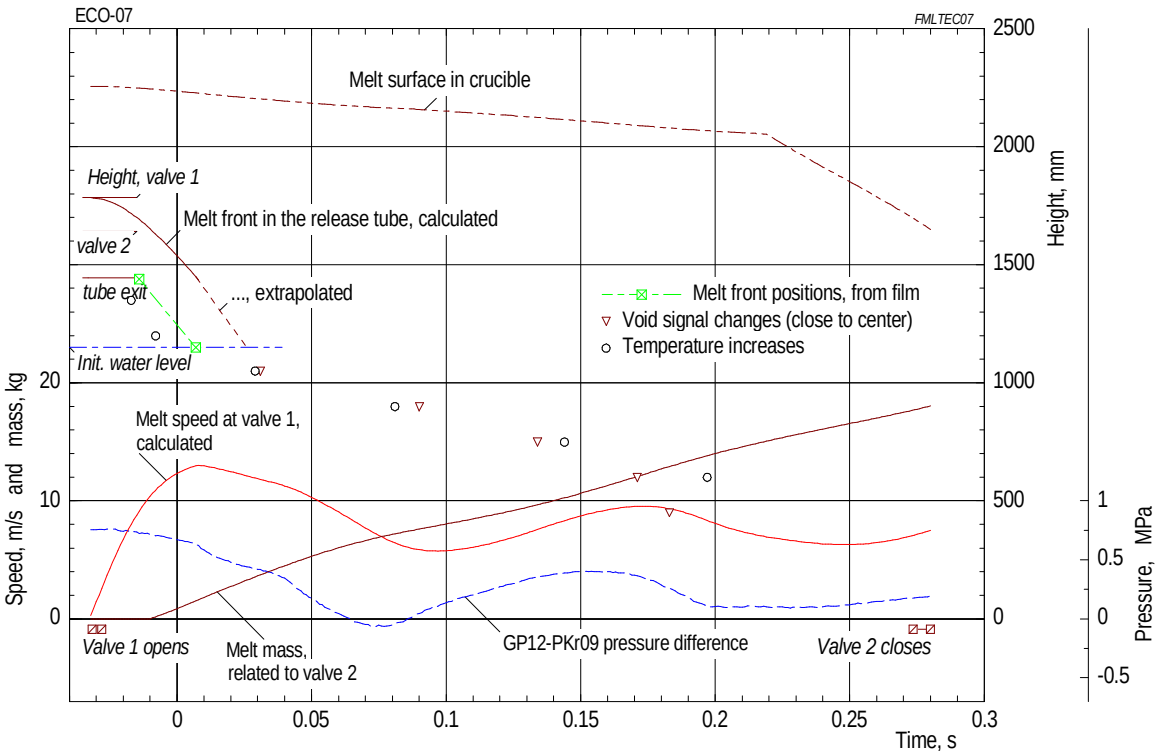

Fig. 5.7.2 ECO-07. Melt release illustrated by calculated and measured data.

The explosion capsules were ignited at 0.296 s, but no steam explosion was triggered. A reason of the missing explosion may be the weak pressure peak, about 0.4 MPa, coming from the explosion capsules (Fig. 5.7.6). The peak which was much weaker than in previous tests was obviously not able to trigger a steam explosion.

Mixing period

The penetration of the melt into the water (see Fig. 5.7.4) occurred in rather unsymmetrical way. The penetration rate seemed to be faster on the 0° side. Speeds between 5.2 and 3.3 m/s were derived along the trace of the void data at 95 mm radius. At the end of melt release, i.e. when valve 2 closed, the axial extensions of the mixing zone at the 0° and 180° sides differed by around 300 mm.

The radial extension of the mixing zone was 200 and 165 mm at the 0° and 180° sides, respectively (Fig. 5.7.4). This gives a cross section that is almost twice as large as that within the restriction tube. Though no void signal changes were measured at a radius larger than 200 mm as well as at a level below 450 mm, there is

positive evidence from the extrapolation of the void signal numbers in Fig. 5.7.4, that the mixing zone extended beyond these limits.

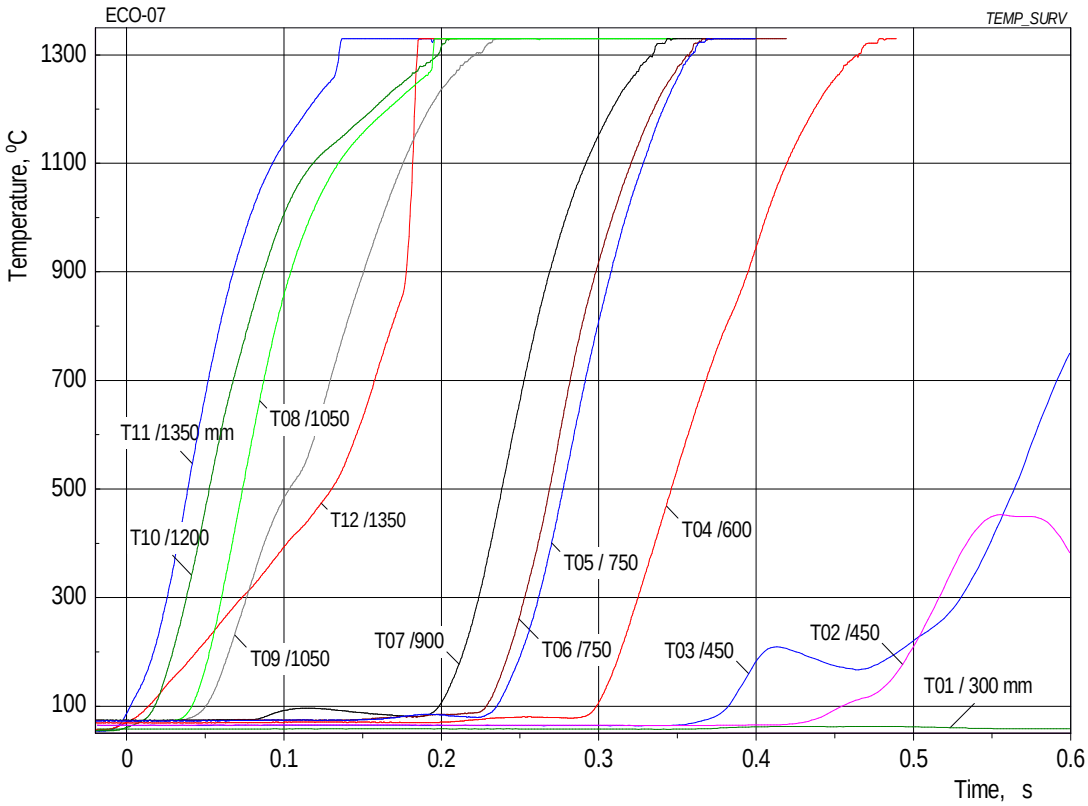

(a) Survey

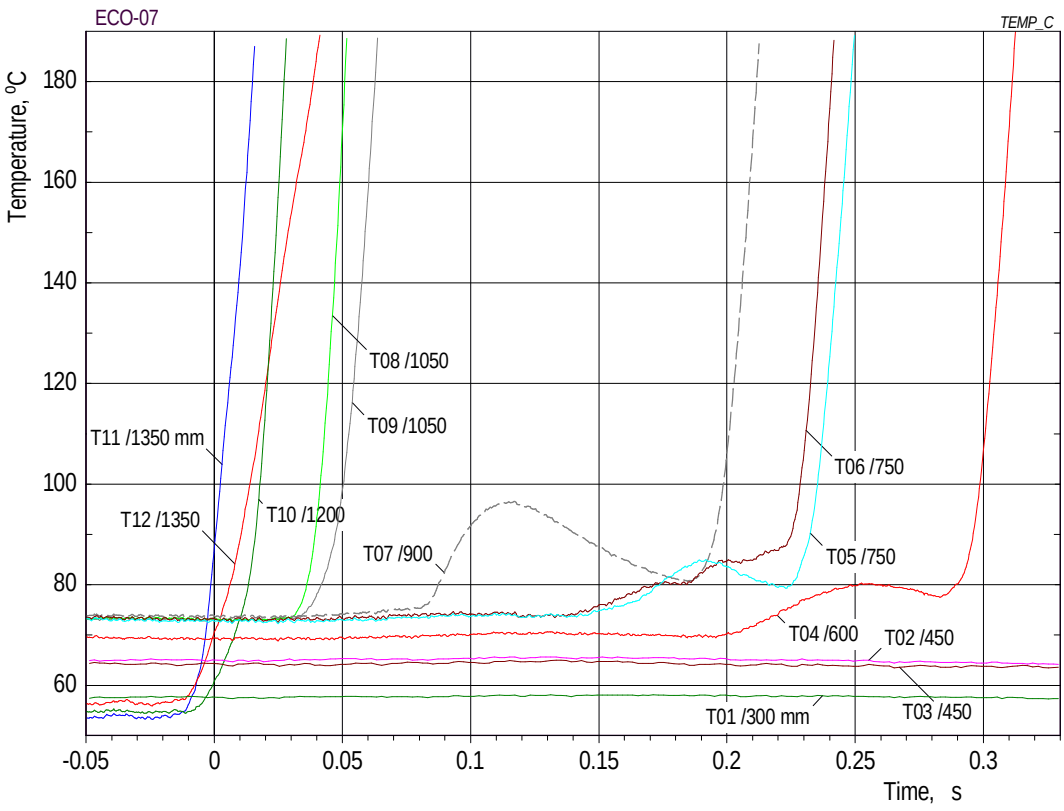

(b) Enlarged scales

Fig. 5.7.3 ECO-07. Temperature time histories depicted in different scales.

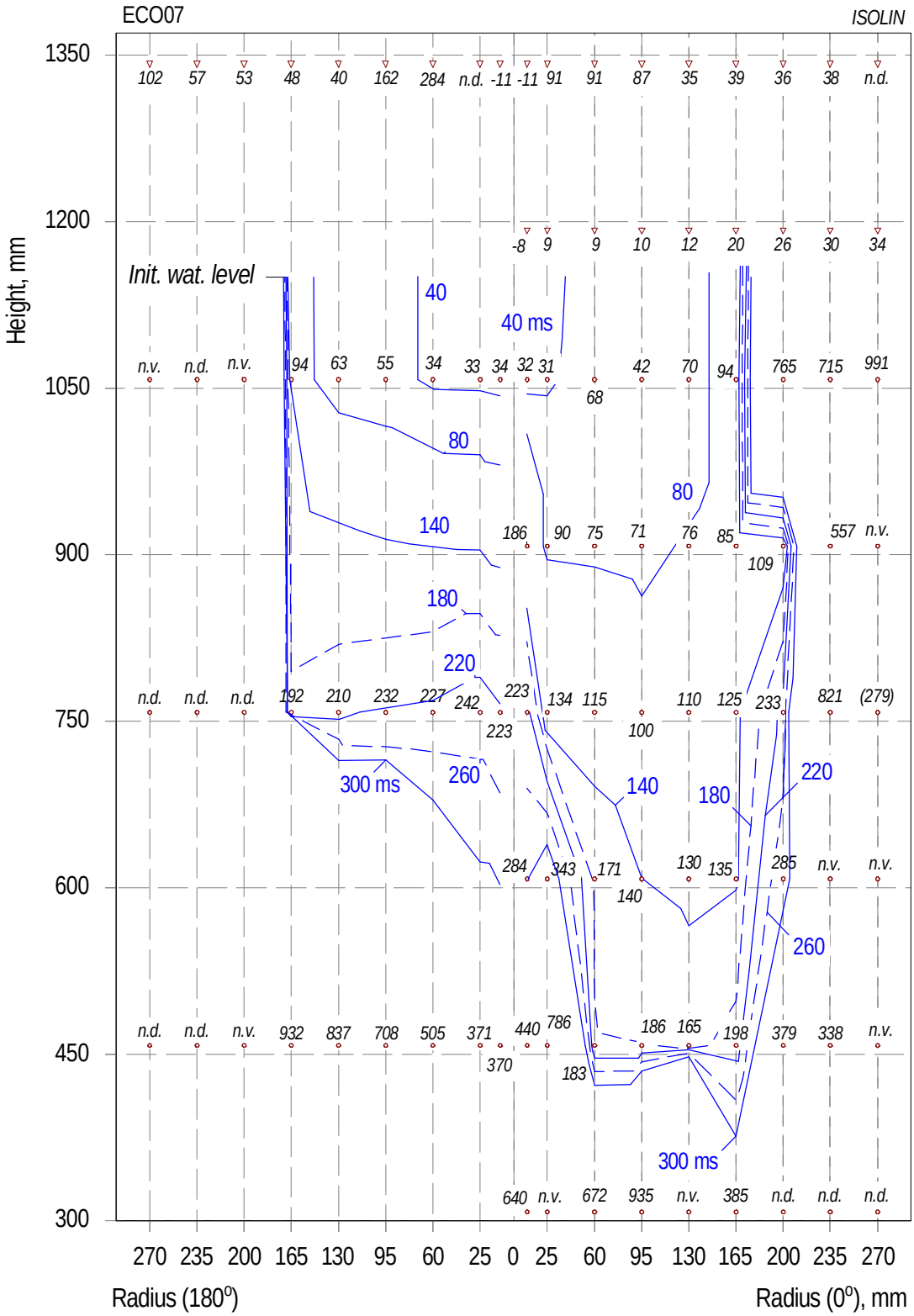

Fig. 5.7.4 ECO-07. Melt penetration in the water with the time as a parameter. Numbers in ms give the instants of first changes in the void signals. Temperature data (at 10 mm radius) denote the starting points of first steep increases. The lines represent outmost boundaries of the mixing zone against the bulk of water. n.v. means: no void detected within one millisecond; n.d. means: no data available. The explosion capsules were ignited at 0.296 s.

Dynamic pressures showing the failed attempt of triggering

The pressures recorded at the various heights (Fig. 5.7.5) show almost identical behaviour during the mixing period. However, from about 0.15 s on (cf. PK04 at 600 mm), abrupt drops occur in the pressure signals obtained in the middle to upper part of the pool. These drops are known to be a thermal effect coming from hotter water contacting the transducer's measuring head. This finding corresponds to the detection of steam (i.e. melt) at the 600 mm level between 0.130 and 0.140 s (Fig. 5.7.4, 0° side).

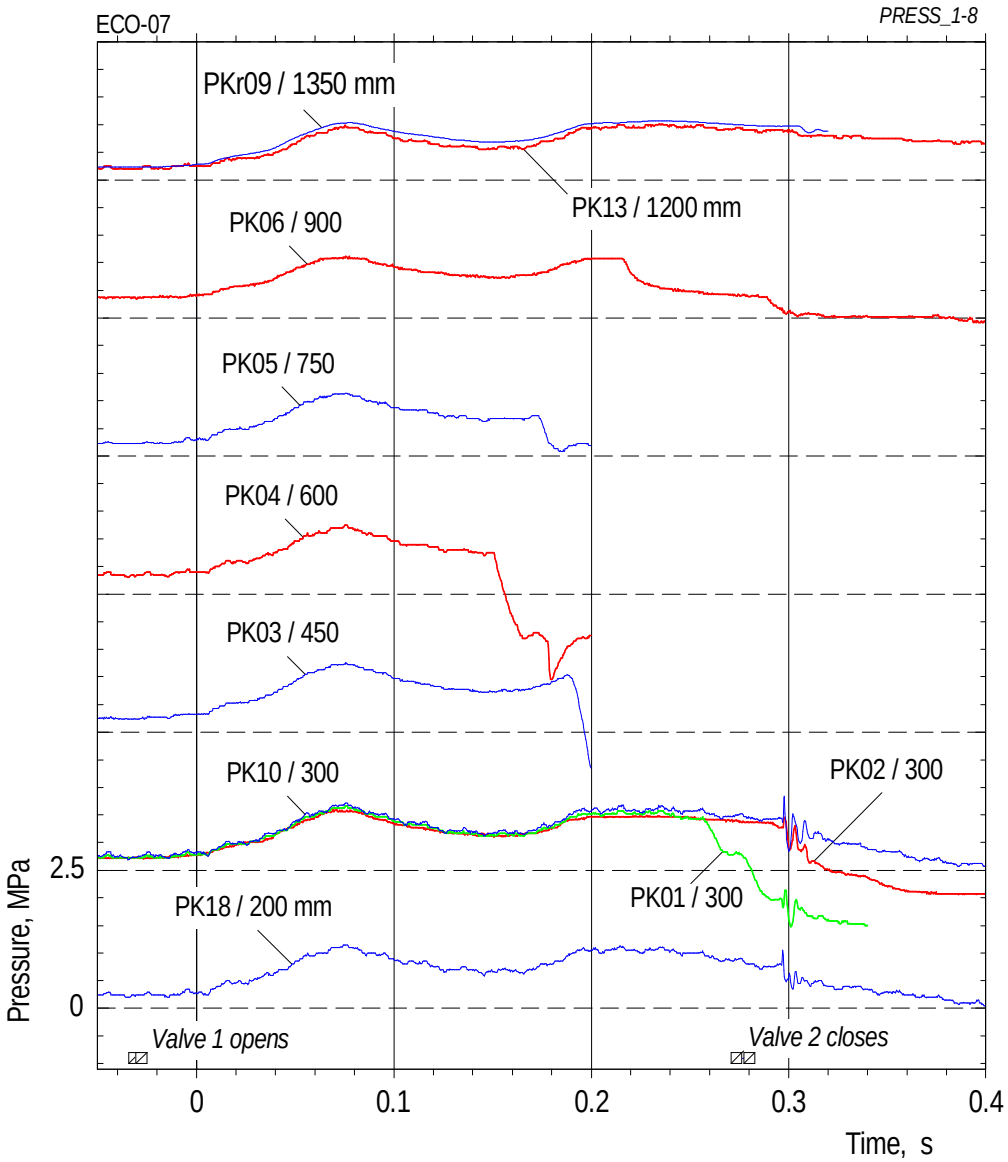

Fig. 5.7.5 ECO-07. Dynamic pressure measurements giving a survey of the mixing period and the time after triggering.
The drops in the signals are a thermal effect exerted on the transducer by a fast change in temperature of the adjacent water.

We conclude from the measurements discussed so far that prefragmentation of the melt caused by the dispersion device together with an unrestricted radial spreading of the fragments led to a more effective quenching than in the other tests performed with the restriction tube. Taking the radius 200 mm as a basis, up to which

void was observed, the cross section of the actual mixing zone is almost twice as large as that within the restriction tube.

The trigger capsules were ignited at 0.2962 s (see the IZ3 and IZ4 signals, Fig. 5.7.6). However, the trigger pulse was extremely weak. Pressure transducers located nearby recorded pressure peaks of up to about 0.6 MPa only. (Note that the resolution of the PK17 signal is not appropriate, due to the large measuring range chosen). No propagation of the pressure took place.

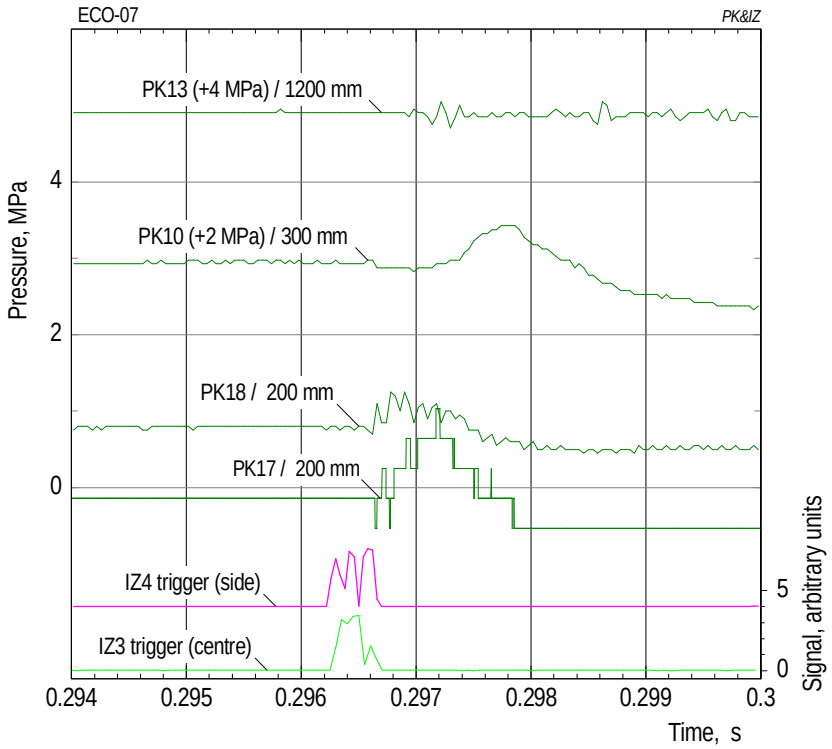

Fig. 5.7.6 ECO-07. Trigger ignition currents (bottom) and the related pressure time histories (top).
Only those pressure signals have been chosen that give a noticeable response to the ignition of the trigger capsules.

The failure of a steam explosion to occur in test 07 gave rise to a more detailed investigation regarding the succession of trigger pulse and steam explosion event. Essential results are summarized in Appendix C.

Taking these results into account, we conclude that the combination of two facts,

- a more effective quenching leading to a lower temperature of the melt fragments and
- a small trigger pressure,

has prevented the triggering conditions of a steam explosion in test 07.

Post test examinations of the melt fragments

The overwhelming part of the injected mass, about 85%, was found in the size between 2 and 10 mm (Fig. 5.7.7). This result is very similar to that of the PM18 PREMIX test /9/. But in contrast with PM18, there are no larger particles in test 07, and a small fraction has diameters below 0.5 mm.

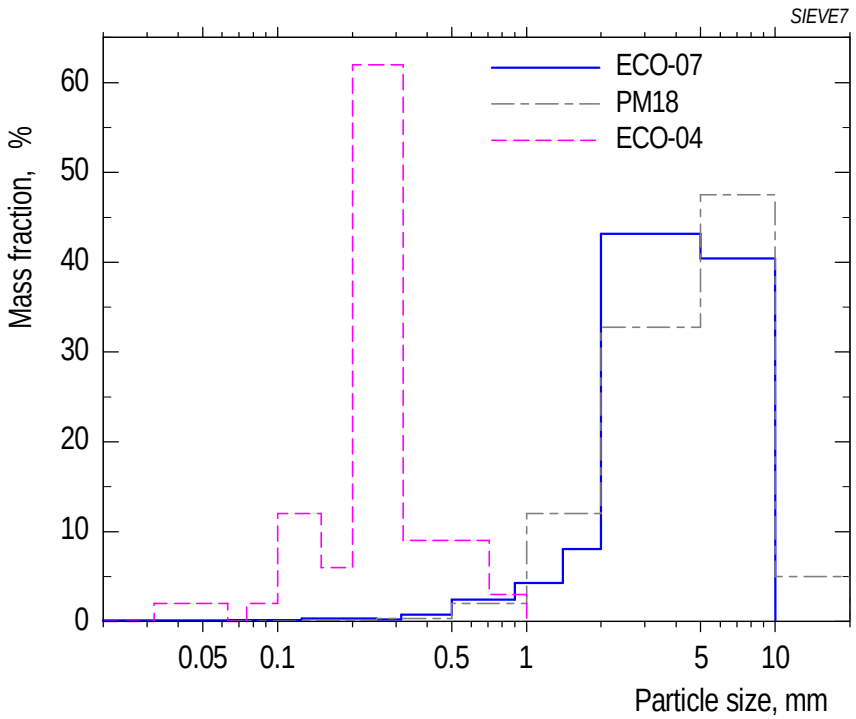

Fig. 5.7.7 ECO-07. Post-test particle size distribution. Comparison is made with the PM18 PREMIX test and test 04.

5.8. Results of ECO-09

Objectives in brief

The purpose of the ECO-09 test was to investigate the effect of a smaller melt release rate on the fragmentation and mixing processes. The other test conditions (see Table 3), especially the system pressure, were similar to those in test 05.

Course of events

Melt release started at -0.04 s when valve 1 was opened (Fig. 5.8.1). At that time, the pressure in the melt generator had attained a value of 0.58 MPa which resulted in a pressure difference of 0.35 MPa. As intended, this is only half of that in test 05.

As anticipated, the time histories of the pressure during the mixing period differed from those in test 05 in several points: The pressure in the test vessel rose markedly, immediately after opening of the valve. The increase, again, took place in two steps, but the stop in between was short. The rates of increase, about 4 MPa/s each, were much smaller than those in test 05. The pressure difference oscillated as in the tests before, but it never became negative.

We assume that the first pressure rise, as in the previous tests, has been promoted by two conditions, (1) the release of gas included in the melt and (2) the evaporation of a water film that had been formed before on the surface of the release tube. We conclude, on basis of the film data entered in Fig. 5.8.2, that the first melt/water contact occurred around time zero, i.e. during the first pressure increase. The meaning of the short plateau after the first pressure rise is not yet clear to us.

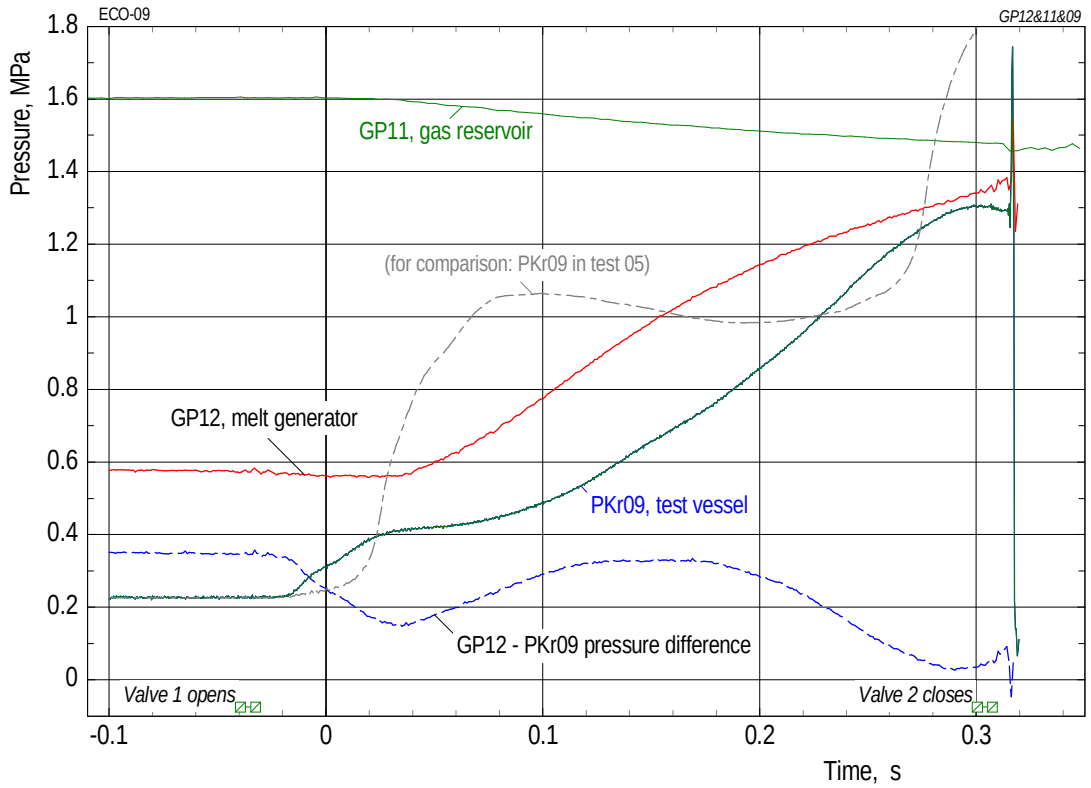

Fig. 5.8.1 ECO-09. Time history of pressures that determined the melt release. Comparison is made with the PKr09 pressure measured in test 05.

Later on, the pressure increase in the test vessel was much lower than that in the preceeding tests conducted with a larger driving pressure, but the increase was con-

tinuous until shortly before the end of melt release. It was such that the pressure difference oscillated but remained positive all times.

The calculated melt speed behaved similarly. Its first maximum, 8 m/s, is much smaller compared to that in test 05 (13 m/s). A second maximum, 9 m/s, is reached before the melt speed decreases to 4 m/s at the end of melt release.

Melt release was terminated by closing valve 2 when the time limit was reached (criterion no 4). From the mass balance, we found that the maximum melt mass, i.e. 18 kg, had been released. This result is larger by about 10 % than in test 05, although the calculated average speeds of melt were similar. The result of this test shows, again, that the time history of the pressure in the mixing zone is strongly dependent on the melt release rate.

The trigger capsules were ignited at 0.313 s. The first pressure rises due to the steam explosion were recorded by the PK16 and PK01 transducers located at the 200 and 300 mm level, respectively, at 0.3144 s. The peak pressures were well above 100 MPa.

The forces of the steam explosion exerted on the upper part of the test apparatus was such that the screws connecting the melt generator to the opening valve broke. When this happened, valve 2 had already been closed. From there, no melt mass escaped from the test vessel. However, some of the plugs in the test vessel wall equipped with measuring instruments became leaky due to the enormous pressure. A large part of the water and with it half of the finely fragmented melt was lost through the leaks. The other half remained in the bottom part of the test vessel.

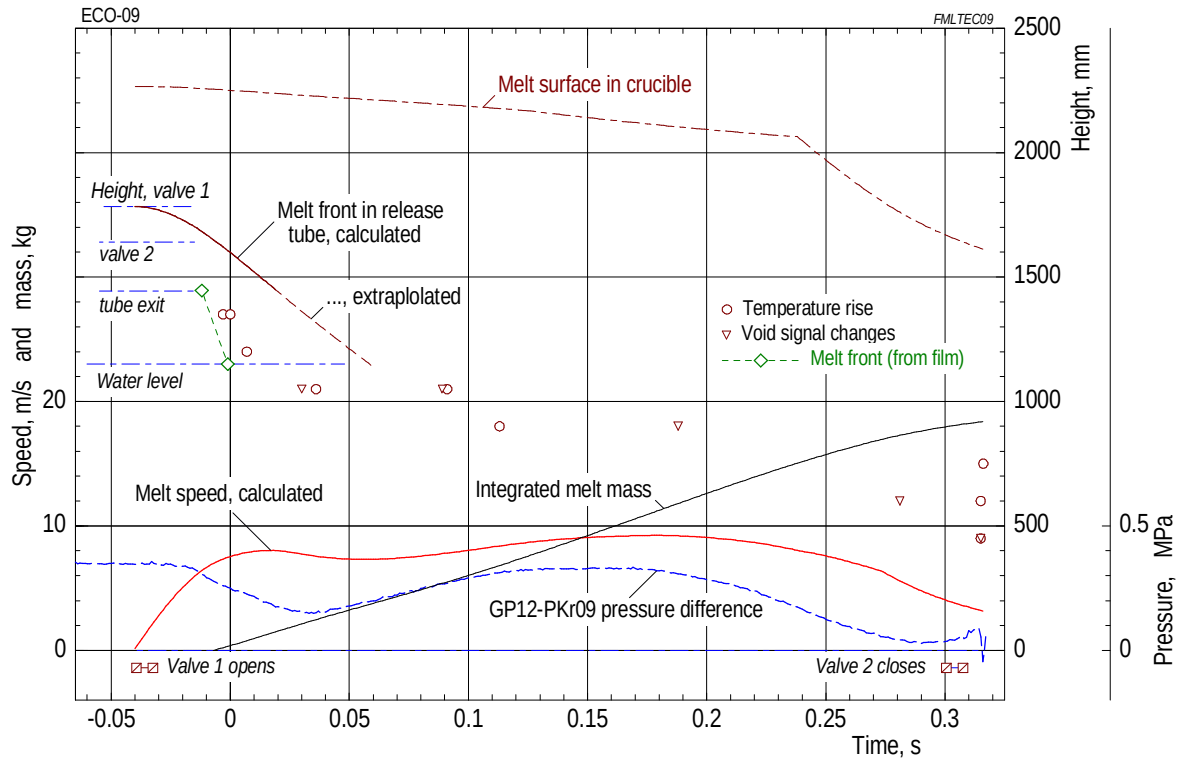

Fig. 5.8.2 ECO-09. Melt release illustrated by calculated and measured data.

Mixing period

The evaluation of the film frames and the temperature and void data leads to the conclusion that the first melt-water contact occurred between zero time and 0.020 s. Compared to that, the melt front is retarded in the calculation. The experimental find-

ing of a faster melt front is, as in earlier tests, attributed to the expansion of gas released with the melt as well as to the evaporation of a water film. These effects are not accounted for in the numerical model. Nonetheless, the calculation predicts, like in test 05, rather well the mass of the melt actually released (18 kg).

In test 09, for the first time, two pressure transducers, PK19 and PK20, and two thermocouples, T18 and T19 (cf. Table 2), were mounted flush with the bottom of the melt generator case to observe the conditions developping in the gas volume during the mixing and steam explosion periods. The temperature signals are drawn in Fig. 5.8.4, the pressure signals in Fig. 5.8.5, together with other measurements that are used for comparison. We conclude from the time histories of the signals that these four instruments suffered severely from heat radiation coming from the melt stream, though they were protected by low (open) steel tubes against splashes of melt. This means that the temperature and pressure records do not discribe real conditions in the gas space. We rely, as in the previous tests, on the record of the PKr09 pressure transducer that was mounted flush with the vessel wall and protected against heat radiation by the restriction tube as well as by an additional (open) cap. The behaviour of the pressure signals during the explosion period is dicussed below.

As in all tests with the dispersion device, a rather unsymmetrical melt penetration in the water was registered in test 09 during the mixing period. This is illustrated by the broad scatter in time of the void and temperature data shown in Fig. 5.8.2 as well as by the numbers and lines drawn in Fig. 5.8.7. This kind of melt penetration makes an estimation of the axial propagation speed difficult. Yet, a trace of steam is identified in the void data on the 180° side marked by the 29, 203, and 292 ms numbers at 95 and 130 mm radii. Along that trace, we obtain velocities of 1.7 and 3.4 m/s (see Fig. 6.3). These values are, with reservations as to the uncertainty mentioned, a bit lower than those in the preceding tests performed with a larger driving pressure.

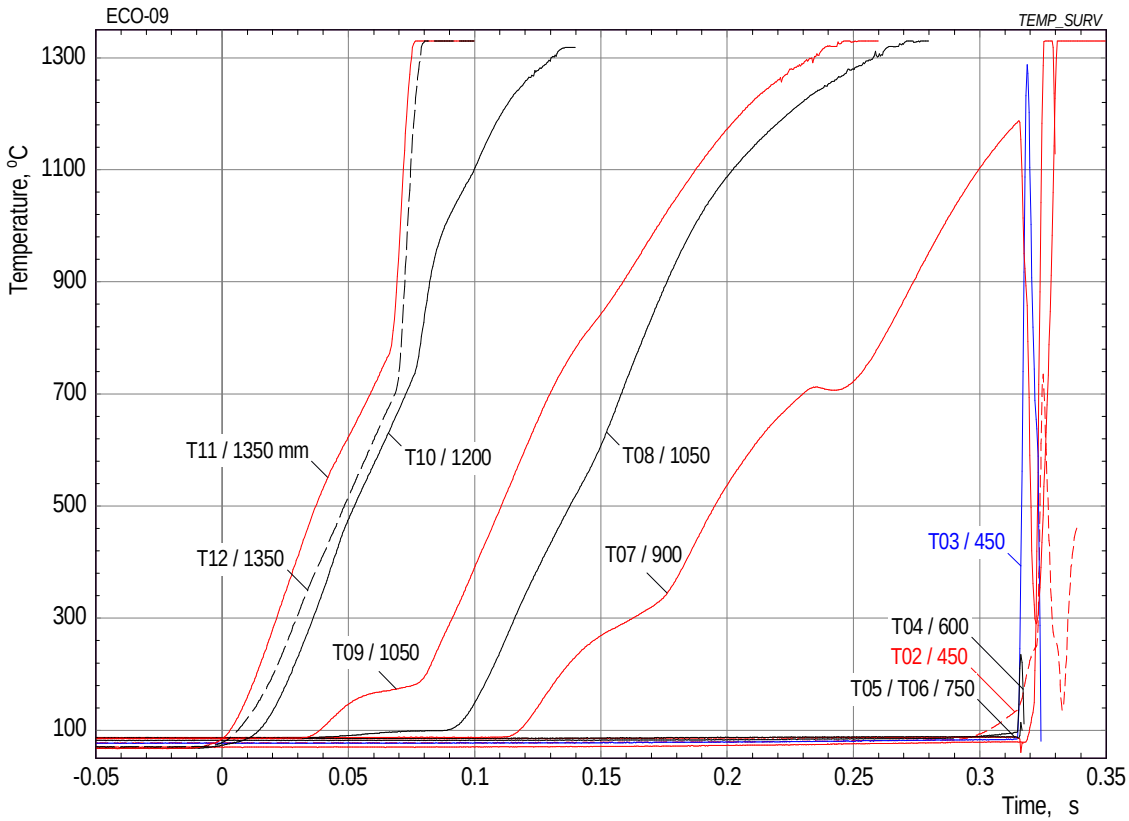

Fig. 5.8.3 ECO-09. Temperature signals giving a survey.

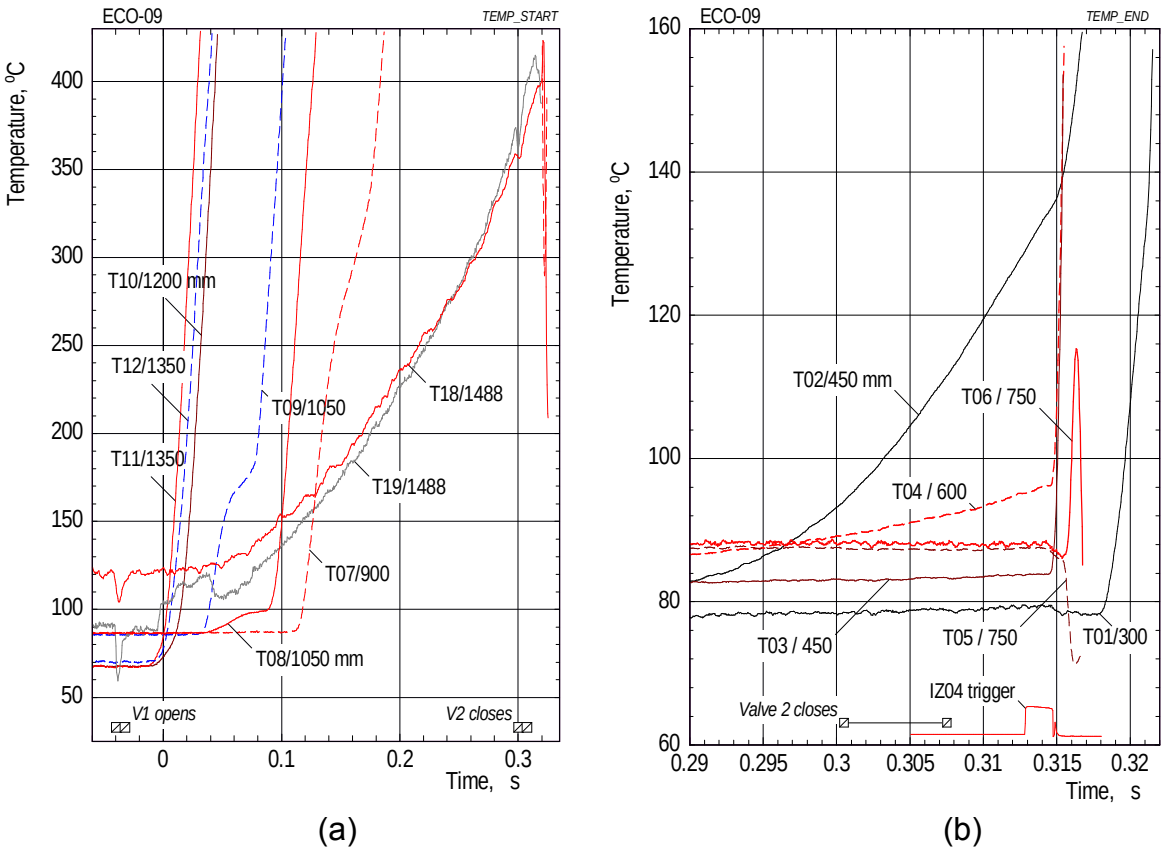

Fig. 5.8.4 ECO-09. Temperature signals showing details at the beginning (a) and at the end (b) of the mixing period.

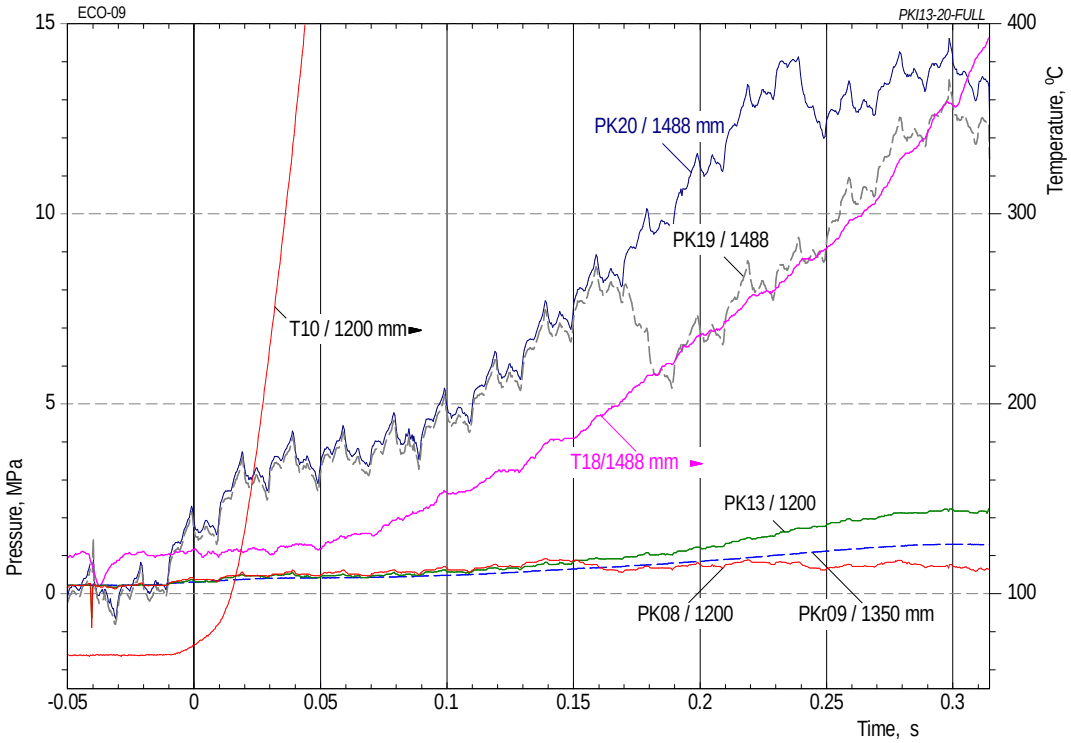

Fig. 5.8.5 ECO-09. Pressure and temperature measurements illustrating the situation above the initial water level during the mixing period.
(Remark: A noise signal occurred in some signals at -0.04 s.)

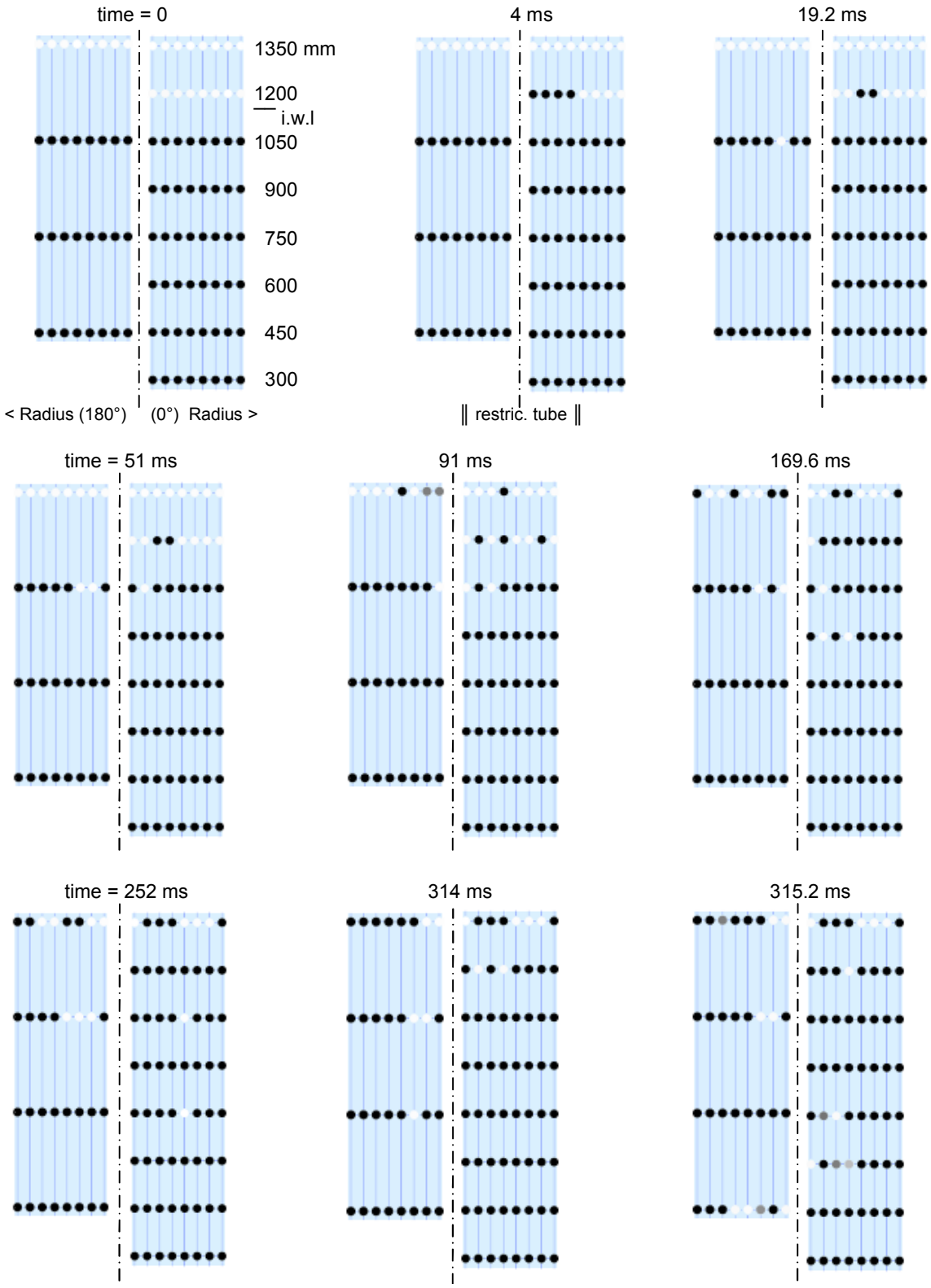

Fig. 5.8.6 ECO-09. Melt penetration mode illustrated by the local distribution of steam and water at increasing times.
The steam explosion started at 0.3144 s.

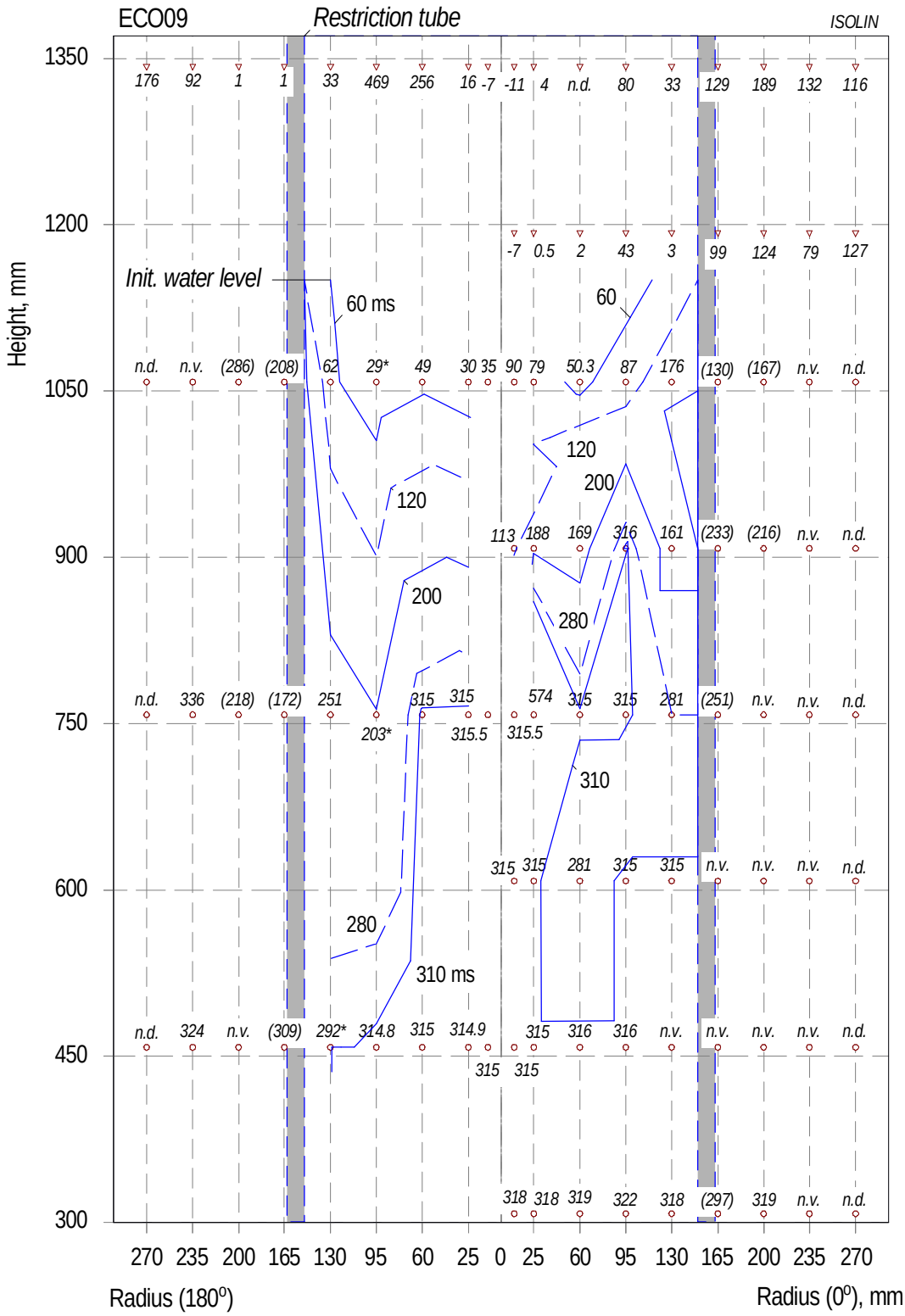

Fig. 5.8.7 ECO-09. Melt penetration in the water with the time as a parameter. The lines represent outmost boundaries of the mixing zone to the bulk of water. Numbers in ms denote the instants of first void signal changes as well as the starting points of first steep temperature increases. Numbers in parentheses have not been used in the interpolation; those marked by a '*' have been used in calculating the melt progression rate. n.v. means: no void detected within one millisecond; n.d. means: no data available. The steam explosion started at 0.3144 s.

On the other side, in the central area, no steam was detected below the 750 mm level prior to the steam explosion. Immediately after the steam explosion, with a delay of less than one millisecond, steam was indicated in the centre at level 750 mm as well as at several positions of the 600 and 450 mm measuring lances. It is safe to assume that part of the melt had been in the region between the 750 and 450 mm levels. But it was, with two exceptions, not detected prior to the steam explosion.

On this basis, the lower level of melt penetration was determined to be between 300 and 200 mm. The first number is obtained from the extrapolation of the void data (Fig. 6.3), the second is the level where the first pressure rise was measured (see PK16 in Fig. 5.8.8). Both numbers have been used to calculate the lower and upper limits of the effective water volume listed in Table 6.2. The melt-to-water mass ratio amounts to 0.30 ... 0.27.

The steam explosion event

The interaction started in the bottom part of the water pool (see PK16 to PK18 signals in Fig. 5.8.8). The first pressure rise occurred at 0.3144 s, i.e. 1.5 ms after the trigger capsules had been ignited. The pressures recorded at 200 and 300 mm height increased within a time of less than 0.2 ms; they exceeded the measuring range of 100 MPa by far (typically during more than 0.25 ms). The pressure event proceeded upward with decreasing magnitude reaching the 1200 mm level at 0.3152 s. From these numbers, a speed of propagation of 1125 m/s can be derived.

The fact that the steam explosion started in the lower part of the water pool indicates that part of the melt must have reached this region without being noticed by the void probes. This assumption is supported by the finding that several void probes mounted at the 450 and 600 mm levels indicate steam within a time span of less than one millisecond after the start of steam explosion (e.g., the 315 numbers, Fig. 5.8.7)

Some thought are given now to the behaviour of the PK19 and PK20 pressure measurements. Both signals suffered from a drop in voltage at the start of the steam explosion. This drop was, as found in several cases in previous tests, obviously due to an abrupt temperature change in the immediate environs of the measuring head. Since these had considerably been heated during the mixing period by radiation coming from the melt (cf. the preceding section), one could conclude that the change in temperature was brought about by a cooling effect of water particles thrown up.

Anyhow, the signals showed strong increases at around 0.316 s, i.e. during the decline period of all the pressures measured at lower elevations. The pressure increases were obviously caused by the impact of a larger mass of water thrown up by the steam explosion. The PK19 and PK20 pressure data exceeded the measuring range of 100 MPa for more than 3 ms. As the decline of both signals is very much retarded, compared with that of the other signals, we conclude that the long-term behaviour (both signals lastly drop below zero level!) suffers from a thermal effect.

The above impact caused a reflected pressure wave that was measured as a second pressure event. It started in the uppermost part of the test vessel (cf. PK13 and PK09, Fig. 5.8.8) at 0.3168 s, i.e. with a short delay to the increase in PK20. The pressure consisted of several interactions, lasted for more than three milliseconds and proceeded down to level 450 mm loosing its magnitude.

A peculiar detail, that may be connected to the water impact, can be observed in Fig. 5.8.9 (b): The elastic deformation of the crushing material, amounting to 1.7 mm by the end of mixing, shortly dropped to zero. After that, the movement proper of the piston (i.e. the plastic deformation) started and with it the DMS force.

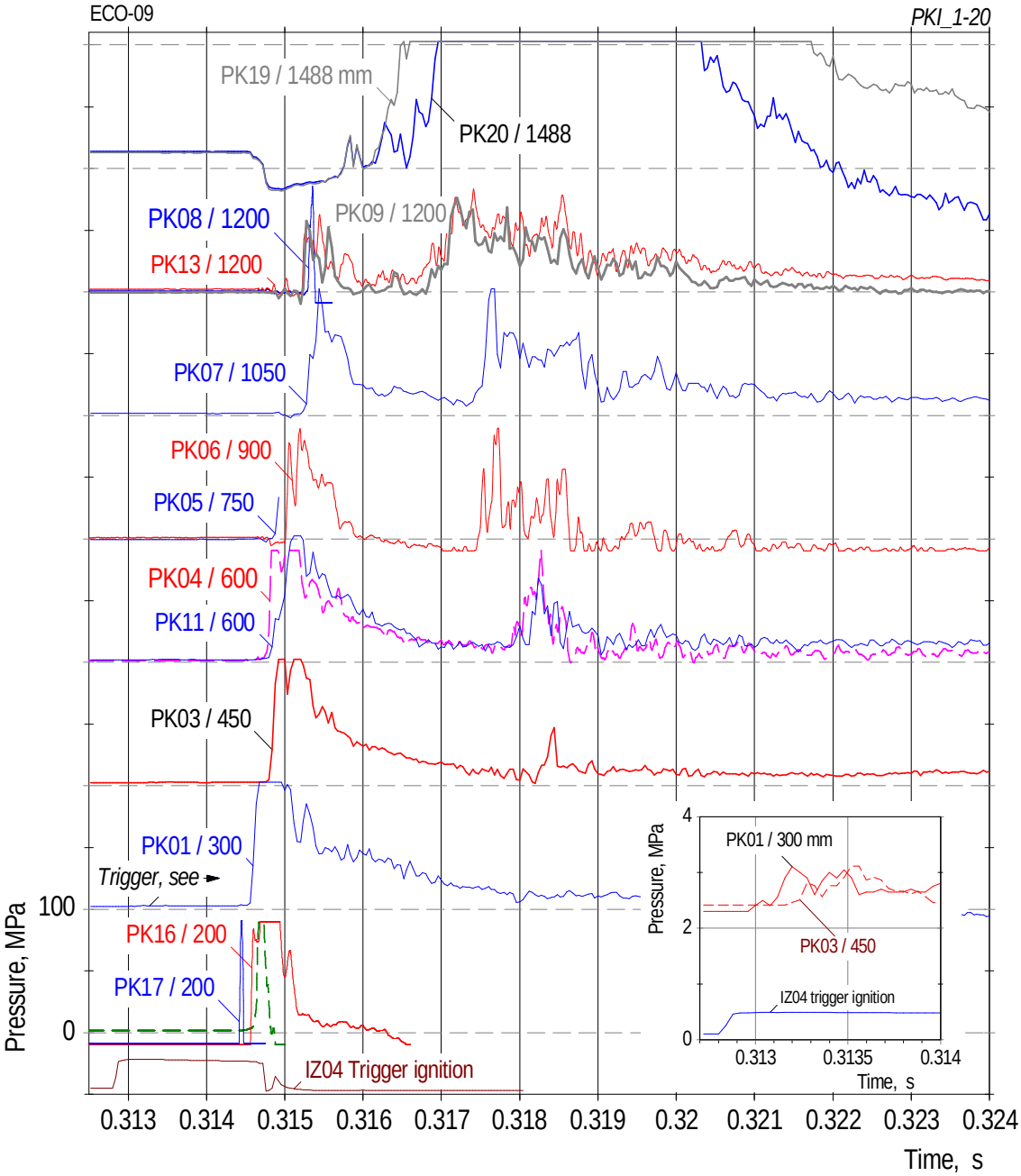

Fig. 5.8.8 ECO-09. Dynamic pressures measured during the steam explosion. The labels also give the axial height. Remarks: 1. Dynamic pressure data were generally calibrated such that they take on the test vessel pressure at the time -0.1 s (here: 0.228 MPa). 2. Drops in the signals are a general thermal effect exerted on the transducer by a sudden change in temperature of the adjacent water. The small picture shows in larger scales the propagation of the trigger pressure.

Evaluation of the energy conversion

In ECO-09, a new charge of crushing material was used in the layers 1 to 3 (for the arrangement and forces see Appendix B). Layers 4 and 5 consisted of the customary material. The result was a bit surprising: Layer 1 was only weakly compressed, whereas layers 2 and 3 were not affected at all. Layers 4 and 5 were markedly compressed (see Table 5.8.1). The sum of compression was 0.046 m.

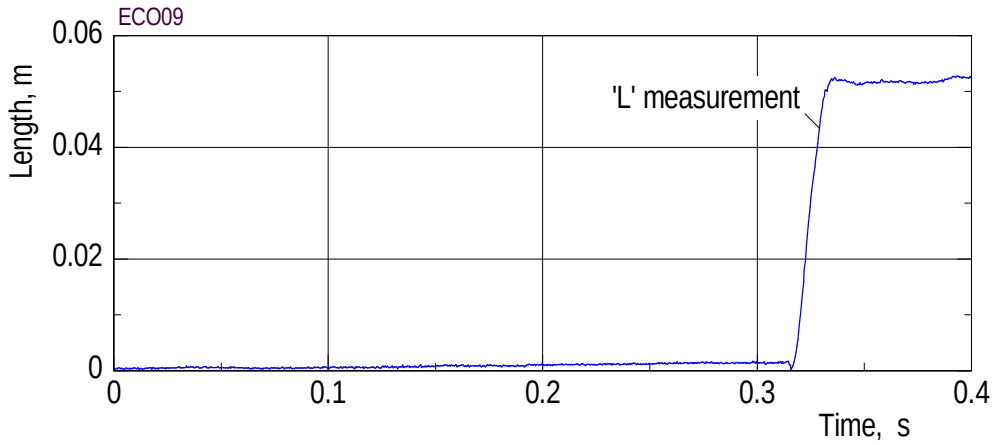

(a) Survey (long time)

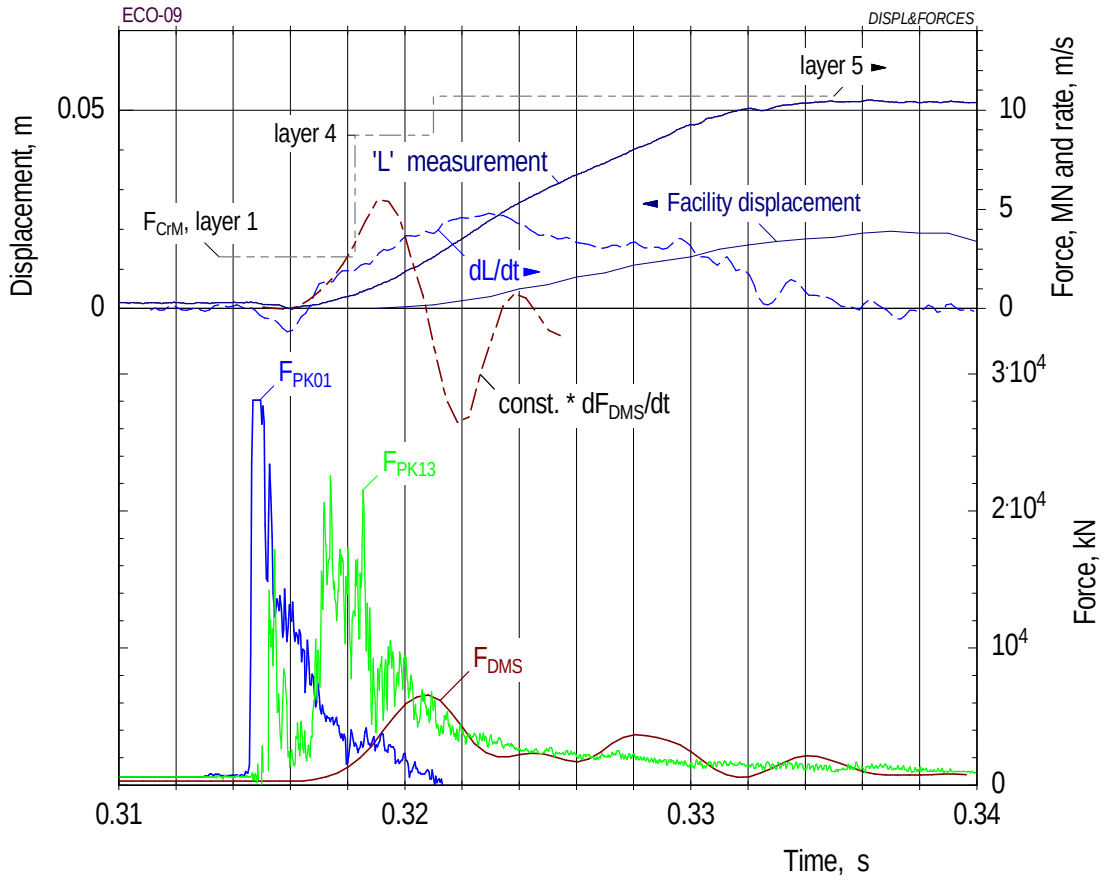

(b) Steam explosion phase

Fig. 5.8.9 ECO-09. Measurements quantifying the extent of the steam explosion: The piston movement, L, the lifting of the facility, and forces derived from pressure and strain gauge data. The F_{CrM} forces (impressed to the layers 1, 4, and 5 of the crushing material) are drawn in the order of their probable chronological response. Two differential functions are also plotted.

If one regards the forces listed in Table 5.8.1, one would expect a much larger compression of layer 1 than the one measured, 0.0035 m. We assume (although the sequence of the F_{CrM} forces has been drawn in Fig. 5.8.9 in a customary way), that under the test conditions the force required to compress layer 1 was much larger than that given in Table 5.8.1, i.e., at least in the order of magnitude of that in layer 4.

For the assessment of energy conversion, we use the mechanical work listed in Table 5.8.1: W = 0.405 MJ.

The heat content of the melt, based on a mass of 18 kg, is 68.4 MJ. This gives an energy conversion ratio of η = 0.59%.

The motion of the whole facility, evaluated from the high-speed video film, started at about 0.319 ms and reached a height of 0.02 m (see Fig. 5.8.9).

Table 5.8.1 Test 09. Mechanical work calculated from the deformation of the various layers.

Layer no	Area, m^2	Force [1], MN	Deformation, m	Work, MJ
1	0.088	5.012	0.0035	0.018
2	0.159	9.055	0	0
3	0.230	13.10	0	0
4	0.327	7.783	0.0105	0.082
5	0.401	9.544	0.032	0.305
Sum			0.046	0.405

[1] see also Appendix B, Table B.3.

Post test examinations

Though only half of the melt released could be recovered, a sieve analysis was made. The particle size distribution (Fig. 5.8.10) shows the result typical of a test with steam explosion: the size of the largest fraction is between 0.125 mm and 0.25 mm.

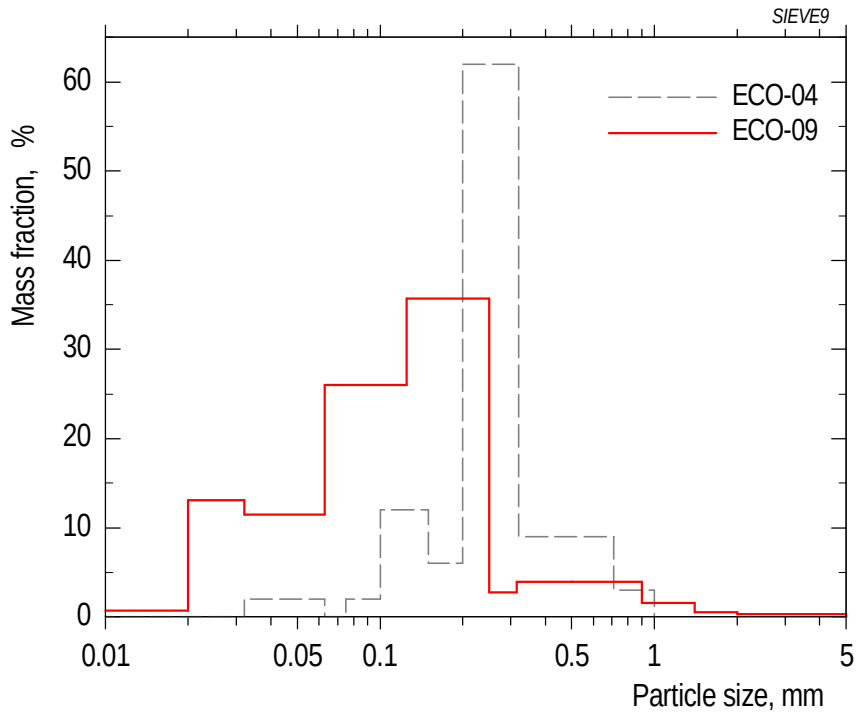

Fig. 5.8.10 ECO-09. Particle size distribution of the melt fragments that could be recovered after the test. Comparison is made with the result in test 04.

6. SUMMARY AND CONCLUSIONS

Steam explosions are a safety concern in the analysis of LWR core melt accidents. Occurrence and consequences (maximum possible energy conversion) are not yet fully understood. ECO has been a unique facility for a direct measurement of the energy conversion (thermal into mechanical) in a strong confinement with a piston moving against a stack of crushing material. In these tests, corium has been simulated by molten alumina at a temperature of 2600 K which has about the same thermal energy content per unit volume as molten corium at about 2900 K.

Melt jet delivery, premixing, explosion, and mechanical consequences are well characterized by different, elaborate instrumentation. This includes an array of void sensors to observe premixing, and an array of pressure transducers to observe origin, progression, intensity, and number of explosions.

In total, 8 tests have been performed under various conditions (see Table 6.1). The objective of the variations was to increase the melt mass released as well as the energy conversion ratio. Of course, the increase in energy conversion ratio went along with a strong increase in the magnitude of the steam explosion pressures.

Table 6.1 Summary list of the essential parameter variations and the yield.

Test number		**01**	**02**	**03**	**04**	**05**	**06**	**07**	**09**
Driving pressure	low	x	x	x					x
	high				x	x	x	x	
System pressure, water temperature	normal	x	x						
	elevated			x	x	x	x	x	x
Start of melt release	steel foil	x	x	x					
	fast valve				x	x	x	x	x
Melt jet	compact	x	x	x	x				
	devided					x	x	x	x
Pool diameter	full	x	x	x				x	
	reduced				x	x	x		x
Melt released	kg	5.8*	2.9	0.9	9.6	16.4	15.2	15.2	18.0
Energy conversion ratio	%	<0.1	<0.1	<0.1	0.42	2.39	0.80	0	0.59

* from the smaller (10 kg) melt generator

In the first three tests, in which the full pool diameter was used, we observed very low energy conversion ratios (below 0.1 %). Melt release started with the melt-through of the steel foil. This condition resulted in an initially narrow melt jet that needed several to a few tens of milliseconds to occupy the full tube diameter. A spontaneous explosion occurred in the second test, ECO-02, with an open system. In all the following tests the system was closed again while the system pressure and the water temperature were increased to 2.5 MPa and about 80 °C, respectively.

A substantial increase in energy conversion (to 0.42 %) was achieved in test 04. The pool diameter had been reduced to obtain a larger melt-to-water mass ratio. Additionally, the melt delivery was modified by increasing the driving pressure and by starting the melt release by means of another fast slide valve. Still, melt penetration was fast such that only half of the possible melt mass had been released when the melt reached the lowermost measuring level. It was in this test that, for the first time, the pressure in the test vessel increased steeply after the start of mixing (Fig. 6.1).

Another substantial increase was achieved in test 05 (2.39 %) by installing the melt jet divider. This device enhanced fragmentation of the melt jet and seemed to retard melt penetration. The result was a highly coherent thermal interaction that started in the lower part of the water pool with one clearly identifiable pressure peak. A melt mass of more than 16 kg, i.e. close to the maximum capacity, was released. It was the strongest explosion observed in the test series, with peak pressures significantly above the measuring range of 50 MPa.

Test 06 was a reproducibility test. The initial conditions and the mass of melt released were almost identical with test 05. The interaction started at a higher axial location and the peak pressures exceeded the increased measuring range of 90 MPa. However, the width of the pulse was smaller than in test 05 and it consisted of several interactions. The energy conversion was about one third of that in test 05. It is not clear what caused these differences in behaviour and result. Most probably, these come from different structures of the mixing zones as will be discussed in more detail below.

In test 07, conducted without the restriction tube, no explosion occurred. One of the reasons for the missing explosion might be that the trigger pulse was extremely weak in this test. The missing radial restriction provided a much larger volume of water available for steam condensation which may have prevented the development of another condition necessary for a steam explosion, namely premixing conditions. The particle size distribution of the melt fragments was similar to that of a quenching test without steam explosion.

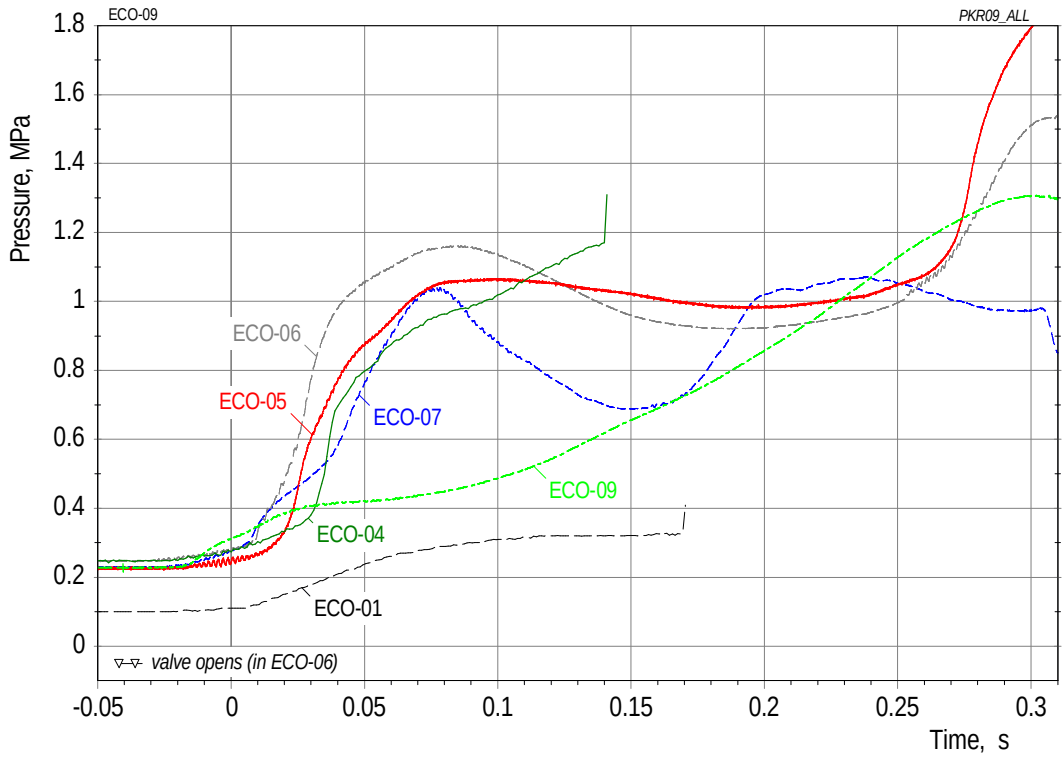

Fig. 6.1 Time histories of pressures recorded in the gas volume before and during mixing.

Test 09 was started with a reduced driving pressure. This condition strongly influenced the pressure time history during melt release: The pressure rise was less steep than in the preceding tests (cf. Fig. 6.1). The full melt mass was released, but no further enhancement of the energy conversion was achieved.

In a first conclusion and with view to the high peak value of interaction pressures observed, the low energy conversion ratios measured are somewhat surprising. A possible explanation may come from the short duration of the pressure pulses. They are essentially over when the piston starts to move. This means that the pressure decrease following the first event(s) is not due to expansion (i.e., doing work) but due to thermal losses from the heated (partly supercritical) water to the surrounding water.

The characteristics of the explosion phase are tightly connected to the conditions formed during the mixing period. Special interest was devoted to the steep increases in pressure. Figure 6.1 shows the pressure time histories of the essential tests.

The pressure increase in test 01 (non-heated!) was very weak. To avoid a pressure increase during the premixing period, the test vessel was vented in test 02. The spontaneous steam explosion that occurred in this test was possibly due to the unimpeded evaporation after melt-water contact. So the venting option was abandoned. Instead, from test 03 on, the initial pressure was raised to 0.25 MPa to avoid a spontaneous steam explosion. Since the water could not be heated to a temperature above 80 °C, it was substantially subcooled (by 30 ... 50 K, initially). The subcooling was much higher (typically around 150 K) at the instant of explosion considering the pressure rise to 0.9 ... 1.1 MPa and assuming not much heating of the water during the short premixing period.

Let us return to these typical steep pressure increases observed in tests 04 to 07. (The slow initial increases are attributed to the evaporation of some water that had condensed in the release tube during the heat-up period.) The steep increases are caused by the intense interaction of melt and water starting directly after the first melt-water contact. An intense interaction leads to a strong melt fragmentation and high evaporation rates. Here, the small free volume above the water plays an important role.

Contributors to a steep pressure rise may be high initial driving pressure and melt delivery rates, respectively. Examples for a low driving pressure and, hence, a low pressure rise are tests 01 and 09. It occurs that especially the high melt velocity may lead to some fragmentation of the melt already on its way towards the water surface or to a stronger fragmentation after its impact on the water. The radial restriction of the mixing zone by the steel tube seems to play a minor role in this context (see the ECO-07 curve in Fig. 6.1).

In the tests with a longer melt delivery period (tests 05 and 06), we observe that the pressure in the test vessel levels off (even drops slightly) after it has reached its first maximum of about one MPa. This behaviour might be a consequence of a relatively strong reduction of the melt flow velocity due to a low or negative pressure difference, e.g. via a less effective melt fragmentation.

Before last conclusions are drawn, the most important result of the ECO tests is summarized in Fig. 6.2. The graph gives the energy conversion ratio vs. the melt-to-water mass ratio. It includes tentative estimates of the uncertainties in determining the variables. At first, a few principal statements are made on the variables used in the graph.

1. The mechanical energy is, as mentioned, really work done against structures outside the interaction region. Note that such contributions as the kinetic energy of the water, the compression of gas in some enclosure, the deformation of the restriction tube, or losses due to leaks and friction, are not accouncted for.

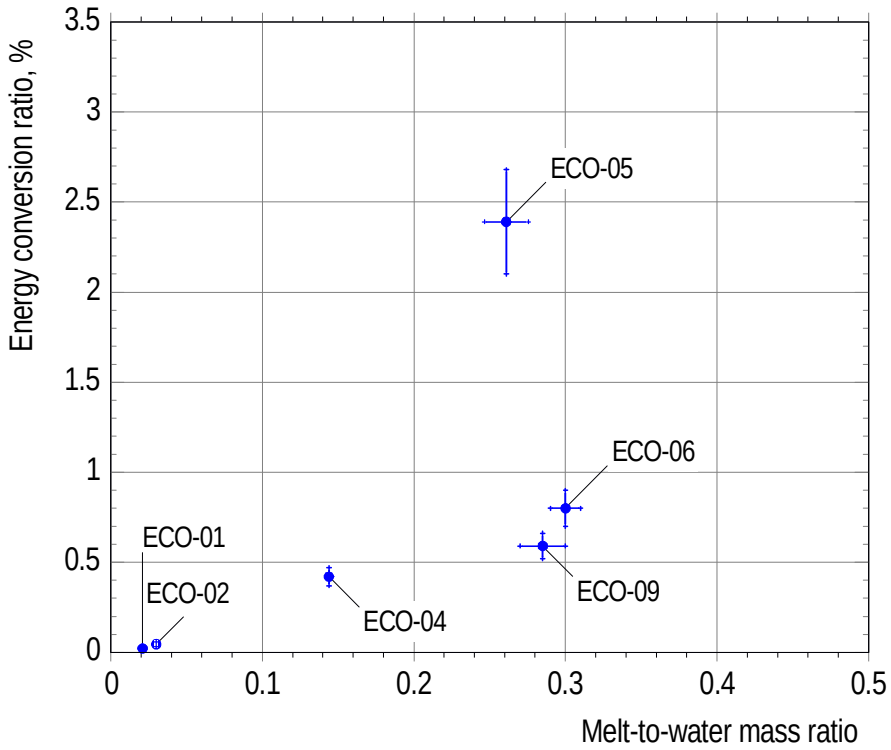

Fig. 6.2 Energy conversion ratio versus the melt-to-water ratio.

2. We have based the energy conversion ratio on the initial heat content of all the released melt mass. In all tests, a complete fine-fragmentation of the introduced melt mass was observed. So, all the melt may have contributed to the explosion. But we have not subtracted any heat losses from the melt into subcooled water during premixing. These depend on a variety of conditions, such as the degree of fragmentation, the local void fraction, the dwell time in the mixture, etc.. Calculations on the MATTINA multiphase computer model /13/, in which the conditions of test 04 /14/ and, more recently, of test 05 were simulated, predict, for the time of explosion, reductions of 20 to 25% in the enthalpy of the total melt released /15/.

3. The water mass used to determine the melt-to-water mass ratio is considered as the one that is available for the condensation of steam during the mixing and explosion periods. The radial and axial extensions of the respective water volume have been defined in Section 4.6, the values are compiled in Table 6.2.

The important scatter of the energy conversion ratios shown in the graph, especially those of the otherwise quite similar tests 05, 06 and 09, indicates that steam explosions are subject to large random variations. This implies that even the result of test 05 cannot be considered as an experimentally determined maximum - even under the special conditions of this experimental setup. The result of test 05 suggests that coherent interactions are more energetic than incoherent ones – which is no surprise.

The energy conversion that we measure with the crushing material is a lower limit. The actual value may be higher than the value that we used for evaluating the energy conversion ratio. Besides the errors coming from the measurement and the assumptions (estimated in Section 4.7 and accounted for in Fig. 6.2), there are three additional kinds of error, respectively energy losses.

Firstly, the force required to compress the crushing material depends to some extent on the deformation velocity. This effect has partly been accounted for.

Secondly, as already discussed, there is more mechanical energy released within the test vessel, that is not transferred to the crushing material. E.g., accounting for the acceleration of water would increase the efficiency from 2.39 to 2.8% in test 05.

Thirdly, there are energy losses due to friction and leakage. The test design represents a compromise between these two. There are seals to reduce leakage flow from the test vessel but they must not cause too much friction. In addition, in tests 05 and 09, there were leaks induced by high pressures during the explosion. Each loss is difficult to quantify.

Summarizing these items, it follows that realistic values of the conversion ratio are 30 % larger than the nominally evaluated ones.

The ECO experiments also demonstrate that relatively weak triggers can set off steam explosions at ambient pressures above 1 MPa (up to 1.9 MPa). This result adds to the data base on triggering (by pressure pulses) at high ambient pressures, cf. the review by Fletcher /16/. At the same time, the success of such weak triggers supports the idea that the occurrence of sufficient spontaneous triggers cannot be excluded in accident situations.

The number of ECO tests under similar conditions has not been large enough to determine the possible range of energy conversion ratios and the influence of individual parameters.

The detailed data available make the experiments useful for explosion code testing and verification.

Table 6.2 Compilation of data used in the calculation of the variables plotted in Fig. 6.2. The data refer to the instant of steam explosion.
The range of melt penetration has partly been obtained by extrapolation of lines drawn in Fig. 6.3.

Test		01	02	04	05	06	09
Melt mass released, kg		5.76	2.86	9.6	16.4	15.2	18
Water							
Effect. cross section, m^2		0.273	0.273	0.07	0.07	0.07	0.07
Level of melt penetr., mm		200	800	200	300 - 200	450 - 400	300 - 200
Related water column, m		1.00	0.35	0.95	0.85 - 0.95	0.70 - 0.75	0.85 - 0.95
Effective volume, m^3		0.2730	0.0956	0.0665	0.06 - 0.067	0.049 - 0.053	0.06 - 0.067
M / W mass ratio, -	1. Average	0.021	0.030	0.144	0.260	0.300	0.285
	2. Range	0.021	0.030	0.144	0.276-0.247	0.310-0.290	0.30 -0.27
Conversion ratio, %	1. Nominal	0.022	0.045	0.42	2.39	0.80	0.59
	2. Range	0.016-0.028	0.032-0.058	0.37 - 0.47	2.10 - 2.68	0.70 - 0.90	0.52 - 0.66

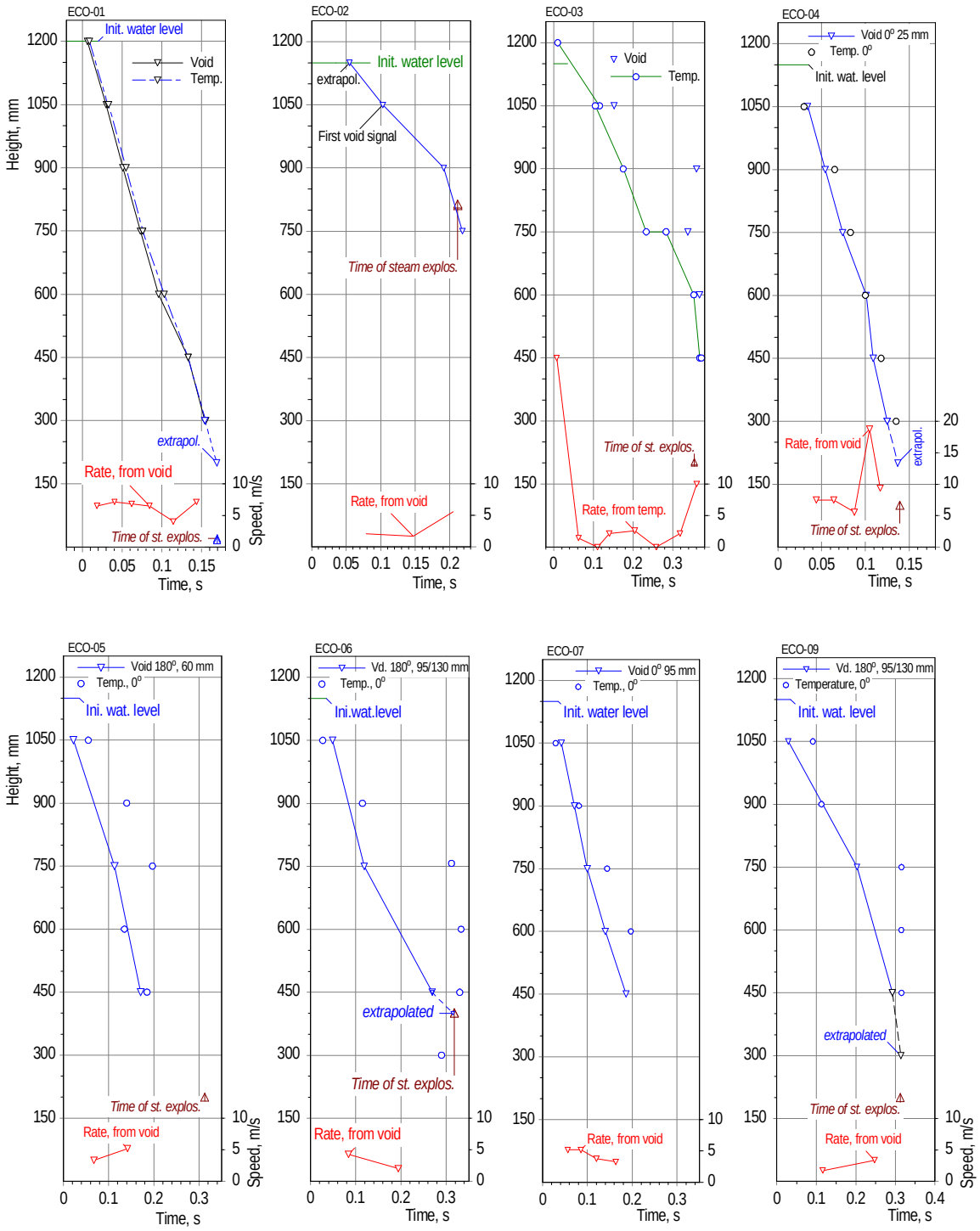

Fig. 6.3 Axial progression of melt in the water in the various tests. Extrapolated data have partly been used in the construction of Fig. 6.2 (compare also Table 6.2).

7. REFERENCES

1. Corradini, M. L., “Vapor explosions: A review of experiments for accident analysis”, Nuclear Safety **32** (1991) 337-362.
2. Cronenberg, A. W. and Benz, R., “Vapor explosion phenomena with respect to nuclear reactor safety assessment”, in: Lewins, J. and Becker, M. (Eds.), Advances in Nuclear Science and Technology **12** (1980), 247-338.
3. Reid, R.C., “Rapid Phase Transitions from Liquid to Vapor”, Adv. Chem. Eng. **12** (1983), 105-208.
4. Berthoud, G., “Vapor Explosions”, Annu. Rev. Fluid Mech., 2000, 573-611.
5. Huhtiniemi, I. and Magallon, D., “Insight into steam explosions with corium melts in KROTOS”, Nucl. Eng. Des. **204** (2001), 391-400.
6. Magallon, D. and Huhtiniemi, I., “Corium melt quenching tests at low pressure and subcooled water in FARO”, Nucl. Eng. Des. **204** (2001), 369-76.
7. Magallon, D., Bang, K.-H., Berthoud, G., Bürger, M., Corradini, M.L., Jacobs, H., Meignen, R., Melikhov, O., Morii, T., Moriyama, K., Sairanen, R., Song, J.-H., Theofanous, T.G., OECD Programme SERENA (Steam Explosion Resolution for Nuclear Applications), Work Programme and first results, 10th International Topical Meeting on Nuclear Reactor Thermal Hydraulics (NURETH-10), Seoul, Korea, October 5-9, 2003; CD-ROM Paper G00107.
8. Albrecht, G., Cherdron, W., Imke, U., Jacobs, H., Kaiser, A., Schütz, W., and Will, H., 2001, “Experiments on Melt-Coolant Interaction Processes, including Steam Explosions”, Trans. 16th Int. Conf. on Structural Mechanics in Reactor Technology (SMiRT 16), Washington, D.C., August 12-17, 2001; Madison, Wis.: Omnipress, 2001; CD-ROM Paper 383.
9. Kaiser, A., Schütz, W., Will, H., “PREMIX Experiments PM12-PM18 to Investigate the Mixing of a Hot Melt with Water“, FZKA-6380, Forschungszentrum Karlsruhe, 2001.
10. Nazare, S., Ondracek, G., Schulz, B., “Properties of Light Water Reactor Core Melts”, Nuclear Technology **32** (1977) 239-246.
11. Magallon, D., Huhtiniemi, I., Dietrich, P., Berthoud, G., Valette, M. Schütz, W., Jacobs, H., Kolev, N., Graziosi, G., Sehgal, R., Bürger, M., Buck, M., von Berg, E., Colombo, G., Turland, B., Dobson, G., Monhardt, D., “Characterisation of Molten-Fuel Coolant Interaction Processes (MFCI)”, FINAL REPORT, EUR 19567 EN, 2000.
12. Steinbrück, M., private communication.
13. Jacobs, H., Väth, L., Thurnay, K., “Constitutive relations for multiphase flow modelling”, Proc. of OECD/CSNI Spec. Mtg on Fuel-Coolant Interactions,Tokai-mura, Japan, May 19-21, 1997, Japan Atomic Energy Research Institute Report JAERI-Conf 97-011 (January 1998) Part I, 205-217.
14. Cherdron, W., Jacobs, H., Kaiser, A. and Schütz, W., “Measurements of Steam Explosion Loads: the ECO Experiments”, Trans. 11th Int. Topical Meeting on Nuclear Reactor Thermal Hydraulics (NURETH-11), Avignon, France, October 2-6, 2005; CD-ROM Paper 011.
15. Jacobs, H., private communication.
16. Fletcher, D.F., “A review of the available information on the triggering state of a steam explosion”, Nuclear Safety **35** (1994), 36-57.

Acknowledgement

The authors thank all the collegues from IRS who helped performing the experiments and evaluating the data. We also thank Dr. H. Jacobs (IKET), who initiated the light-water reactor experimental programme in IRS on premixing and energy conversion, for valuable discussions from the very beginning. DI. H. Will is especially appreciated for his important contributions to layout, construction, and testing of the facility.

Access to Data Base

The essential data, such as pressure and temperature measurements shown in the graphs of this report, as well as a pdf file can be downloaded from the STRESA FZK Data base by entering the web address:

http://nuklear-server.fzk.de/stresa%5Ffzk/

APPENDIX A: Melt supply procedure

Contents in brief outlines

In this Appendix, additional information is given on the melt supply procedure arranged in four parts:

A1. For all relevant tests, actions of the *operational control system*, reactions of the system, and *characteristic events* are listed in chronological order in Tables A1.1 to A1.8.

A2. Schematics of the first design and an improved version of the *larger melt generator* are shown in Figure A2.1.

A3. The *melt dispersion device*: Information on a *preliminary test* with water, in which the effect of such a device was demonstrated, and a photograph of the actual design are given in Figure A3.1. The arrangement in the azimuthal direction is shown in Figure A3.2.

A4. The numerical simulation of melt release.

A5. Several film frames are given of the high-speed endoscope camera observing the melt release flow in test 06.

A1: Course of events

Table A1.1. ECO-01. Course of events connected with actions of the operational control system.

Time related to		Event
Ignition (s)	GR03 signal (ms)	
0	-16136	Ignition of the thermite.
13.734	-2402	Melt front reaches the bottom of crucible.
15.552	-584	Melt front reaches detectors GD01/02, 20 mm above steel foil.
15.574	-562	GR01 signal, produced by GD02; start of cameras.
15.590	-546	Order to close GV01 valve (ventilation of crucible).
15.830	-306	Order to open gas feeding valves.
16.076	-60	Order to close gas feeding valves.
16.108	-28	Signal of melt detector GD03 at the outlet
16.136	**0**	**GR02 signal, produced by the GD03 sensor.**
16.191	55	Order to open gas feeding valves.
16.268	132	Steam detected at 450 mm level (V021)
16.290	154	Steam detected at 300 mm level (V011)
16.295	159	Order to close gas feeding valves.
16.296	160	Order to close melt slide valve.
16.304	168 / 172	Slide valve starts to move / is closed
16.305	169	Ignition of the explosion capsules
16.588	452	Generation of the flash light

Table A1.2. ECO-02. Course of events connected with actions of the operational control system.

Time related to		Event
Ignition (s)	GR03 signal (ms)	
0	-17716	Ignition of the thermite
14.229	-3487	Melt front reaches bottom of crucible
16.461	-1255	Melt front reaches detectors GD02, 30 mm above steel foil
16.467	-1249	GR01 signal, produced by GD02, initiates start of cameras
16.483	-1233	Order to close GV01 valve (ventilation of crucible)
16.508	-1208	Melt front reaches detectors GD01, 30 mm above steel foil
16.732	-985	Order to open gas feeding valves.
16.9121	-805 to -278	Repeated orders to close / open gas feeding valves
17.476	-240	Generation of flash light
17.712	-4	Signal of GD03 melt detector.
17.716	**0**	**GR02 signal, produced by the GD03 sensor.**
17.717	1	Signal of GD04 melt detector.
17.897	181	Order to open gas feeding valves.
17.906	190	Survey video camera (25 f/s) observes illumination coming from the steam opening lines.
17.927	211	Strong pressure rise, $5 \cdot 10^3$ MPa/s, due to spontaneous nucleation
17.928	212	PKu14 pressure (600 mm height) reaches 2 MPa limit
17.930	214	Order to close the melt slide valve and the two steam opening lines
17.933	217	Steam detected at 300 mm level (V011)
17.934	218	Ignition of the explosion capsule
17.937	221 / (226)	Slide valves (melt and steam) start to move / (are closed)
18.073	357	Steam detected at 450 mm level (V021)
19.730	383	Steam detected at 450 mm level (V031)

Table A1.3. ECO-03. Course of events connected with actions of the operational control system.

Time related to		Event
Ignition (s)	GR03 signal (ms)	
0	-26480	Ignition of the thermite
17.141	-9339	Melt reaches bottom of crusible
25.109	-1371	Signal of melt detector GD02, 30 mm above steel foil
25.119	-1361	GR01 signal, produced by GD02
25.137	-1343	Order to close GV01 valve (ventilation of crucible)
25.262	-1218	Signal of melt detector GD01, 30 mm above steel foil
25.349	-1131	Signal that GV01 is closed.
25.325	-1128	Order to open gas feeding valves
26.132	-348	Generation of flash light
26.476	-4	Signal of melt detector GD03 at the outlet
26.480	**0**	**GR03 signal, produced by the GD03 sensor.**
26.489	9	Signal of melt detector GD04 at the outlet
26.823	343	Order to close slide valve 2 (release time limit reached)
26.828	348	Slide valve starts to move
26.829	349	Order to close gas fitting valves
26.831	351	Slide valve is closed
26.834	354	Ignition of the explosion capsule
26.866	386	Steam detected at 450 mm level (V031)
26.878	398	Steam detected at 300 mm level (V011)
27.041	561	Steam detected at 450 mm level (V021)

Table A1.4. ECO-04. Course of events connected with actions of the operational control system.

Time related to		Event
Ignition (s)	GR03 signal (ms)	
0	-24498	Ignition of the thermite.
23.535	-963	Melt front reaches detector GD02, 30 mm above steel foil.
23.541	-957	GR01 signal, produced by GD02.
23.557	-941	Order to close GV01 valve (ventilation of crucible).
23.833	-665	GV01 is closed, order to open gas feeding valves.
24.052	-446	Signal of melt detector GT17, melt front reaches space above slide valve1.
24.076	-422	GR2 signal, produced by GT17.
24.085	-413	Order to close gas feeding valves.
24.469	-29	Order to open slide valve1.
24.474	-24 / -22	Slide valve starts to move / is open.
24.495	-3	Signal of GD03 melt detectors.
24.498	**0**	**GR03 signal, produced by the GD03 sensor.**
24.508	9	Order to open gas feeding valves.
24.606	108	Steam detected at 450 mm level (V021).
24.609	111	Steam detected at 450 mm level (V031).
24.624	126	Steam detected at 300 mm level (V011).
24.625	127	Order to close slide valve 2.
24.631	133 / 137	Valve 2 starts to move / is closed.
24.633	135	Order to close gas feeding valves.
24.638	140	Ignition of the explosion capsule.
24.638	140	Start of steep pressure increase in the test vessel.

Table A1.5. ECO-05. Course of events connected with actions of the operational control system.

Time related to		Event
Ignition (s)	GR03 signal (ms)	
0	-26475	Ignition of the thermite.
21.114	-5361	Melt front reaches bottom of crucible (GT14)
25.559	-916	Melt front reaches 30 mm level above steel foil (GD01).
25.585	-890	Order to close GV01 valve (ventilation of crucible).
25,826	-649	GV01 is closed.
25.828	-647	1. Order to open gas feeding valves.
26.019	-456	Signal of melt detector GT17, melt front reaches space above slide valve 1.
20,036	-439	GR2 signal, produced by GT17.
26.065	-410	Order to close gas feeding valves.
26.434	-41	Order to open slide valve 1.
26.445	-35 / -30	Slide valve starts to open / is open.
26.472	-3	Signal of GD03/4 melt detectors.
26.475	**0**	**GR03 signal, produced by the GD03/4 sensors.**
26.475	0	Order to open gas feeding valves.
26.773	298 / 305	Order to close slide valve 2 / valve 2 is closed.
26.779	304	Order to close gas supply valves.
26.785	310	Ignition of the two explosion capsules.
26.790	315	First steep pressure rise due to steam explosion.
26.796	321	First steam indicated at 450 mm height (V022).

Table A1.6. Course of events in ECO-06 connected with the operational control system. (V)* means information was gained from video film.

Time related to		Event
Ignition (s)	GR03 signal (ms)	
0	-26579	Ignition of the thermite.
23.412	-3167	Melt front reaches bottom of crucible (GT14).
25.460	-1119	Melt front reaches GD01 detector.
25.462	-1117	GR1 signal, produced by GD01.
25.482	-1097	Order to close GV01 valve (ventilation of crucible).
25.705	-874	Order to open gas feeding valves.
25,696	-610	Order to close gas feeding valves.
26.110	-469	Signal of melt detector GT16, melt front reaches space above slide valve1.
26,130	-449	GR2 signal, produces by GT16.
26.430	-149 (V)*	Start of video recording.
26.530	-49	Order to open slide valve1.
26.537	-42 / -36	Slide valve1 starts to open / is open.
26.543	-36 (V)*	First luminous signal by melt on video film.
26.560	-19 (V)*	Melt front reaches lower end of release tube (estimated).
26.562	-17	Order to open gas feeding valves.
26.572	-7 (V)*	Melt contacts water surface.
26.576	-3	Signal of GD03/4 melt detectors at the outlet.
26.579	**0**	**GR03 signal, produced by the GD03 sensor.**
26.880	301	Order to close slide valve2.
26.885	306	Order to close gas supply valves.
26.887	308	Slide valve2 is closed.
26.893	314	Ignition of the two explosion capsules.
26.894	315	First pressure rises due to the explosion capsules.
26.899	320	Steam detected at 450 mm level (V021).
26.900	321	Temperature rise on themocouple T03, 450 mm.
26.904	325	Temperature rise on themocouple T02, 450 mm.

Table A1.7. Course of events in ECO-07 connected with the operational control system. (V)* means information was gained from video film.

Time related to		Event
Ignition (s)	GR03 signal (ms)	
s	ms	
0	-21801	Ignition of the thermite.
18.3820	-3419	Melt front reaches bottom of crucible (GT14).
20.6640	-1137	Melt front reaches GD01 detector, 50 mm above steel foil.
20.6650	-1136	GR1 signal, produced by GD01.
20.6650	-1136	Order to close GV01 valve (ventilation of crucible).
20.6750	-1126	Signal from GD02 detector, 50 mm above steel foil.
20.8900	-911	Order to open one gas feeding valve.
21.1005	-700.5	Order to close gas feeding valve.
21.301	-500	Start of fast video recording; pretime 500 ms.
21.3500	-451	Signal of melt detector GT17 detector, melt front reaches space above slide valve1.
21.4850	-316	Order to open gas feeding valve.
21.5155	-285.5	Order to close gas feeding valve.
21.7640	-37	Order to open slide valve1.
21.7695	-31.5 / -28	Upper slide valve starts to open / is open.
21.7870	-14 (V)*	First luminous patch by melt visible at the outlet.
21.7980	-3 / -2	Signal of GD03/04 melt detectors.
21.8000	-1	Order to open all gas feeding valves.
21.8010	**0**	**GR03 signal produced by the GD03 sensor.**
22.0745	273.5	Order to close slide valve2.
22.0765	275.5	Order to close gas supply valves.
22.0790	278	Slide valve2 starts to move.
22.0810	280	Slide valve2 is closed.
22.0970	296	Ignition of the two explosion capsules.
22.1720	371	Steam detected at 450 mm level (V031).
22.3180	423/517	Temperature rise on thermocouple T02, 450 mm level.
22.3330	362/531	Temperature rise on thermocouple T03, 450 mm level.
22.5865	7855	Steam detected at 450 mm level (V021).
23.0135	12125	Steam detected at 300 mm level (V011).

Table A1.8. ECO-09. Course of events connected with actions of the operational control system. (V)* means information was gained from video films.

Time related to		Event
Ignition (s)	GR03 signal (ms)	
0	-33173	Ignition of the thermite filling.
23.523	-9650	Melt front reaches bottom of crucible (GT14).
31.826	-1347	Melt front reaches GD01 detector.
31.831	-1342	Order to close GV01 valve (ventilation of crucible).
32.048	-1125	Order to open gas feeding valve, 50 mm above steel foil.
32.069	-1104	Signal received from GD02 detector.
32.494	-677	Order to close gas feeding valve.
32.700	-473	Melt front reaches GT17 detector (in space above slide valve). GT16 detector responds 9 ms later.
32.721	-452	GR02 signal produced by GT17
32.958	-215	Order to open MV23 gas feeding valve.
33.025	-148 (V)*	Flashlight synchronizes video camera. At the same time melt from a first leak illuminates part of the pipe work.
33.127	-46	Order to open upper slide valve.
33.134	-39 / -32	Upper slide valve starts to open / is open.
33.152	-21	Order to open one gas feeding valve.
	-17 (V)*	First luminous patch by melt visible in video film.
	-12 (V)*	Melt front reaches lower end of release tube (estimated).
	-1 (V)*	Melt contacts water surface.
33.170	-3	Signal of the GD03/4 melt detectors.
33.173	0	**GR03 signal, produced by the GD03 sensor.**
33.270	7	Order to open all gas feeding valves.
33.468	295	Order to close lower slide valve.
33.473	300	Order to close gas feeding valves.
33.474	301 / 308	Lower slide valve starts to move / is closed.
33.4823	312.9	Rise in ignition current of the two explosion capsules.
33.486	313	Pressure rise due to explosion capsules.
33.4874	314.4	First rise in pressure (PK17), start of steam explosion.
33.4879	314.9	Steam indicated by void probe V031.
33.489	316	Piston starts to move.
33.492	319	Whole test apparatus starts to move.
33.512	≈339	The pressure in the melt generator starts to decrease indicating a second melt leak.

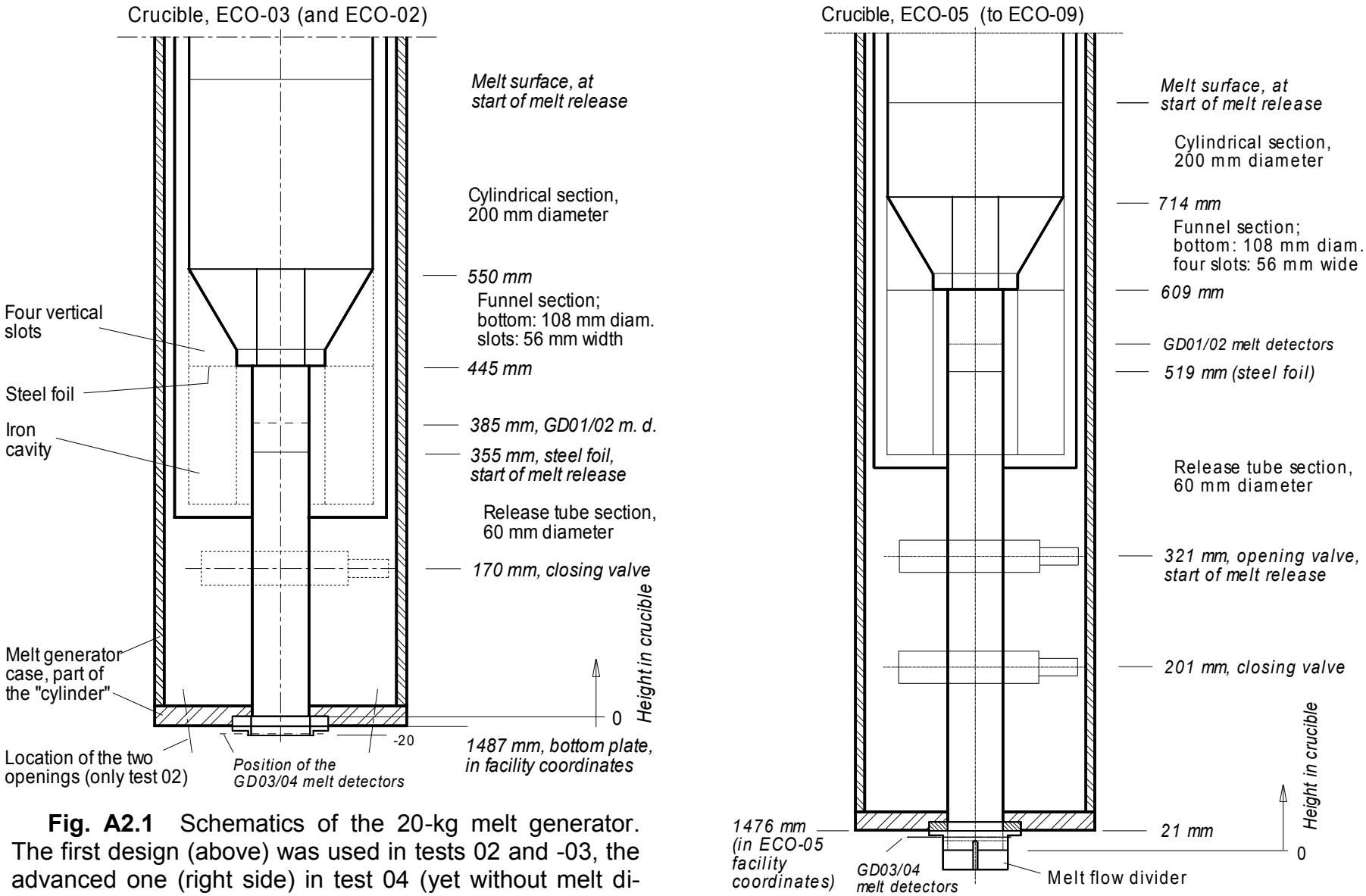

Fig. A2.1 Schematics of the 20-kg melt generator. The first design (above) was used in tests 02 and -03, the advanced one (right side) in test 04 (yet without melt divider) and in tests 05 to -09.

A3: Design of the melt flow divider based on preliminary tests with water

(a) Test with water showing the division of the flow.

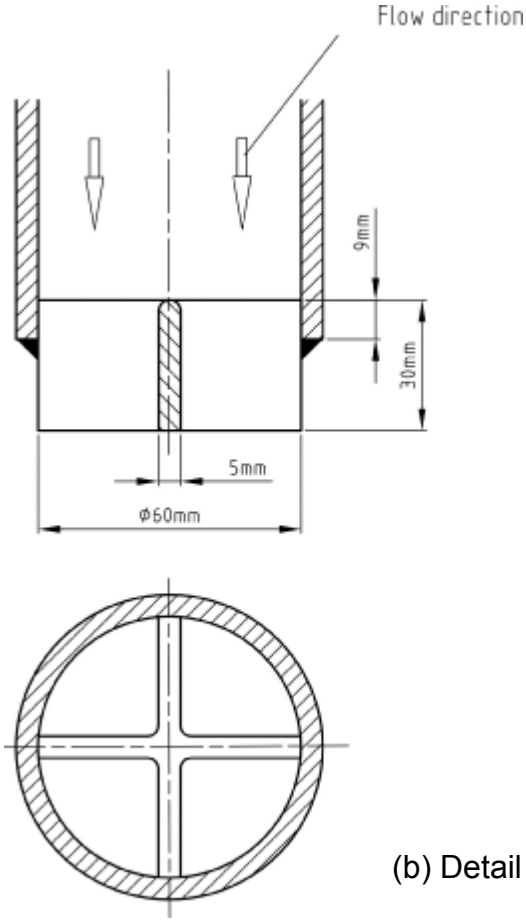

(b) Detail

(c) Actual design

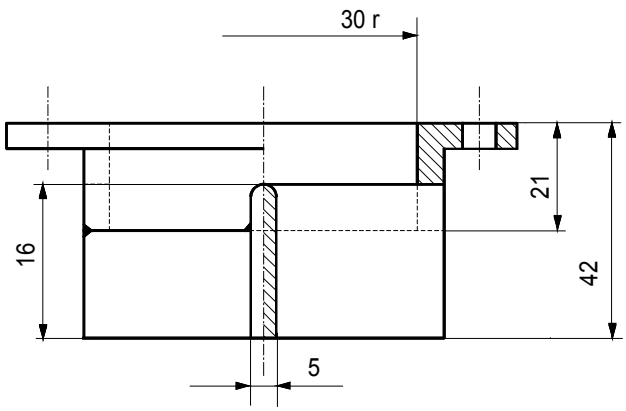

(d) Essential dimensions

Fig. A3.1 Melt flow divider as used from test 05 on. The photograph (a) shows a preliminary test with water, in which the principle of flow division was demonstrated. The view from below (c) illustrates the built-in situation. Two interwoven two-wire cables served as melt detectors.

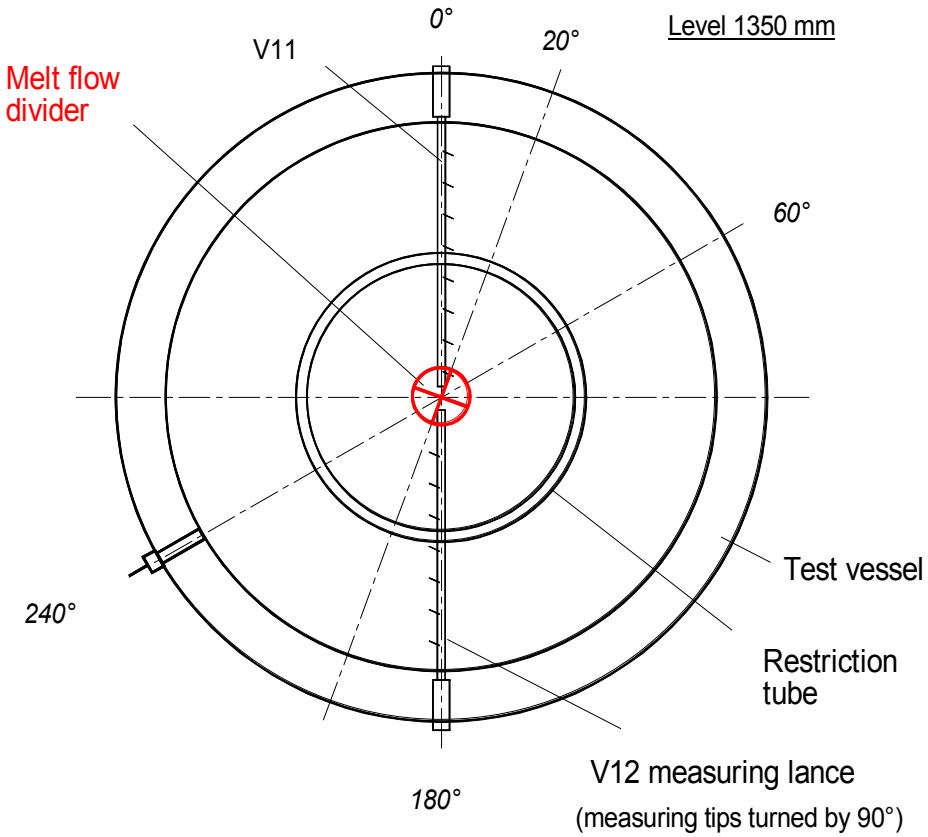

Fig. A3.2 Arrangement of the melt flow divider in the azimuthal direction in test 05. A turn existed of 20° (-10° in tests 06 to 09) related to the void measuring lances.

A4: Numerical simulation of the melt release

The one-dimensional numerical model is based on the following momentum equation that describes the flow of melt in a pipe:

$$dv=dt/h* (g*h - 0.5*(v+0.5*dv)^2*zk + p_d(t)/rho), \quad (A4.1)$$

or, in the difference form,

$$\Delta v=\Delta t/h*(g*h - 0.5*(v+0.5*\Delta v)^2*zk + p_d(t)/rho), \quad (A4.2)$$

where

v and Δv are the velocity and the change in velocity, respectively,

t and Δt are the time variable and the time step (0.001 s in general), respectively,

g and h are the gravity constant and the actual geodetic height of the melt,

p_d is the time dependent pressure difference acting on the melt,

rho is the density, and

zk is a composed number accounting for acceleration and for friction losses; here: $zk = 1+\varsigma+\lambda*l/d$, where l and d are actual length and diameter of the melt release tube, respectively; λ and ς denote the tube friction losses and inlet / outlet resistances, respectively.

In the discretization, the lower end of the melt release tube (cf. Fig. A2.1) is taken as the origin of the axial coordinate. The most important input variable is the difference of the pressures measured in the melt generator atmosphere and in the gas space of the test vessel, GP12 and PKr09, respectively.

Another input is the maximum mass of (alumina) melt to be released, m_0. The latter is 18 kg in case of the larger melt generator. The height of the melt in the crucible at the start of calculation is calculated on basis of this mass. The melt density (2800 kg/m^3) was set to 80% of the theoretical density. By that, a portion of 10 – 20 vol% of gas in the melt is accounted for.

In the calculation, constant frictional losses and a homogeneous flow of melt in the tube are assumed. As for the actual flow cross section, a small average crust thickness of one millimeter is considered that reduces the tube internal diameter. Table A4.1 gives a survey of the essential parameters.

The major output data are the flow speed (always related to the tube cross section), the integrated melt mass, and the height of the melt surface in the crucible.

The results of the calculation of the first three tests suggested that the actual initial flow pattern of the melt did not agree with that of the numerical model (full tube cross section all the time). We concluded that the melt flow, because of the finite time required to complete melt through of the steel foil, is starting as a small jet, and the flow occupies the full tube cross section only after several tens of milliseconds. Modelling a gradual growth of the jet diameter had an effect on the integration of the melt mass such that the mass actually released was obtained at the end of the calculation. No measures were taken to modify the melt speed function.

The calculation of melt release from test 04 on was easier since the starting time was given by the opening time of valve 1. From test 05 on, the loss coefficients were chosen to be ς_e=0.2 at the entrance to the release tube, λ=0.1 within the tube, and ς_a=0.1 at the lower end. In the cases with the melt flow divider, ς_a=0.6 was used.

The loss coefficients (which are in fact somewhat larger than those generally used in single-phase flow in smooth pipes) together with the assumed density and the

slightly reduced tube diameter resulted in melt masses released that agree with those found in the tests. It should be noted that a set of similar parameters gave also good results in the calculations of melt release performed in the PREMIX test series /9/.

The calculation is started at the time when the slide valve opens (tests 04 to 09). In the calculations for test 01 to 03, the instant when melt through of the steel foil started had to be assessed. In doing so, characteristics in the measurements were considered, e.g. the first decrease in the melt generator pressure.

The initial axial height of the melt surface in the crucible is calculated on basis of the maximum mass of melt to be released, i.e. 18 kg. The flow of melt starts from the state of rest, i.e., v=0 at t=0.

The portion of melt mass that passes the location of the closing valve during the time Δt is given by

$$\Delta m(t_i) = 0.5 * (v_{i-1} + v_i) * \Delta t * rho * A_{tube}\,, \qquad \text{(A4.3)}$$

where A_{tube} is the cross section of the melt release tube. The time step is Δt = 1 ms. The mass fractions are integrated to give the total mass:

$$m(t_i) = m(t_{i-1}) + \Delta m(t_i). \qquad \text{(A4.4)}$$

The melt surface in the crucible is considered to move evenly at any time. The area of the funnel cross section is treated as a function of the axial coordinate.

In tests 01 to 03, additional assumptions had to be made in the calculation to obtain the same mass of melt as released in the test:

- In test 01, it was assumed that melt through of the foil took 15 ms. This means that the melt occupied the full tube cross section only after that time.
- In test 02, the diameter of the melt jet was set to 0.03 m (=const.). The frictional losses were calculated using the tube diameter.
- In test 03, the jet diameter had to be reduced even larger: it was varied from 0.002 to 0.025 m within the release time of about 0.4 s. The frictional losses were calculated as in test 02.

Table A4.1 Geometrical data and friction coefficients used in the calculation.

Test	Effective tube (jet) diameter, m	Inlet resistance coefficient, ς_e, -	Tube friction coeff., λ, -	Tube outlet resistance coeff., ς_a, -
ECO-01	0.043	0.2	0.1	-
ECO-02	(0.03)	0.2	0.1	-
ECO-03	(0.002 – 0.025)	0.2	0.1	-
ECO-04	0.058	0.1	0.05	-
ECO-05$^+$	0.058	0.2	0.1	0.6
ECO-06$^+$	0.058	0.2	0.1	0.6
ECO-07$^+$	0.058	0.2	0.1	0.6
ECO-09$^+$	0.058	0.2	0.1	0.6

$^+$ Tests performed with the melt dispersion device.

A5: Information gained from the high-speed endoscope camera

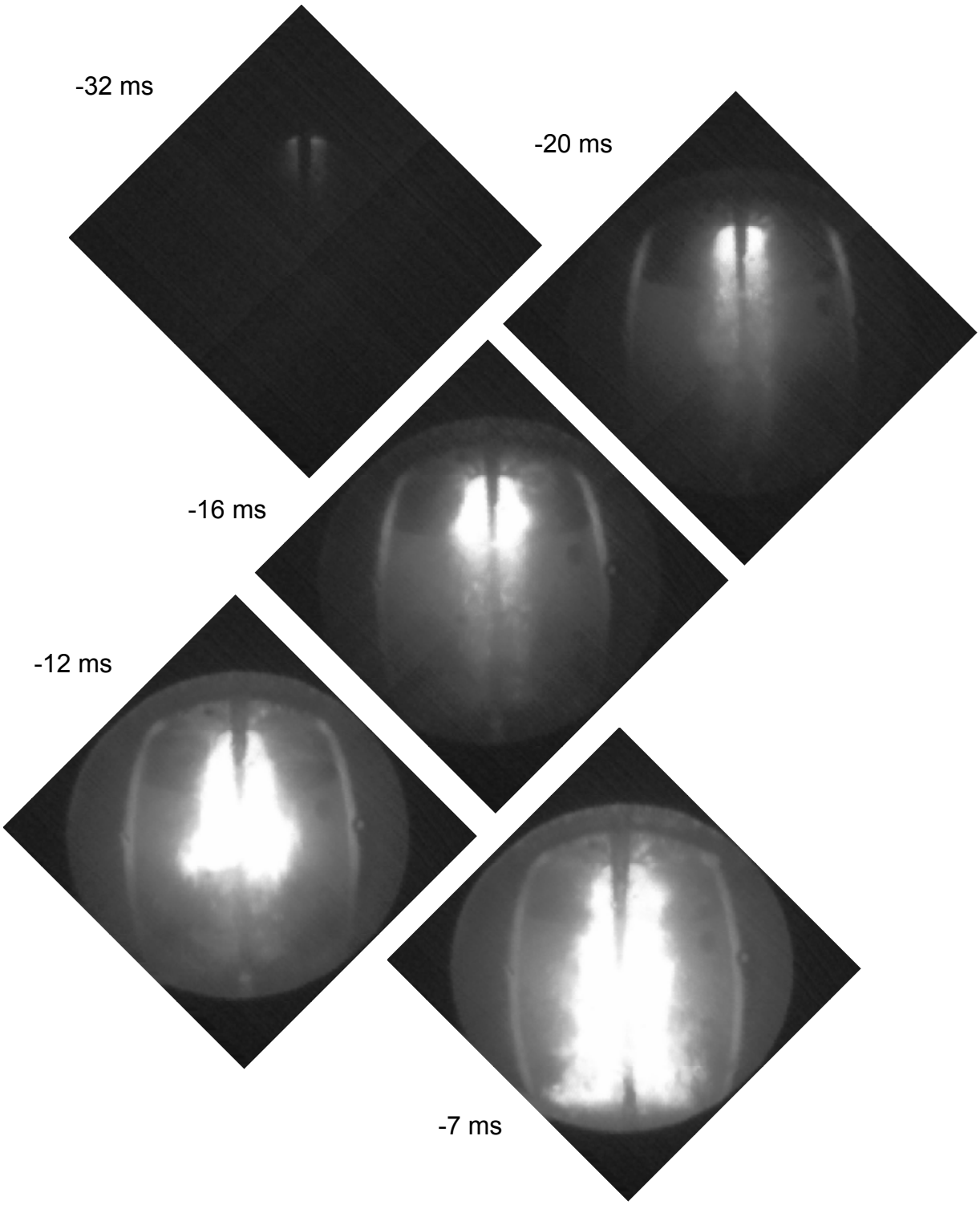

Fig. A5.1 A sequence of film frames taken during test 06. The flattening of the bright contour (at -7 ms) indicates that the melt flow has arrived at the water surface.

APPENDIX B: Crushing material data

Two kinds of crushing materials, called Charge 1 and Charge 2 supplied by different manufacturers, were used in the various layers in ECO test series. In tests 01 to 06, Charge 1 was applied. A combination of Charge 1 and Charge 2 had to be used in tests 07 to 09 (see Table B.1) because Charge 1 was no more fully availabe.

Normally, the strength of the crushing material is expected to be almost constant during compression. For the case of slow, i.e. quasi-static deformation, the manufacturers give strengths of σ = 27.6 and 29.8 N/mm² for Charge 1 and 2, respectively. These values might be up to 30% larger under dynamic loads, was an additional indication. The forces, $F = \sigma A$, given in the table, were calculated using the above strengths for static deformation, where A is the respective area of the layer.

The Charge 2 material was used only in the three uppermost layers (see Table B.1). Since only elements of 150 mm diameter were available, a number of five, nine, and 13 elements had to be used in the layers 1 to 3, respectively, to approximately meet the required force (see Fig. B.2 below).

Table B.1 Properties of the crushing material using the manufacturers' data. N.o.e. means number of elements; Chg means charge.

Layer	Test 01 to 06					Test 07 to 09				
	N.o.e.	Chg	Diam. m	Area m^2	Force MN	N.o.e.	Chg	Diam. m	Area m^2	Force MN
1	1	1	0.36	0.102	2.723	5	2	0.15	0.088	2.599
2	1	1	0.48	0.181	4.833	9	2	0.15	0.159	4.680
3	1	1	0.57	0.255	6.810	13	2	0.15	0.230	6.771
4	1	1	0.645	0.327	8.731	1	1	0.645	0.327	8.731
5	1	1	0.715	0.401	10.707	1	1	0.715	0.401	10.707

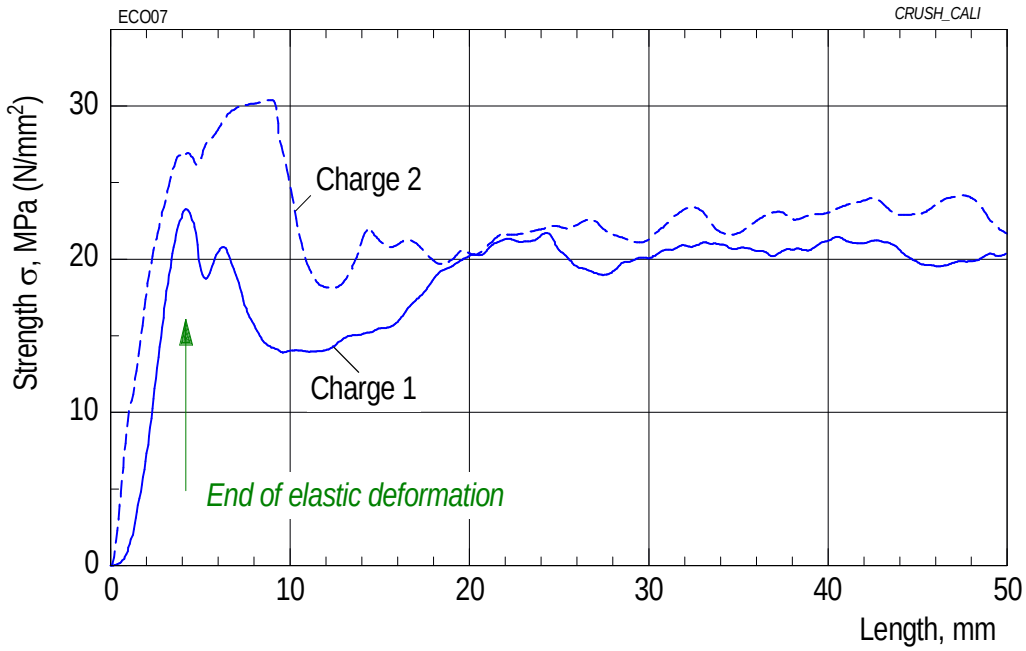

Fig. B.1 Calibration tests performed under quasi-static conditions.

Calibration tests were performed to check the data given by the manufacturers and to find out the stress dynamic loads would exert on the two materials. Each probe was subjected to quasi-static and dynamic loads.

The results of *quasi-static deformation* performed with rates of 0.007 m/s are presented in Fig. B.1. As one can see, the initial characteristic of the stress functions (formation of an elastic deformation) is similar to that known from tests with solid probes. The plastic deformation starts after a deformation of about 4 mm has been reached. Up to a deformation of 20 mm, the strength of Charge 2 is much larger than that of Charge 1. The difference becomes smaller for larger deformations.

We calculated from the lines in Fig. B.1 mean strengths of 18.4 and 22.6 N/mm², respectively, taking a deformation length of 50 mm. In both cases, these values are lower than those given by the manufacturers for the deformation under quasi-static loads. The so calibrated values are smaller by 33 % in Charge 1 and by 24 % in Charge 2.

The calibration tests under *dynamic loads* were performed using the kinetic energy of a falling body. The mass of the falling body was 242 kg, the falling height 3.8 m. The evaluation of the high-speed video film gave a mean deformation rate of about 3 m/s. (In the ECO experiments, much larger deformation rates, up to 15 m/s, were found!).

The results are summarized in Table B.2. The specimen in tests no 1 and no 2 were cut out of a Charge-1 layer kept in reserve. The mean strength was calculated using the deformation length attained.

Table B.2 Calibration tests performed under dynamic conditions.

Calib. test no	Charge no	Diameter, m	Area, m²	Deformation, m	Strength, N/mm²
1	1	0.15	0.0176	0.021	24.4
2	1	0.15	0.0176	0.022	23.2
3	2	0.15	0.0176	0.009	≈ 57
4	2	0.15	0.0176	0.009	≈ 57

For Charge 1, the strength measured under dynamic conditions is about 30 % larger than that measured under static conditions, but even under these conditions the value is 14 % lower than that given by the manufacturer.

The results for Charge 2 are different in two respects. The strength measured under dynamic conditions is larger than the static values by a factor of 2.5 (compare the numbers 57 in Table B.2 with the mean of the dashed line in Fig. B.1 which is ≈22). The strengths of the two materials differ by a factor of 2.4 (Table B.2, last column). It is assumed that the deformation starts with a peak strength which is still larger than the calculated mean value. This behaviour may explain why, as reported in test 09 (Section 5.8), the energy absorption elements used in layer 1 showed only little, those in layer 2 and 3 no deformation.

We decided to use the material data found in the calibration tests under dynamic conditions in our calculations of the mechanical work. The deformation forces of the various layers calculated with these data are given in Table B.3.

Table B.3 Deformation forces calculated on basis of the results obtained under dynamic loads in the calibration tests. N.o.e. means number of elements.

Layer	Test 01 to 06					Test 07 to 09				
	N.o.e.	Ch.	Diam., m	Area, m^2	Force, MN	N.o.e.	Ch.	Diam., m	Area, m^2	Force, MN
1	1	1	0.36	0.102	2.428	5	2	015	0.088	5.012
2	1	1	0.48	0.181	4.308	9	2	0.15	0.159	9.055
3	1	1	0.57	0.255	6.069	13	2	0.15	0.230	13.10
4	1	1	0.645	0.327	7.783	1	1	0.645	0.327	7.783
5	1	1	0.715	0.401	9.544	1	1	0.715	0.401	9.544

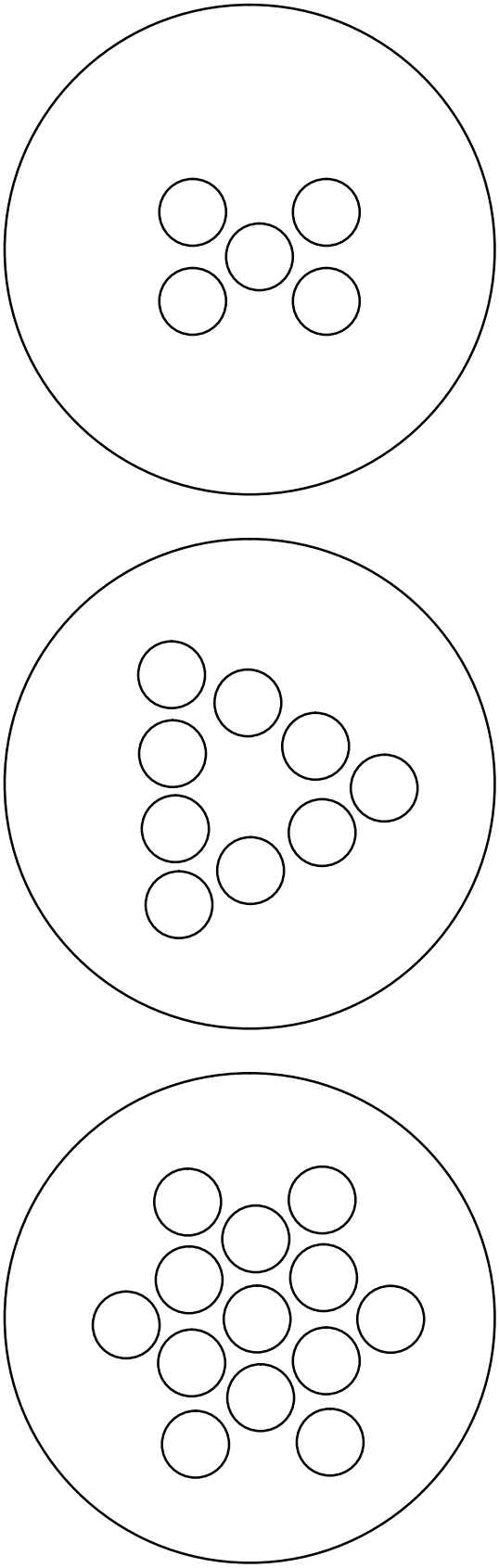

Fig. B.2 Test 07 to 09. Arrangement of the crushing material elements placed in the layers 1 to 3 (from top to bottom).

APPENDIX C: Investigations on the trigger pulse

Separate tests of the trigger capsules have been performed at several occasions before and during the test series. Figure 5.1.7 includes an early example in which a single capsule, mounted in the centre of the bottom, produced a peak with a pressure increase ΔP of about 7 MPa. In the later tests performed with two capsules (after test 02), pressure increases of 4.5 – 5.5 MPa have been seen. The situation in the essential tests is the following:

- (a) The small peak close to the beginning of the event in test 04 (Fig. 5.4.6) with a ΔP of 5.7 MPa quite certainly shows the trigger pulse.
- (b) In the tests 05 and 06, the triggers had a ΔP of 2.9 and 4.2 MPa, respectively. It appears that they were weakened by void close by. The steam explosions occurred with a delay of 2.5 and 3.5 ms, respectively (cf. Figs. 5.5.6 and 5.6.6).
- (c) In test 09, the trigger pulse had (in the PK01 signal) a ΔP of about 0.7 MPa only. The steam explosion followed with a delay of 1.5 milliseconds. Possibly, in this test, the trigger at the side (no data are available from the central trigger!) ignited with a delay of about 1.7 ms.

The measurement of an extremely low trigger ΔP of 0.4 MPa in test 07 has given rise to a more intensive investigation regarding the reliability of the explosion capsules used in ECO. Special tests were performed in a small vessel (0.016 m^3) that could be partly filled with water and be pressurized. At pressures up to 1.7 MPa the trigger capsules exploded as expected. This removed the concern that the capsules might not have performed properly in test 07 due to water having penetrated into the charge. On the other hand it is questionable whether the low trigger ΔP can be explained by especially large void close by. The absence of the restriction tube has allowed the multiphase zone to extend closer to the vessel wall but also has made more subcooled water available for condensation of the steam.